

# 1 Technical note: Surface fields for global environmental modelling

2 Margarita Choulga<sup>1</sup>, Francesca Moschini<sup>1</sup>, Cinzia Mazzetti<sup>1</sup>, Stefania Grimaldi<sup>2</sup>, Juliana  
3 Disperati<sup>3</sup>, Hylke Beck<sup>4</sup>, Peter Salamon<sup>2</sup>, Christel Prudhomme<sup>1</sup>

4 <sup>1</sup>European Centre for Medium-Range Weather Forecasts (ECMWF), Reading, RG2 9AX, United Kingdom

5 <sup>2</sup>Joint Research Centre (JRC), European Commission, Ispra, 21027, Italy

6 <sup>3</sup>Fincons Group, Vimercate, 20871, Italy

7 <sup>4</sup>King Abdullah University of Science and Technology (KAUST), Thuwal, Saudi Arabia

8 *Correspondence to:* Margarita Choulga (margarita.choulga@ecmwf.int) and Christel Prudhomme  
9 (christel.prudhomme@ecmwf.int)

10 **Abstract.** Climate change has resulted in more frequent occurrences of extreme events, such as flooding and  
11 heavy snowfall, which can have a significant impact on densely populated or industrialised areas. Numerical  
12 models are used to simulate and predict these extreme events, enabling informed decision-making and planning  
13 to minimise human casualties and protect costly infrastructure. LISFLOOD is an integrated hydrological model  
14 underpinning the European and Global Flood Awareness Systems (EFAS and GloFAS, respectively) developed  
15 by the Copernicus Emergency Management Service (CEMS). The CEMS\_SurfaceFields\_2022 dataset is a new  
16 set of high-resolution surface fields at 1 and 3 arc min (approximately 2 and 6 km at the [Equator](#)  
17 respectively) covering Europe and the global land surface (excluding Antarctica) respectively, based on a wide  
18 variety of high-resolution and up-to-date data sources. ~~The dataset has been created together with upgrades to the~~  
19 ~~open source LISFLOOD code. The set~~ [The dataset](#) encompasses (i) catchment morphology and river network, (ii)  
20 land use, (iii) vegetation cover type and properties, (iv) soil properties, (v) lake information, and (vi) water  
21 demand. This manuscript details the complete workflow to generate CEMS\_SurfaceFields\_2022 fields, including  
22 data sources and methodology. ~~The use of these fields is expected to significantly improve accuracy, detail, and~~  
23 ~~realism of~~ [Whilst created together with upgrades to the open source LISFLOOD simulations code, the CEMS\\_](#)  
24 [SurfaceFields\\_2022 fields can also be used independently for a wide range of applications, including as input for](#)  
25 [other of hydrological, Earth system models](#) ~~System or environmental modelling~~, or for carrying out general  
26 ~~statistical~~ analyses across ~~various~~ spatial scales, ranging from global and regional to local levels [\(especially useful](#)  
27 [for regions outside Europe\)](#), ~~expected to improve accuracy, detail, and realism of applications.~~

## 28 1 Introduction

29 Current numerical Earth system models are highly complex. Thanks to the availability of High Performance  
30 Computers, cloud computing, and a wide range of high-resolution environmental data derived from the use of  
31 ground, unconventional and satellite measurement sensors, numerical global models are even able to reach  
32 kilometre-scale horizontal resolution. But increase in spatial resolution also means that the Earth system and  
33 environmental models have to represent more surface and atmospheric processes and their interactions, which can  
34 become challenging, for example in complex orographic areas. Model accuracy heavily depends on the quality of  
35 the input surface fields (i.e. how realistic and up-to-date they are), and it is essential to minimise errors in surface  
36 fields. New high-resolution (i.e. 10-100 m) surface datasets based on daily satellite observations are now  
37 frequently released and continuously supported by e.g. the Copernicus program (e.g. Global Land Cover:  
38 Buchhorn et al., 2021; GHSL-BUILT-S: Pesaresi and Politis, 2022; Schiavina et al., 2022), which helps in  
39 achieving the goal of minimising surface field errors. It was shown, e.g. in Kimpson et al. (2023, ~~in review~~), that  
40 the use of accurate and up-to-date underlying information to generate model's input surface fields can substantially  
41 reduce skin temperature errors even at 30 km horizontal resolution (Kimpson et al., 2023 ~~in review~~).  
42 Following the digital revolution of cloud archiving and computing, where data, software and [information](#)  
43 [technology \(IT\)](#) infrastructure can be accessed by anyone from everywhere, the Earth systems and environmental  
44 modelling community has also moved from codes developed by a single organisation and few contributors, to so-  
45 called 'community models' where a reference code is open for free use and/ or development according to sharing  
46 principles. Such models include Joint UK Environmental Simulator JULES, a land surface model whose  
47 development is coordinated by the UK Met Office and UKCEH (Best et al., 2011; Clark et al., 2011; Marthews  
48 et al., 2022), OpenIFS, a Numerical Weather Forecast model available to external users for research and training  
49 (Sparrow et al., 2021; Carver, 2022; Huijnen et al., 2022; Köhler et al., 2023), the Community Land Model CLM,  
50 an Earth System Model with strong climate component maintained by the National Centre for Atmospheric  
51 Research but available for use by the wider research community (Lawrence et al., 2019), or LISFLOOD-OS, a  
52 spatially distributed water resources model developed by the Joint Research Centre (JRC; Van Der Knijff and De  
53 Roo, 2008) and available for use and development through a share code repository ([available online: https://ec-](#)

54 [jrc.github.io/lisflood/#lisflood](https://ec-jrc.github.io/lisflood-code/); <https://ec-jrc.github.io/lisflood-code/>, last  
55 [accessed: 21.01.2024](https://ec-jrc.github.io/lisflood-code/).

56 To promote the seamless development of science, and facilitate research community efforts in working with the  
57 same code and input data, providing feedback, and improving the code and the data itself, powerful web-based  
58 platforms can be used. One of them is the Google Earth Engine (GEE; Gorelick et al., 2017), a free-of-charge  
59 platform that provides easy, web-based access to an extensive catalogue of satellite imagery and other geospatial  
60 data in an analysis-ready format. The data catalogue is embedded into Google computing platform that lets you  
61 easily implement all personal workflows, which facilitates global-scale analysis and visualization (GEE: FAQ,  
62 2023). GEE was chosen for the generation of a new vast surface field set due to its high resolution data catalogue  
63 and powerful computation capabilities.

64 This manuscript presents the methodology used to prepare the CEMS\_SurfaceFields\_2022 dataset containing all  
65 surface fields necessary to run the LISFLOOD-OS model at [resolutions ~2 km at the equator or 1 arc min](#) (over  
66 Europe) and [~6 km at the equator or 3 arc min](#) (globally). CEMS\_SurfaceFields\_2022 ~~can also be used~~ used in  
67 the set-up of the Early Warning Systems of the Copernicus Emergency Management Service of the European  
68 Union for the European (European Flood Awareness System EFAS version 5; Smith et al., 2016;  
69 <https://www.efas.eu/>)2016; information available online: <https://www.efas.eu/>, last accessed: 21.01.2024) and  
70 global (Global Flood Awareness System GloFAS version 4; Hirpa et al., 2018; Alfieri et al., 2020; Harrigan et  
71 al., 2023; information available online: <https://www.globalfloods.eu/>), last accessed: 21.01.2024) domains  
72 ~~expected to become operational during in December 2023. The detailed explanation, encompassing (EFASv5 and~~  
73 ~~GloFASv4). Details on~~ raw data collection, scientific protocol, and technical details, ~~with methods aim to allow~~  
74 the adequate understanding and interpretation of the surface field datasets ~~(openly available from the data~~  
75 ~~catalogue of the JRC, and for EFAS~~ [https://data.jrc.ec.europa.eu/dataset/f572e443-7466-4adf-87aa-](https://data.jrc.ec.europa.eu/dataset/f572e443-7466-4adf-87aa-e0847a169f23)  
76 ~~e0847a169f23, for GloFAS~~ <https://data.jrc.ec.europa.eu/dataset/68050d73-9e06-499e-a441-de5053eb0e86>), with  
77 ~~clear methodological protocols that can be replicated or adapted easily~~ any interested user to prepare alternative  
78 ~~fields over a~~ generate their own datasets by replicating or adapting the workflow to different fields, geographical  
79 domain, spatial resolution, or different content as relevant for downstream application. Finally, the resulting  
80 ~~The~~ manuscript is structured as follows: Section 2 provides an overview of the surface fields ~~are expected to be a~~  
81 ~~useful resource not only for hydrological modelling but also for weather prediction, Earth system modelling,~~  
82 ~~environmental modelling, or statistical analysis in,~~ explains the criteria to select reference data, where and how  
83 they were processed, and outlines the general, ~~with a spatial methodology to produce the surface fields;~~ Section 3  
84 to Section 8 details the reference data and specific methodology applied to each surface field category, including  
85 examples of application; Section 9 provides all the relevant information for data access; Section 10 discusses the  
86 challenges of creating a consistent high resolution continental and global scale ~~allowing for global, regional and~~  
87 ~~even national applications. set of consistent surface fields and the opportunities disclosed by their availability.~~

## 88 2 Surface fields for distributed environmental modelling

### 89 2.1 General information

90 Environmental models, especially land surface and hydrological models, simulate how water moves across  
91 canopy, surface, subsurface, ground and eventually river channels using mechanistic equations that describe the  
92 physics of these processes. Each model represents processes with more or less complexity, depending on the  
93 model purpose and expected output (Rosbjerg and Madsen, 20052006). With most represented terrestrial  
94 processes depending on the landscape, information describing the spatial variation in the geophysical and  
95 vegetation characteristics is needed. Such characteristics include morphological features (e.g. channel geometry,  
96 orography or slope), soil hydraulic property, land and vegetation features (e.g. ecosystem cover type, leaf area  
97 index (LAI), evaporation rates, crop type, planting and harvesting dates), and if relevant, human intervention  
98 information such as population density or type of water usage.

99 LISFLOOD is a semi-distributed, physically based hydrological model which has been designed for the modelling  
100 of rainfall-runoff processes in large and transnational catchments (Bates and De Roo, 2000; De Roo et al., 2000;  
101 De Roo et al., 2001; Van Der Knijff and De Roo, 2008; Van Der Knijff et al., 2010; Burek et al., 2013). In its  
102 most prominent application, LISFLOOD is used by the Copernicus Emergency Management Services' EFAS and  
103 GloFAS to provide medium range and seasonal riverine flow forecasts. (Alfieri et al., 2020). LISFLOOD is also  
104 widely used for a variety of applications, including water resources assessment (drought forecast); analysis of the  
105 impacts of land use changes, river regulation measures, water management plans; climate change analysis (e.g.  
106 Vanham et al., 2021).

107 To facilitate users' uptake and enable the seamless development of science, LISFLOOD has been released as open  
108 source in 2019, i.e. LISFLOOD-OS. The open-source suite includes the LISFLOOD hydrological model and a  
109 set of auxiliary tools for model setup, calibration, and post-processing of the results. For instance, the pre-

processor LISFLOOD-LISVAP can be used to compute evapotranspiration, which is one of the three meteorological variables, along with total precipitation and average temperature, strictly required as input to the hydrological model.

The modelling of runoff processes in different climates and socio-economic contexts then requires a set of raster fields (i.e. set of surface fields presented in this manuscript) to provide information of terrain morphology, surface water bodies, soil properties, land cover and land use features, water demand. The total number of fields range between 66, when only the essential rainfall-runoff processes are modelled, to a total 108 for a more comprehensive model set-up in which, for instance, lakes, reservoirs, water demand for anthropogenic use are included (<https://ec-jrc.github.io/lisflood-model/>), available online: <https://ec-jrc.github.io/lisflood-model/>, last accessed: 21.01.2024).

~~In this section, we introduce the main characteristics of environmental fields dataset produced, grouped according to their role in process representation (name in brackets next to each field correspond to the name in the data repository). The main model's field (i.e. in technical field for model operation/ running sense) is 'mask' – a Boolean field that defines model boundaries, i.e. grid\_cells over which the model performs calculations and grid\_cells which are skipped (e.g. ocean grid\_cells). Whilst the surface fields described in this manuscript follow some specific requirements of the LISFLOOD-OS model, they are a source of versatile information that can be used for any environmental modelling application, either directly, or following a transformation, as relevant, as a full set or as a few consistent fields.~~

## 2.2 Reference data and methodology

### ~~2.1 To produce CEMS SurfaceFields 2022 surface fields only open source, freely available, updated as recently as possible, with recognised reference on their quality data sources were used (see Appendix 1 for all relevant reference data details). Catchment morphology and river network~~

~~Morphology and channel shape information are essential for the computation of snow melting, temperature sealing, and river routing. Land morphology is derived from elevation and its variability within a single cell can be represented through slope, standard deviation, aspect, etc. River drainage information, derived from elevation, is used to connect the model cells according to the direction of the surface runoff, with channel geometry information used for routing processes.~~

~~The dataset contains 14 morphology and river network variables:~~

- ~~● Morphologic information: local drainage direction (i.e. flow direction from one cell to another; *LDD*, dimensionless), upstream area (*upArea*,  $m^2$ ), grid-cell area (*pixarea*,  $m^2$ ), grid-cell length (*pixleng*,  $m$ ), standard deviation of elevation (*chvstd*,  $m$ ), gradient (i.e. elevation gradient; *gradient*,  $m/m$ );~~
- ~~● Kinematic wave equation for routing: channel bottom width (*chanbw*,  $m$ ), channel length (*chanlength*,  $m$ ), channel gradient (*changrad*,  $m/m$ ), Manning's roughness coefficient for channels (*chanman*,  $s/m^{1/3}$ );~~
- ~~● River network information: channel mask (i.e. presence of river channel; *chan*, dimensionless), channel side slope (i.e. channel's horizontal distance divided by vertical distance; *chans*,  $m/m$ );~~
- ~~● Open water evaporation: bankfull channel depth (*chanbnlf*,  $m$ ), channel flood plain (i.e. width of the area where the surplus of water is distributed when the water level in the channel exceed the channel depth; *chanflpn*,  $m$ );~~

### ~~2.21 Land use fields~~

~~Land use is an essential component of environmental models. Many models use a sub-grid-cell approach where a single-grid cell can include several different land uses with each land use being subject to different prominent physical processes. This approach allows to keep a high level of accuracy when representing how different types of land cover affect e.g. the hydrological cycle (e.g. evaporation is different in urban areas compared to forests) while limiting the increase in computational time.~~

~~The dataset differentiates between six different land uses:~~

- ~~● Forest: areas where the main hydrological processes are canopy interception, evapotranspiration from canopies, canopies drainage and evapotranspiration, root uptake and evaporation from the soil (fraction of forest; *fracforest*, dimensionless fraction);~~
- ~~● Sealed surface: impervious areas where there is no water infiltration into the soil, i.e. water is accumulated in the surface depression, yet evaporates, but once the depression is full, water is transported by a surface runoff (fraction of sealed surface; *fracsealed*, dimensionless fraction);~~
- ~~● Inland water: open water bodies where the most prominent hydrological process is evaporation (fraction of inland water; *fracwater*, dimensionless fraction);~~

- ~~• Irrigated crops: areas used by agriculture—water is abstracted from ground water and surface water bodies to irrigate the fields. The main hydrological processes connected with the irrigated crops are canopy interception, evapotranspiration from canopies, canopies drainage and evapotranspiration, root uptake and evaporation from the soil (fraction of all irrigated crops, excluding rice; *fracirrigated*, dimensionless fraction);~~
- ~~• Irrigated rice: areas used to grow rice with flooded irrigation agricultural technique, when water is abstracted from the inland water bodies and delivered to the rice fields. The main hydrological processes connected with rice fields are soil saturation, flooding, rice growing phase, soil drainage phase (fraction of irrigated rice; *fracrice*, dimensionless fraction);~~
- ~~• Other land cover: used in canopy interception, evaporation from the canopies, canopy drainage, plant evapotranspiration, evaporation from the soil hydrological processes. The relative importance of these processes depends on the LAI (fraction of other cover types; *fracother*, dimensionless fraction).~~

### 2.31 ~~Vegetation properties~~

~~Vegetation related information contributes to the computation of precipitation interception, evaporation, transpiration, and root water uptake. Depending on the model, vegetation dynamics can be represented with different degrees of complexity including in hydrology processes, vegetation growth and feedback on climate (Bonan et al., 2002). Rice being the world's most important food crop and having specific water demands, its water cycle is often considered explicitly, with planting and harvesting dates being critical information to represent the inter-annual variability in its water demand, provided the maximum three growing seasons. The variables allow to model how vegetation affects the hydrology, with a particular focus on root water uptake and transpiration depending on vegetation type and vegetation state (e.g. water stress conditions). For example, the crop group number depends on the critical amount of soil moisture below which water uptake from plants is reduced as they start closing their stomata.~~

~~The dataset describes vegetation properties through four variables (note that LAI consists in total of 36 10 day average fields) for each of forest (*\_f*), irrigated crops (*\_i*) and other land cover types (*\_o*), and another six (two types times three seasons) variables for rice:~~

- ~~• Transpiration rate: crop coefficient (*cropecoef\_f*, *cropecoef\_i*, *cropecoef\_o*, dimensionless);~~
- ~~• Water uptake: crop group number (*cropgrp\_n\_f*, *cropgrp\_n\_i*, *cropgrp\_n\_o*, dimensionless);~~
- ~~• Surface runoff generation and water routing: Manning's surface roughness coefficient (*manning\_s\_f*, *manning\_s\_o*,  $s/m^{1/2}$ ), rice planting and harvesting days (*riceplantingday1*, *riceplantingday2*, *riceplantingday3*, calendar day number; *riceharvestday1*, *riceharvestday2*, *riceharvestday3*, calendar day number);~~
- ~~• Water interception and evaporation: leaf area index (*laif*, *laui*, *laio*,  $m^2/m^2$ ).~~

### 2.41 ~~Soil properties~~

~~In land surface and distributed hydrological models, the water movement, storage and plants' water uptake from the soil are often described by the soil/ water retention curve (SWRC). The SWRC is derived empirically by measuring how water is retained and released by different soil types. Throughout time different SWRC have been developed and integrated into models, the most widely applied are Van Brooks and Corey (Brooks and Corey, 1964), Fredlund and Xing (Fredlund and Xing, 1994), van Genuchten (van Genuchten, 1980), and Gardner (Gardner, 1956) SWRCs. Different SWRC equations require different parameters, some shared between different SWRC concepts, e.g. referring physical soil characteristics such as water saturated and unsaturated content, hydraulic conductivity and pore size, others uniquely describing the SWRC function shape, not directly related to soil properties. Often, for computational reasons, the soil profile from ground level to bedrock depth is sliced into layers, at the modeller's choice, and the SWRC function is applied to each soil layer.~~

~~The dataset includes variables required to apply the Van Genuchten SWRC equations (van Genuchten, 1980) to describe the water dynamics through a vertical soil profile composed of three layers (1, 2, 3), each variable is required for each soil layer and for forest (*\_f*) or non forest (*\_o*) land use, with different soil depth in forest (*\_f*) and non forest (*\_o*) areas following root depth values from Allen et al. (1998), further referred as FAO56, (total of 29 variables; see Section 4.4 for detailed definition and calculation):~~

- ~~• Soil profile: surface layer depth (*soildepth1\_f*, *soildepth1\_o*, mm), middle layer depth (*soildepth2\_f*, *soildepth2\_o*, mm), subsoil depth (*soildepth3\_f*, *soildepth3\_o*, mm);~~
- ~~• Soil hydraulic properties: saturated (*thetas1\_f*, *thetas1\_o*, *thetas2\_f*, *thetas2\_o*, *thetas3*,  $m^3/m^3$ ) and residual (*thetar1*, *thetar2*, *thetar3*,  $m^3/m^3$ ) volumetric soil moisture content, pore size index (*lambda1\_f*,~~



~~$\lambda_{o1}, \lambda_{f2}, \lambda_{o2}, \lambda_{o3}$ , dimensionless), Van Genuchten equation parameter ( $g_{nu1-f}, g_{nu1-o}, g_{nu2-f}, g_{nu2-o}, g_{nu3}$ ,  $\text{cm}^{-1}$ ), saturated soil conductivity ( $ksat1-f, ksat1-o, ksat2-f, ksat2-o, ksat3$ , mm/day).~~

## 2.51 ~~Lakes~~

~~Lakes (and reservoirs) are important as they influence the atmosphere regionally and globally as well as the river discharge. The area covered by lakes is used for computing evaporation from open water surfaces. In LISFLOOD the volume of evaporated water is not subtracted from the storage volume of lakes. Here the dataset only includes data on lake extent and not reservoirs (generally smaller): lake mask (i.e. presence of lakes consistent with fraction of inland water;  $lakemask$ , dimensionless).~~

## 2.61 ~~Water demand~~

~~Some environmental models explicitly represent a number of the human interventions impacting on the water cycle. One of the most common is water demand, which represents the withdrawal of water from natural water sources (e.g. rivers, reservoirs, groundwater) to satisfy the water demand for anthropogenic use. The segregation of the total water demand for anthropogenic use into four main sectors, namely domestic, energy, industrial, and livestock water withdrawal, enables a more accurate representation of the processes. Following the Food and Agriculture Organisation of the United Nations (FAO) terminology (Kohli et al., 2012), domestic water withdrawal represents indoor and outdoor household water use as well as other uses (e.g. industrial and urban agriculture) connected to the municipal system (e.g., water use by shops, schools, and public buildings). Electricity (energy) water withdrawal is the water use for the cooling of thermoelectric and nuclear power plants. Water withdrawal for industry is the water used for fabricating, processing, washing, cooling or transporting products, also includes water within the final products and water used for sanitation within the manufacturing facility. Livestock withdrawal is the demand for drinking and cleaning purposes of livestock.~~

~~Higher accuracy in environmental modelling is achieved by differentiating water demand sources and by allocating different levels of priority to different usages. Within LISFLOOD, for instance, water demand for the energy sector and flooded irrigation (rice crops) is supplied by surface water bodies only, while non flooded irrigation, domestic, industrial, livestock water demand can be supplied by both groundwater and surface water bodies. Moreover, domestic water demand has the highest priority in case of water scarcity conditions.~~

~~It must be noted that the fields of water demand for agriculture are not included in this dataset because LISFLOOD computes crops water demand internally by accounting for climatic conditions, information on land cover (see Section 2.2), crops properties (see Section 2.4), and soil properties (see Section 2.5). Conversely, fields representing the volume of water to satisfy the domestic, energy, industrial, and livestock demand must be provided as input. Domestic, industrial, energy, and livestock water demand volumes have seasonal (e.g. due to temperature differences) and inter-annual variations (e.g. due to population changes and different economic conditions). In order to account for this variability, in LISFLOOD the four sectoral water demand fields provide daily water demand data with monthly or annual variability from 01.01.1979 to 31.12.2019: the water demand values are provided in mm/day, one field per month (the first day of each month is used as representative timestamp for the entire month) for domestic and energy demand, one value per year (the monthly fields are repeated twelve times per each year) for industrial and livestock demand.~~

~~The dataset includes water demand for four main sectors (note that each sector consists in total of 12 daily water demand fields per 41 (1979-2019) years, so 492 fields per sector) for: livestock ( $liv$ , mm/day), industry ( $ind$ , mm/day), energy production, ( $ene$ , mm/day) and domestic use ( $dom$ , mm/day). The temporal extension of the water demand fields presented in this manuscript includes the most recent information of water demand at the time of the dataset's preparation. Readers that are interested in using more recent water demand data are invited to follow the protocol presented in Section 4.6 to further extend in time the provided fields.~~

## 2.7 Specific requirements for the dataset

~~The dataset produced follows the specific requirements of LISFLOOD for EFAS (European domain, 1 arc min resolution at mid-latitude of the domain (47.50 N) is ~1.25 km) and GloFAS (Global domain) implementation, summarised in Table 1.~~

**Table 1. Dataset files technical specifications.**

Type	Specification
------	---------------

Format	NetCDF
Projection	EPSG:4326 – WGS84: World Geodetic System
Horizontal resolution	Europe: 1 arc min (~1.86 km at the Equator) [file size 4530x2970 grid cells] Globe: 3 arc min (~5.57 km at the Equator) [file size 7200x3600 grid cells]
Domain bound	Europe: [North = 72.25 N; South = 22.75 N; West = 25.25 W; East = 50.25 E] Globe: [North = 90.00 N; South = 90.00 S; West = 180.00 W; East = 180.00 E]
Missing value (i.e. NoData) location	Over land: none Over ocean: all ocean grid cells have missing value (i.e. ocean is masked based on ‘mask’ field)
Missing value (i.e. NoData) number	For Integer variable type: 0 For Real variable type: 999999.0
Variable type	Integer: Int8 Real: Float32

### 266 3 Reference data and overall methodology

267 This section describes all data sources used to produce dataset’s surface fields introduced in Section 2. All data  
 268 considered were open source, freely available, updated as recently as possible, with recognised reference on their  
 269 quality. Note that whilst the majority of surface fields contain no time element, vegetation and water demand  
 270 fields explicitly describe the annual cycle (vegetation, rice) or annual time evolution (water demand) and therefore  
 271 have more stringent requirements regarding the data source. Global single-source datasets (e.g. Te Chow, 1959;  
 272 Supit et al., 1994; Allen et al., 1998; Buchhorn et al., 2021) were favoured to regional and/ or multiple data sources  
 273 that needed to be combined in order to produce the required data unless sub-set information was of much better  
 274 quality (e.g. Moiret-Guigand, 2021). CEMS SurfaceFields 2022 surface fields are based on 25 different data  
 275 sources and consist of 140 gridded fields grouped into six following groups: (i) catchment morphology and river  
 276 network, (ii) land use, (iii) vegetation cover type and properties, (iv) soil properties, (v) lake information, and (vi)  
 277 water demand.

### 278 3.1 Catchment morphology and river network

#### 279 3.1.1 Digital Elevation Model

280 **The MERIT DEM: Multi Error Removed Improved Terrain Digital Elevation Model v.1.0.3** [15 October,  
 281 2018] (further referred as MERIT DEM) is a high accuracy global DEM at 3 arc second resolution (~90 m at the  
 282 Equator) covering land area from 90 N to 60 S, selected for its ability to clearly represent landscapes such as river  
 283 networks and hill valley structures even in flat areas where height errors could be larger than topography  
 284 variability (Yamazaki et al., 2017; Bhardwaj, 2021; Chai et al., 2022). It is derived from seven different open-  
 285 source datasets, delivered as 57 GeoTiff files 30° by 30° region each, at 90 m resolution (in total 90.0 GB),  
 286 representative of the year 2018. More detail on method, data content and access can be found in Yamazaki et al.  
 287 (2017) and MERIT DEM web page <http://hydro.iis.u-tokyo.ac.jp/~yamada/MERIT-DEM>.

288 The MERIT DEM was used to compute standard deviation of elevation, gradient and channel geometry fields.

#### 289 3.1.2 Hydromorphology

290 **The Catchment based Macro-scale Floodplain (CaMa Flood) Global River Hydrodynamics Model v4.0**  
 291 **maps** (further referred as CaMa Flood) are used for the basic maps describing all physical properties of the river  
 292 network. It is derived from MERIT Hydro (MERIT Hydro is a global hydrography dataset, created by using  
 293 elevation (i.e. MERIT DEM) and several inland water maps; more detail can be found in Yamazaki et al. (2019)  
 294 and MERIT Hydro web page <http://hydro.iis.u-tokyo.ac.jp/~yamada/MERIT-Hydro>) for high resolution river  
 295 routing applications using the FLOW algorithm (Yamazaki et al., 2009; Yamazaki et al., 2011). The maps include  
 296 information on channel length, river topography parameters, floodplain elevation profile, channel width and  
 297 channel depth. The maps exist at 15, 6, 5, 3 and 1 arc min resolutions covering land area from 90 N to 60 S,  
 298 representative of the year 2017, and for each resolution, they are available as one single file with all variables in  
 299 NetCDF format (for 1 arc min 737.0 MB). More detail on method, data content and access can be found in  
 300 Yamazaki et al. (2011) and CaMa Flood web page <http://hydro.iis.u-tokyo.ac.jp/~yamada/cama-flood/index.html>. Note that whilst the CaMaFlood maps were originally generated for the specific use of the  
 301 CaMa Flood model, they can also serve as basic to derive alternative maps for other environmental models, as  
 302 done here.

303 The CaMa Flood maps were used to create the local drainage direction (LDD), upstream area, channel geometry  
 304 and land masks fields.  
 305

### 3.2.1.1 Land-use fields

#### 3.2.1 Land-cover

~~The Copernicus Global Land Service (CGLS) Land Cover (LC) 100m map (further referred as CGLS LC100) is a global land cover map of the year 2015 (Buchhorn et al., 2020). It is derived from the PROBA V 100 m satellite image collection, a database of high quality land cover training sites and ancillary datasets, reaching an accuracy of 80 % at Level1 (Buchhorn et al., 2021). It contains 23 classes for discrete classification and 10 classes for continuous cover fractions, and it is delivered as 15 files in GeoTiff format (in total 39.3 GB) at 100 m resolution covering land area from 90 N to 60 S and representative of the year 2015. More detail on method, data content and access can be found in Buchhorn et al. (2021) and Copernicus web site <https://land.copernicus.eu/global/products/1c>.~~

~~The CGLS LC100 was used to generate crop parameters and Manning's surface roughness coefficient for forest and other land cover types, to generate forest, inland water, and sealed surface fraction fields, following a basic quality check on large water bodies (i.e. correcting Fox Basin and Caspian Sea).~~

~~The Coordination of Information on the Environment (CORINE) Land Cover (CLC) inventory for 2018 (further referred as CLC2018) is a set of maps describing the land cover/ land use status of 2018 covering 39 countries in Europe with a total area of over 5.8 Mkm<sup>2</sup>. The dataset is derived from satellite imagery (mainly Sentinel 2, based on a constellation of two satellites orbiting Earth at altitude of 786 km 180° apart revisiting equator every 5 days, and for gap filling Landsat 8, making a constellation together with Landsat 9 satellite orbiting Earth at altitude of 705 km each revisiting equator every 16 days) and in situ data and contains 44 classes, delivered as one GeoTiff raster file (125.0 MB) at 100m resolution covering land area over Europe, representative of the time period 2017-2018. The overall accuracy for CLC2018 is 92 % for the blind analysis (i.e. validation team had no knowledge of the CLC2018 thematic classes) but there are regional variations: the Black Sea geographical region has the lowest accuracy of 84 %; country wise overall accuracy vary from 86 % for Portugal to 99 % for Iceland, lowest accuracy being linked to the landscape complexity (Moiret Guigand, 2021). More detail on method, data content and access can be found in Büttner and Kosztra (2017) and Moiret Guigand (2021); and Copernicus web site <https://land.copernicus.eu/pan-european/corine-land-cover/clc2018>.~~

~~The CLC2018 was used to generate the irrigated crop fraction and rice fraction fields.~~

#### 3.2.2 Crop cover

~~The Spatial Production Allocation Model (SPAM) Global Spatially Disaggregated Crop Production Statistics Data for 2010 v2.0 (further referred as SPAM2010) is a global dataset generated in 2020, which redistributes crop production information from country and sub-national provinces level to a finer grid cell level (IFPRI, 2019). It is derived from numerous data sources, including crop production statistics, cropland data, biophysical crop "suitability" assessments, spatial distribution of specific crops or crop systems, and population density. SPAM2010 contains estimates of crop distributions within disaggregated units (based on a cross-entropy approach) for 42 crops and two production systems (irrigated and rainfed), and is delivered as 84 files in shapefile format at 10 km (5 arc min) resolution covering land area from 90 N to 60 S and representative of the year 2010 (in total 2.2 GB). Based on crop expert judgement from international (i.e. International Rice Research Institute, International Maize and Wheat Improvement Center) and national organisations (i.e. The Chinese Academy of Agricultural Sciences) SPAM2010 over Europe and America is more accurate than over Africa and South East Asia, with best performance in allocating rice; grid-by-grid comparison of crop areas with independent Cropland Data Layer (produced by using satellite images and vast amount of ground truth) over continental United States shows coefficient of determination ( $R^2$ ) 0.7-0.9 and root mean square error (RMSE) 231-307 ha indicating a relatively high reliability, with highest  $R^2$  and lowest RMSE values are for maize and soybean (Yu et al., 2020). More detail on method, data content and access can be found in Yu et al. (2020) and MapSPAM web site <https://mapspam.info>.~~

~~SPAM2010 was used to compute the irrigated crop and rice fractions, crop parameters and Manning's surface roughness coefficient for irrigated crop fields.~~

### 3.3 Vegetation properties

#### 3.3.1 Crop properties

~~The Food and Agriculture Organisation (FAO) of the United Nations Irrigation and Drainage Paper No. 56 (further referred as FAO56) is a publication covering geographically referenced statistics for crop development stages, crop coefficients, crop height, rooting depth, and soil water depletion fraction for common crops found across the world; it also covers procedures for information aggregation, e.g. on the grid. It is delivered as an article with a set of tables and equations and can be considered as the most complete source of information on crop~~

properties. More detail on method and data content can be found in Allen et al. (1998) and FAO online crop information web page <http://www.fao.org/land-water/databases-and-software/crop-information/tobacco/en/>. FAO56 was used to compute the crop coefficients for forest, irrigated crops and other land cover types (online crop information was specifically used for tobacco); and for intermediate computations such as depletion fraction for different crop and surface types (table), crop height and root depth fields.

Intara et al. (2018) is a publication covering oil palm roots architecture. Intara et al. (2018) was used for oil palm root depth information in addition to FAO56.

Burek et al. (2014) is a publication covering summarised information for crop coefficients, rooting depth, crop group number and Manning's surface roughness coefficient for different surface types. Burek et al. (2014) was used for built up, bare/ sparse vegetation, snow & ice, permanent inland water, ocean & seas, herbaceous wetland, moss & lichen surface types crop coefficients, rooting depth, crop group number and Manning's surface roughness coefficient information in addition to FAO56 and other sources.

**The Wofost 6.0 crop simulation model description** (further referred as SUPIT) is a publication on developing, validating, and testing new or already existing agrometeorological models (Supit et al., 1994). It contains crop group information for several crops as examples, and relation of a crop group from water depletion fraction. The publication is delivered as a book with a set of tables and equations. Information on crop group is still considered up to date. More detail on method and data content can be found in Supit et al. (1994). SUPIT was used to compute the crop group fields for forest, irrigated crops and other land cover types.

### 3.3.2 River hydraulics properties

~~The Open Channel Hydraulics manual~~ (further referred as CHOW) is a publication on open channel hydraulics, including basic principles and different types of flows, i.e. uniform, gradually varied, rapidly varied, and unsteady (Te Chow, 1959). It contains information on roughness coefficient over different surfaces. The publication is delivered as a book with a set of tables and equations. More detail on method and data content can be found in Te Chow (1959).

CHOW was used to compute the Manning's surface roughness coefficient fields for forest, irrigated crops and other land cover types.

### 3.3.3 Vegetation time evolution

~~The Copernicus Global Land Service (CGLS) Leaf Area Index (LAI) 1km Version 2 collection~~ (further referred as CGLS LAI) is a set of global maps without missing data describing vegetation dynamics—the annual evolution of LAI at 10 day intervals over the period of 1999–2020. The dataset is derived from SPOT/VEGETATION and PROBA-V data. The dataset's root mean square deviations over 20 GBOV sites over the period 2014–2018 is 0.92, compared to 1.19 for MODIS C6 LAI product (Martinez Sanchez, 2020). The dataset is delivered as one multi-band file per year in NetCDF (netCDF4 CF 1.6) format (14.7 GB per year) at 1 km resolution covering land area from 90 N to 60 S and representative of the 10-year period of 2010–2019. More detail on method, data content and access can be found in Smets (2019) and Martinez Sanchez (2020), and Copernicus web site <https://land.copernicus.eu/global/products/lai>.

CGLS LAI was used to compute the LAI fields for forest, irrigated crops and other land cover types.

### 3.3.4 Crop time evolution

~~The RiceAtlas v3~~ (further referred as RiceAtlas) is a spatial database of global rice calendars and production. It contains information on start, peak and end dates of sowing, transporting and harvesting rice, derived from global and regional databases, national publications, online reports, and expert knowledge. It is delivered as 7 files in shapefile format (in total 195.8 MB) for administrative units (in total 2725 spatial units) at 1 km resolution for the national production totals to match the years 2010–2012 (Laborte et al., 2017a). RiceAtlas is 10 times more spatially detailed, and has 7 times more special units comparing with other global datasets (Laborte et al., 2017b). More detail on method, data content and access can be found in Laborte et al. (2017a) and Laborte et al. (2017b). RiceAtlas was used to compute rice planting and rice harvesting days for three different seasons.

## 3.4 Soil properties

~~The International Soil Reference and Information Centre (ISRIC) SoilGrids250m global gridded soil information release 2017~~ (further referred as SoilGrids250m) is an output of special predictions produced by the SoilGrids system, as a set of global soil property and class maps at 250 m resolution. It is derived from soil profile data (from 150,000 sites globally) with the use of machine learning, and contains information on soil characteristics at six standard depths, including soil textures (clay, silt, sand), depth to bedrock, bulk density, organic carbon, pH and cation exchange capacity. It is delivered as 43 files in GeoTiff format (in total 111.8 GB) at 250 meters resolution covering land area with no permanent ice and representative for the year 2010 (according to land cover) (Hengl et al., 2017). SoilGrids250m pH comparison with SSURGO data over California (depth 0–



200 cm) and Soil and Landscape Grid of Australia data over Tasmania (depth 0–5 cm) show high correlation, 0.79 and 0.71 respectively (Hengl et al., 2017). Despite its limited accuracy (i.e. between 30 and 70 %, according to the SoilGrids web site) due to the scarcity of soil profile observations (especially in Central Asia, Arctic regions coastal area and desert), low resolution of covariates data and algorithms, it was selected as the most recent source of information. More detail on method, data content and access can be found in Hengl et al. (2017) and SoilGrids250m web site <https://www.isric.org/explore/soilgrids/faq-soilgrids-2017>. SoilGrids250m was used to compute the soil depth and soil hydraulic properties for forest and non-forest.

### 3.5 Lakes

**The Global Lakes and Wetlands Database** (further referred as GLWD) is a global database of water bodies. It is derived from a combination of global and regional lake data sets, registers and inventories (i.e. point information with descriptive attributes), and digital maps (i.e. polygons, rasterised global land cover and land use maps). The database consists of two global files in shapefile format at spatial resolutions of up to 1:1 million – GLWD 1 with 3067 largest lake and 654 largest reservoir polygons (6.4 MB), and GLWD 2 with 250000 smaller lake and reservoir polygons (32.0 MB); and of one global file in ADF raster format at 30 arc sec resolution – GLWD 3 combines GLWD 1, GLWD 2 and additional information (8.9 MB). Validation against documented data shows that GLWD represents good wetland maximum extent, and describes comprehensively lakes with surface area greater or equal 1 km<sup>2</sup> (Lehner and Döll, 2004). More detail on method, data content and access can be found in Lehner and Döll (2004) and GLWD web site <https://www.worldwildlife.org/pages/global-lakes-and-wetlands-database>. GLWD (i.e. only GLWD 1 and GLWD 2) was used to compute the discrete lake mask field.

### 3.6 Water demand

**AQUASTAT** is the FAO's global information system on water resources and agricultural water management. AQUASTAT collects information on water use via the network of AQUASTAT National Correspondents who are required to fill the annual questionnaire and collaborate with AQUASTAT team in the data validation process. Five types of manual checks are followed by automatic implementation of almost 200 validation rules. The dataset includes data for 180 countries worldwide, yearly data from 1979 to 2019 were used to produce the maps presented by this manuscript. Float, lumped values for each country for the variables "Gross Domestic Product (GDP)", "Industry, value added to GDP", "Agricultural water withdrawal", "Industrial water withdrawal", "Municipal water withdrawal", "Total water withdrawal", and "Irrigation water withdrawal" were obtained in CSV format (2 files, in total 2.0 MB) from the AQUASTAT data acquisition dashboard ([https://tableau.apps.fao.org/views/ReviewDashboard\\_v1/country\\_dashboard](https://tableau.apps.fao.org/views/ReviewDashboard_v1/country_dashboard)). More detail on method, data content and access can be found in AQUASTAT web site <https://www.fao.org/aquastat/en/overview/methodology/>. AQUASTAT variables were used accordingly to compute water demand fields for domestic, industrial, energy, livestock use.

**United States Geological Survey National Water Information System** (further referred as USGS NWIS) is a national database on water use data for the United States (US) with annual statistics provided every 5 years since 1950. The water use data are best estimates produced by the USGS in cooperation with local, state, and federal agencies as well as academic and private organisations. The water use data are lumped values (float numbers) for each state, delivered in plain text format (52 files, in total 56.0 MB). Following variables were used: "Domestic total self-supplied withdrawals, fresh, in Mgal/d", "Public Supply total self-supplied withdrawals, fresh, in Mgal/d", "Industrial total self-supplied withdrawals, fresh, in Mgal/d", "Total Thermoelectric Power total self-supplied withdrawals, fresh, in Mgal/d", "Total Thermoelectric Power power generated, in gigawatt hours", and "Livestock total self-supplied withdrawals, fresh, in Mgal/d". More detail on method, data content and access can be found in USGS NWIS web site <https://waterdata.usgs.gov/nv/nwis/wu>. For this study, data from 1985 to 2015 were used. USGS NWIS variables were used accordingly to refine the global water demand fields for the domestic, industrial, energy, livestock use sectors for the US.

**Global Change Analysis Model** (further referred as GCAM) is an integrated, multi-sector model developed by the Joint Global Change Research Institute (JGCRI) to explore the overall behaviour of human and physical systems dynamics and interactions. GCAM includes five main systems. One of these systems, the water module, provides information about water withdrawals for energy, agriculture, and municipal uses as lumped values of 235 hydrologic basins; a detailed explanation can be found in Calvin et al. (2019). Estimates of industrial, thermoelectric water withdrawals (energy sector) and electricity consumption were computed by running the

475 GCAM model, the output used are two files in CSV format (in total 4.0 MB). Data from the following sectors was  
476 used: "biomass", "electricity", "nuclearFuelGenII", "nuclearFuelGenIII", "regional coal", "regional natural gas",  
477 "regional oil", "SheepGoat", "Beef", "Dairy", "Pork", and "Poultry". More detail on method, data content and  
478 access can be found in the documentation of the open source package [https://github.com/JGCRI/gcam-  
479 core/tree/gcam\\_v6.0](https://github.com/JGCRI/gcam-core/tree/gcam_v6.0).

480 GCAM variables were used accordingly to estimate water withdrawals for industrial, energy, livestock use.

481  
482 **Global scale gridded estimates of thermoelectric power and manufacturing water use** (further referred as  
483 Vassolo and Doll, 2005) is a global scale gridded estimate of water withdrawal for cooling of thermal power  
484 stations and for manufacturing. Estimates of values for the year 1995 are provided with a spatial resolution of 0.5°  
485 by 0.5°. Thermoelectric power water use is based on the geographical location of 63590 thermal power stations.  
486 Manufacturing water use is computed by estimating country specific water withdrawal values, and spatial  
487 downscaling using city night time lights. Dataset verification of Vassolo and Doll (2005) showed satisfactory  
488 representation of thermoelectric power water use but high uncertainty in the representation of manufacturing water  
489 use. The data are delivered as one shapefile (2.5 MB). More details on method, data content and validation, and  
490 data access can be found in Vassolo and Doll (2005).

491 Vassolo and Doll (2005) dataset was used for the computation of energy demand fields.

492  
493 **The Gridded Livestock of the World (GLW) version3** (further referred as GLW3) is a spatial gridded dataset  
494 of the global distribution of eight livestock species for 2010. It is delivered as 8 GeoTiff files at 0.083333° (~10-  
495 km at the Equator) resolution (in total 208.0 MB). The species abundance was converted to total livestock mass.  
496 More detail on method, data content and access can be found in Gilbert et al. (2018).

497 GLW3 was used to spatially disaggregate the water demand for livestock use.

498  
499 **World Bank manufacturing value added and gross domestic product** (further referred as World Bank) data  
500 provide "Manufacturing, value added (constant 2015 US\$)" values (further referred as MVA) and "Gross  
501 Domestic Product GDP (constant 2015 US\$)" values. The data provided as a table, downloaded in CSV format  
502 (6 files, in total 6.0 MB) from <https://data.worldbank.org>.

503 World Bank dataset was used to temporally downscale the values of water demand fields for the industrial and  
504 energy sectors.

505  
506 **The Global Human Settlement Population Grid multitemporal version R2019A** (further referred as GHS-  
507 POP) is a spatial raster dataset that depicts the distribution of population, expressed as the number of people per  
508 grid cell (Freire et al., 2016; Florezyk et al., 2019; Schiavina et al., 2019). GHS POP residential population  
509 estimates for target years provided by CIESIN GPWv4.10 were disaggregated from census or administrative units  
510 to grid-cells, informed by the distribution and density of built-up as mapped in the Global Human Settlement  
511 Layer. The dataset has a spatial resolution of 9 arc sec (~300 m at the Equator) resolution and is delivered as  
512 individual files in GeoTiff format for 1975, 1990, 2000 and 2015 (4 files, in total 6.5 GB; available online:  
513 [https://ghsl.jrc.ec.europa.eu/ghs\\_ pop2019.php](https://ghsl.jrc.ec.europa.eu/ghs_pop2019.php), last accessed: 21.02.2023).

514 GHS POP was used to spatially disaggregate the country, state, basin level information of domestic, industrial,  
515 energy water withdrawal.

516  
517 **Thematic Mapping Country Borders** shapefile (further referred as TM 'country borders') was derived from  
518 Thematic Mapping™, which is a tool enabling web browsers to create thematic maps and associated world  
519 datasets. For this work, the TM World Borders Dataset was downloaded as one shapefile (10.0 MB). **The United  
520 States Census Bureau Cartographic Boundary Files** Shapefile (further referred as US CB) provides the State  
521 boundaries for the USA. For this work, the 2018 version was retrieved as one shapefile (3.2 MB; available online:  
522 [https://www.census.gov/geographies/mapping\\_files/time\\_series/geo/carto-boundary-file.html](https://www.census.gov/geographies/mapping_files/time_series/geo/carto-boundary-file.html), last accessed:  
523 21.02.2023). More detail on method, data content and access can be found in  
524 <http://thematicmapping.org/downloads/>.

525 TM 'country borders' and US CB were used to spatially disaggregate the information of water withdrawal for  
526 domestic, industrial, energy use.

527  
528 **Multi-Source Weather** (further referred as MSWX) is a high resolution (3 hourly, 0.1°), bias-corrected  
529 meteorological product with global coverage from 1979 to 7 months into the future. The data for 42 years  
530 (~316700 files in NetCDF format, in total 128.0 GB) were retrieved via [www.gloh2o.org/mswx/](http://www.gloh2o.org/mswx/). For more  
531 detailed information, see Beek et al. (2022).

532 MSWX 2 meter daily and monthly maximum and minimum air temperature were used to account for the climate-  
533 induced intra- and inter-annual fluctuations of domestic, livestock, and energetic water demand.

534

Huang et al. (2018) is a publication presenting 0.5° resolution global monthly gridded sectoral water withdrawal dataset for the period 1971–2010. Huang et al. (2018) Table 3 (calibrated R coefficient values) and Eq. (2) to (6) for temporal downscaling of domestic and energy water demands were used in this study, respectively.

### 3.7 Surface field creation overview

Considering the high resolution (i.e. hundreds of meters) and volume of data (i.e. GB) of most input datasets used to generate the surface fields, a high performing data manipulation platform was needed. GEE (Gorelick et al., 2017) was selected as it provides (embedded) a vast high resolution data catalogue (e.g. ready available MERIT DEM elevation dataset, CGLS-LC100, and CLC2018 land cover datasets) and powerful computation capabilities. It also allows to upload any raster and vector data (e.g. GeoTiff or shapefiles) and to conduct each surface field tailored computations. All GEE scripts were written in JavaScript to produce GeoTiff files, converted to the final file format (NetCDF) locally after transfer from GEE platform.

To ensure a consistent representation of physical processes at all scales, surface fields should be as coherent as possible among each other – between variables and across scales. Coherency can be achieved by using, where possible, the same input datasets to derive different field types (e.g. unique forest information input to create all forest-related surface fields), and making sure spatial aggregation or disaggregation across scales results in expected values. Figure 1 shows a simplified scheme that relates input datasets (e.g. CGLS-LC100) with the resulting surface fields (e.g. surface cover fractions – forest, inland water, and sealed surface fraction fields), also highlighting fields requiring intermediary and sequential steps (e.g. forest fraction is needed to create soil parameter fields over forested and non-forested areas).

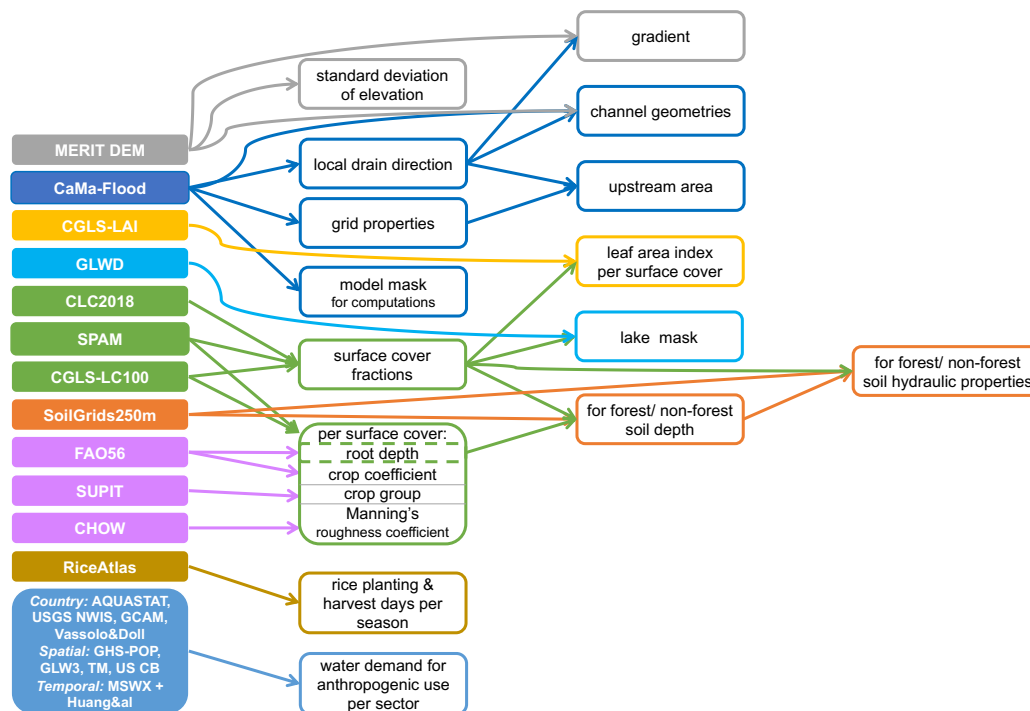
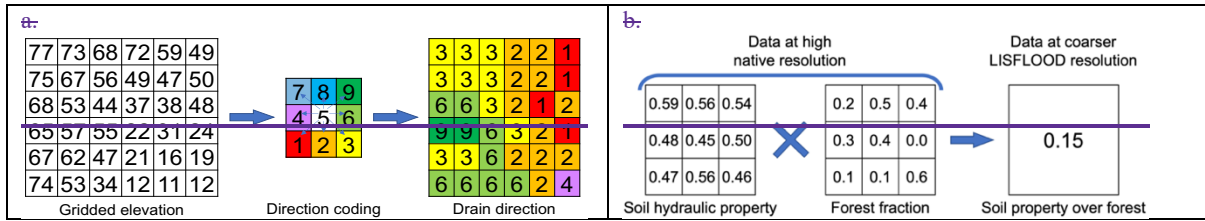


Figure 1. Flow chart connecting input datasets and surface fields created. Dashed border denotes intermediate fields, that are not part of the final dataset catalogue.

For processes with horizontal dependency such as river routing, the relationship between grid\_cells (e.g. how the grid\_cells are connected) must be defined first so that all dependent fields can be generated on the same grid coordinates, spatial resolution and using consistent input data. For example, LDD defines how water moves across the model grid\_cells as a river drainage network (see Figure 2) and strongly depends on elevation data (see Section 3.1.2 for more details). Because of the complex spatial dependency of a river drainage network, LDD must be created directly from elevation data at the required grid and resolution and cannot be resampled from a previous LDD field of a different grid and/or resolution. It is then used to define information on the river network, including upstream drainage area and gradient. Note, Figure 1 misses an arrow from MERIT DEM to LDD only because this step was mainly done by CaMa-Flood developers (see Section 3.1.2 for more details). Four steps are involved in generating a particular surface field (see Table 2, Table 1), with step 3 being the most complex and varied (see Figure 2 for an example), and step 4 being necessary only for some model specifications

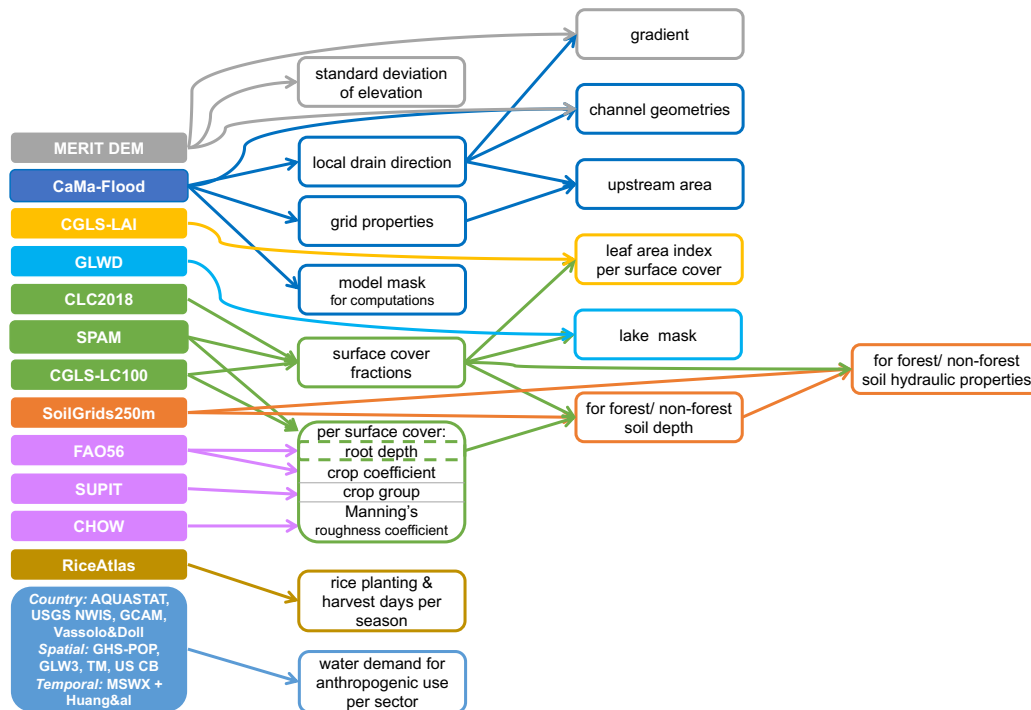
570 (here as required by LISFLOOD). Further details on specific manipulations associated with each field category  
 571 are given in Section 4 as relevant., see Table 2).  
 572



573 **All Figure 2. Examples of data manipulation for (a) transformation of elevation data into LDD (done within CaMa-**  
 574 **Flood), and (b) upscaling with weighted average for one final grid cell of soil hydraulic property over forested area.**

575 **4— Generation of surface fields**

576 This section details the complex data manipulations required to generate the surface fields introduced in Section 2,  
 577 with examples of resulting fields. The techniques applied (see Table 1) to generate CEMS\_SurfaceFields\_2022  
 578 are reproducible to different input data and/ or for different output data specifications. Further details on  
 579 specific manipulations associated with each field category are given in sections below as relevant, where each  
 580 section has a table with exact data source used per surface field, and step-by-step description of transformations  
 581 applied to the data to compute the final fields included in CEMS\_SurfaceFields\_2022 (full technical descriptions  
 582 for all fields needed by the LISFLOOD model are available explained in the LISFLOOD user guide (available  
 583 online: [https://ec-jrc.github.io/lisflood-code/4\\_Static-Maps-introduction/](https://ec-jrc.github.io/lisflood-code/4_Static-Maps-introduction/), last accessed: 21.02.2023/01.2024).  
 584 Although the specific requirements for the dataset were defined by LISFLOOD for EFAS (European domain, 1  
 585 arc min resolution at mid-latitude of the domain (47.50 N) is ~1.25 km) and GloFAS (Global domain)  
 586 implementation, summarised in Table 2, they are consistent with requirements of any other environmental models.  
 587 Regional examples of a sub-set of CEMS\_SurfaceFields\_2022 are provided to show the level of detail available  
 588 at each resolution and field, and to emphasise the consistency through all the fields, a critical requirement for  
 589 environment modelling and analysis, focusing on three regions of the world: the Po River (Europe), the Amazon  
 590 River (South America) and the Brahmaputra River (Asia), with additional examples provided in Appendix 4).  
 591



592 **Figure 1. Flow chart connecting input datasets and surface fields created. Dashed border denotes intermediate fields,**  
 593 **that are not part of the final dataset catalogue.**  
 594



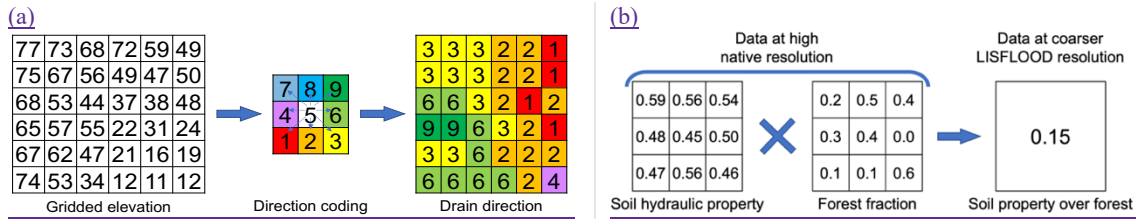


Figure 2.

Examples of data manipulation for (left column, plot a) transformation of elevation data into LDD (done within CaMa-Flood), and (right column, plot b) upscaling with weighted average for one final grid cell of soil hydraulic property over forested area.

Table 2.1. The four steps of a particular surface field generation and associated data manipulations.

Order	Description	Purpose	Function
1	Raw file preparation	Vector gridding, region merging	
		Upscaling (spatial/ temporal aggregation)	Arithmetic mean, mode, sum, standard deviation (weighted) resampling from auxiliary data
2	Unit conversion	Converting values from native to fraction per grid-cell	Surface area, percentage or categorical to fractions per grid-cell (see Annex 1/Appendix 2 for more details)
3	Value computation	Transforming	Mathematical equation/ function needed to generate the output variable
		Reprojecting	Interpolation (changing grid, preserving resolution in meters)
		Upscaling (spatial [default]/ temporal aggregation)	Arithmetic mean, mode, sum, standard deviation (weighted) resampling from auxiliary data (changing resolution, preserving grid)
		Downscaling (spatial [default]/ temporal disaggregation)	Nearest neighbour (changing resolution, preserving grid)
4	Zero/ NoData filling	Replace zero/ NoData by the most appropriate values	Force a minimum/ maximum value to satisfy e.g. calculation precision, physical meaning and/ or model requirement
			LIGHT. Constant value, unweighted global mean, unweighted global mode DEEP. Values from next coarser resolution (up to an agreed maximum resolution); if still missing, method LIGHT

Table 2. Dataset files technical specifications.

Type	Specification
Format	NetCDF
Projection	EPSG:4326 - WGS84: World Geodetic System
Horizontal resolution	Europe: 1 arc min (~1.86 km at the equator) [file size 4530x2970 grid cells]
	Globe: 3 arc min (~5.57 km at the equator) [file size 7200x3600 grid cells]
Domain bound	Europe: [North = 72.25 N; South = 22.75 N; West = 25.25 W; East = 50.25 E]
	Globe: [North = 90.00 N; South = 90.00 S; West = 180.00 W; East = 180.00 E]
Missing value (i.e. NoData) location	Over land: none
	Over ocean: all ocean grid cells have missing value (i.e. ocean is masked based on 'mask' field)
Missing value (i.e. NoData) number	For Integer variable type: 0
	For Real variable type: -999999.0
Variable type	Integer: Int8
	Real: Float32

### 3 Catchment morphology and river network

#### 3.1 General information

Morphology and channel shape information are essential for the computation of snow melting, temperature scaling, and river routing. Statistics such as standard deviation of elevation and other orographic sub-grid parameters critical for radiation parametrization, especially for shadowing effect, whilst channel geometry fields are needed to describe overbank inundation and infer inundated areas in wetland methane and soil carbon modelling, for example. Land morphology is derived from elevation and its variability within a single cell can be represented through slope, standard deviation, aspect, etc. River drainage information, derived from elevation, is

used to connect the model cells according to the direction of the surface runoff, with channel geometry information used for routing processes.

The dataset contains 14 morphology and river network variables (name in brackets in italics correspond to the field's name in the data repository):

- Morphologic information: local drainage direction (i.e. flow direction from one cell to another; *LDD*, dimensionless), upstream drainage area (*upArea*, m<sup>2</sup>), grid cell area (*pixarea*, m<sup>2</sup>), grid cell length (*pixleng*, m), standard deviation of elevation (*elvstd*, m), gradient (i.e. elevation gradient; *gradient*, m/m);
- Kinematic wave equation for routing: channel bottom width (*chanbw*, m), channel length (*chanlenght*, m), channel gradient (*changrad*, m/m), Manning's roughness coefficient for channels (*chanman*, s/m<sup>1/3</sup>);
- River network information: channel mask (i.e. presence of river channel; *chan*, dimensionless), channel side slope (i.e. channel's horizontal distance divided by vertical distance; *chans*, m/m);
- Open water evaporation: bankfull channel depth (*chanbnkf*, m), channel flood plain (i.e. width of the area where the surplus of water is distributed when the water level in the channel exceed the channel depth; *chanflpn*, m).

### 3.2 Reference data and methodology

#### 4.11.1 Catchment morphology and river network

Environmental models require an accurate description of terrain and hydro-morphology to represent the hydrodynamics at the spatial resolution of the model. Here all catchment morphology and river network fields are derived from (i) **The Catchment-based Macro-scale Floodplain (CaMa-Flood) Global River Hydrodynamics Model v4.0 maps** (further referred as CaMa-Flood) – that include information on channel length, river topography parameters, floodplain elevation profile, channel width and channel depth at 3 and 1 arc min resolutions covering land area from 90 N to 60 S, representative of the year 2017, and (ii) **The MERIT DEM (Multi-Error-Removed Improved-Terrain Digital Elevation Model v.1.0.3)** (further referred as MERIT DEM) – a high accuracy global DEM at 3 arc second resolution (~90 m at the equator) covering land area from 90 N to 60 S, representative of the year 2018 (for reference data details see Table 3, Appendix 1). All fields follow a complex sequential workflow (see Figure 3 and Table 1). Note that whilst some river network fields were already directly available from the CaMa-Flood catalogue (e.g. LDD, channel length), they had to be adapted to the specific requirements of LISFLOOD, specifically consistent with an interconnected river network described by the D8 algorithm (O'Callaghan and Mark, 1984; Figure 2a) different to that used by the CaMa-Flood algorithm.

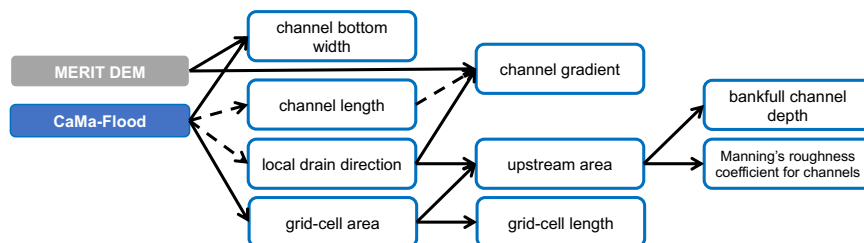


Figure 3. Workflow of complex manipulations to create some of the morphology and river network fields; solid arrows indicate a function transformation, dashed – modification of existing input data to LISFLOOD specifications.

Table 1. Morphology and river network fields, their description, data source and applied transformation; \* denotes transformation following Burek et al. (2014); name in brackets in italics next to each field correspond to the name in the data repository.

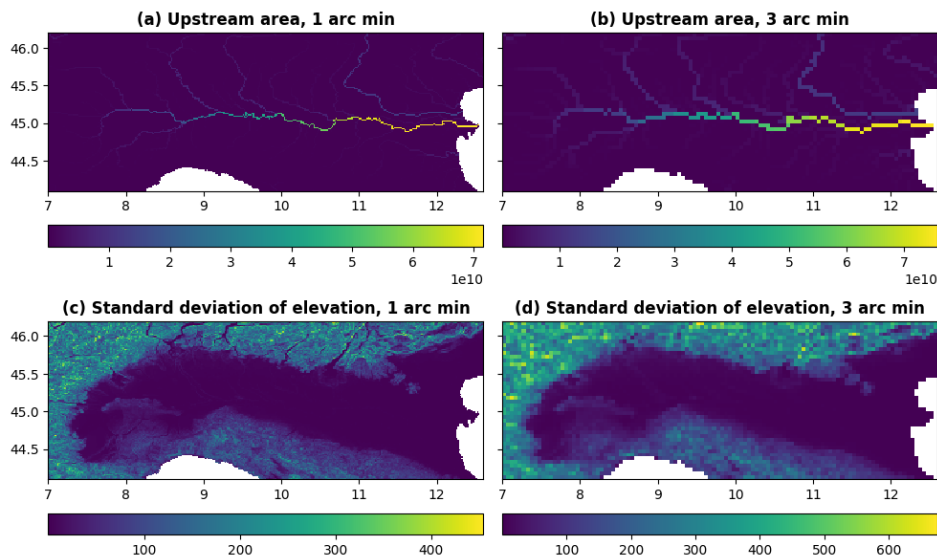
Field type	Description	Data source (variable)	Transformation
Local drainage direction ( <i>LDD</i> )	Connects every grid-cell forming a river network from springs to mouth-	CaMa-Flood (flwd)	Direction coding, ensuring grid-cell connectivity
Grid-cell area ( <i>pixarea</i> )	Area of every grid-cells cell	CaMa-Flood (flwd)	Grid-cell area based on a given coordinate reference system and resolution
Grid-cell length ( <i>pixlength</i> )	Length of every grid-cell	<i>pixarea</i>	$pixlength = \frac{pixarea}{resolution}$ , where resolution – 1.86 km and 5.57 km for 1 and 3 arc min respectively
Upstream drainage area ( <i>upArea</i> )	Accumulated area of all connected grid-cells of the LDD from springs (start;	<i>LDD</i> ; <i>pixarea</i>	PCRaster Accuflux function (Karssenberget al., 2010)

	lowest values) to mouth (end; highest values)		
Standard deviation of elevation ( <i>elvstd</i> )	Amount of elevation variation within a <i>grid-cell</i>	MERIT DEM	Upscaling (spatial) with standard deviation
Gradient ( <i>gradient</i> )	Elevation gradient between two connected <i>grid-cells</i>	MERIT DEM; <i>LDD</i>	$gradient = \frac{abs(elv_{uc} - elv_{dc})}{D_{uc,dc}}$ , where <i>elv</i> – elevation, <i>uc</i> and <i>dc</i> – upstream and downstream cell, <i>D<sub>uc,dc</sub></i> – distance between upstream and downstream cells
Channel bottom width ( <i>chanbw</i> )	Width of the bottom of the channel	CaMa-Flood (width); <i>upArea</i>	Recomputing zero and negative values based on equation* $chanbw = upArea \cdot 0.0032$
Channel length ( <i>chanlength</i> )	Length of river channel in each <i>grid-cell</i> (can exceed grid-size to account for meandering river)	CaMa-Flood (rivlen)	No transformation was carried out
Channel gradient ( <i>changrad</i> )	Gradient (slope) of river channel inside a <i>grid-cell</i>	MERIT DEM; <i>LDD</i> ; <i>chanlength</i>	$changrad = \frac{abs(elv_{uc} - elv_{dc})}{chanlength_{uc}}$ , where <i>elv</i> – elevation, <i>uc</i> and <i>dc</i> – upstream and downstream cell; Note: <i>LDD</i> is used to define <i>uc</i> and <i>dc</i>
Manning's roughness coefficient for channels ( <i>chanman</i> )	Manning's roughness coefficient of river channel for each <i>grid-cell</i>	MERIT DEM; <i>upArea</i>	Transformation based on equation* $chanman = 0.25 + 0.015 \cdot \min\left(\frac{50}{upArea_{km^2}}, 1\right) + 0.030 \cdot \min\left(\frac{elv_m}{2000}, 1\right)$ , where <i>elv</i> – elevation, <i>km<sup>2</sup></i> and <i>m</i> – values in <i>km<sup>2</sup></i> and <i>m</i>
Channel mask ( <i>chan</i> )	Channel presence in the <i>grid-cell</i> indicator. Note LISFLOOD specific requirement to have channels in every 'mask' <i>grid-cell</i>	'mask' (main model's <i>technical-field</i> )	Channel mask is equal to 1 everywhere
Side slope ( <i>chans</i> )	Slope of river banks (i.e. horizontal distance divided by vertical distance)		Side slope of all channels is 45°, hence side slope is equal to 1 everywhere
Bankfull channel depth ( <i>chanbnkf</i> )	Channel depth (i.e. river bed depth)	<i>upArea</i>	Transformation based on equation* $chanbnkf = 0.27 \cdot upArea_{km^2}^{0.33}$ , where <i>km<sup>2</sup></i> – values in <i>km<sup>2</sup></i>

646 **4.2 Land use fields**

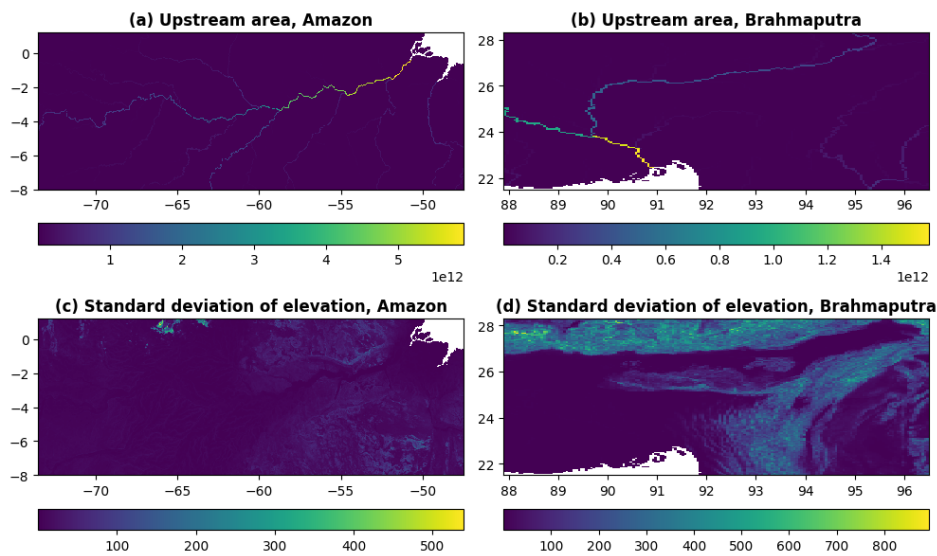
647 **3.3 Regional examples**

648 Most fields in catchment morphology and river network category are quite technical and hard to interpret. The  
649 ones that can be easy digested are upstream area and standard deviation of elevation which are presented in Figure  
650 3 for Po River area in 1 arc min and 3 arc min resolution, and in Figure 4 for Amazon River and Brahmaputra  
651 River areas at 3 arc min resolution. The field of standard deviation of elevation shows high level of detail over the  
652 Brahmaputra River and the benefit of high resolution dataset is clearly seen over the Po River.  
653



654  
655  
656  
657

**Figure 3. Upstream drainage area in square meters (upper row, plots a and b) and standard deviation of elevation in meters (lower row, plots c and d) at 1 arc min (~1.9 km at the equator, left column, plots a and c) and 3 arc min (~5.6 km at the equator, right column, plots b and d) resolution for Po River area in Italy.**



658  
659  
660  
661

**Figure 4. Upstream drainage area in square meters (upper row, plots a and b) and standard deviation of elevation in meters (lower row, plots c and d) at 3 arc min (~5.6 km at the equator) resolution for Amazon River area (left column, plots a and c) and Brahmaputra River area (right column, plots b and d).**

## 662 4 Land use fields

### 663 4.1 General information

664 Land use is an essential component of environmental models. Many models use a sub-grid cell approach where a  
 665 single grid cell can include several different land uses with each land use being subject to different prominent  
 666 physical processes. This approach allows to keep a high level of accuracy when representing how different types  
 667 of land cover affect e.g. the hydrological cycle (e.g. evaporation is different in urban areas compared to forests)  
 668 while limiting the increase in computational time. Application of land surface fractions include grid cell weighted  
 669 average skin temperature calculations, biogenic flux calculations, urban planning, and climate mitigation plan  
 670 preparation. For example, sealed surface fraction is necessary for carbon budget calculations and trace gas  
 671 emissions in general, more explicitly for anthropogenic and residential emission calculations, and irrigated crop  
 672 and irrigated rice fractions (combined with rice planting and harvesting days) useful for crop yield and methane  
 673 emissions modelling.



The dataset differentiates between six different land uses (name in brackets in italics correspond to the field's name in the data repository):

- Forest: areas where the main hydrological processes are canopy interception, evapotranspiration from canopies, canopies drainage and evapotranspiration, root uptake and evaporation from the soil (fraction of forest; *fracforest*, dimensionless fraction);
- Sealed surface: impervious areas where there is no water infiltration into the soil, i.e. water is accumulated in the surface depression, yet evaporates, but once the depression is full, water is transported by a surface runoff (fraction of sealed surface; *fracsealed*, dimensionless fraction);
- Inland water: open water bodies where the most prominent hydrological process is evaporation (fraction of inland water; *fracwater*, dimensionless fraction);
- Irrigated crops: areas used by agriculture – water is abstracted from ground water and surface water bodies to irrigate the fields. The main hydrological processes connected with the irrigated crops are canopy interception, evapotranspiration from canopies, canopies drainage and evapotranspiration, root uptake and evaporation from the soil (fraction of all irrigated crops, excluding rice; *fracirrigated*, dimensionless fraction);
- Irrigated rice: areas used to grow rice with flooded irrigation agricultural technique, when water is abstracted from the inland water bodies and delivered to the rice fields. The main hydrological processes connected with rice fields are soil saturation, flooding, rice growing phase, soil drainage phase (fraction of irrigated rice; *fracrice*, dimensionless fraction);
- Other land cover: used in canopy interception, evaporation from the canopies, canopy drainage, plant evapotranspiration, evaporation from the soil hydrological processes. The relative importance of these processes depends on the LAI (fraction of other cover types; *fracother*, dimensionless fraction).

#### 4.2 Reference data and methodology

In models explicitly accounting for sub-grid variability, the fraction of each land use in every cell must be provided so that process representation for each land use can be weighted accordingly. Here, the majority of land use fields are derived from **The Copernicus Global Land Service (CGLS) Land Cover (LC) 100m map** (further referred as CGLS-LC100) – a set of global land cover maps at 100 m resolution covering land and ocean area from 90 N to 60 S, representative of the year 2015; rest of the land use fields (i.e. irrigated crops and irrigated rice fractions) are derived from (i) **The Spatial Production Allocation Model (SPAM) – Global Spatially-Disaggregated Crop Production Statistics Data for 2010 v2.0** (further referred as SPAM2010) – a global dataset with crop distribution and production information at 10 km (5 arc min) resolution covering land area from 90 N to 60 S, representative of the year 2010, and (ii) **The Coordination of Information on the Environment (CORINE) Land Cover (CLC) inventory for 2018** (further referred as CLC2018) – a set of maps describing the land cover/ land use status at 100 m resolution covering land area over Europe (i.e. 39 countries), representative of the time period 2017-2018 (for reference data details see Appendix 1). The derivation of fractions of the five land use classes used in LISFLOOD (and additional ocean fraction for consistency check) are derived from super high resolution datasets each following follow specific steps (see Figure 5) summarised in Table 2. Note that LISFLOOD requires all ‘mask’ (main model’s technical field) grid\_cells to have at least one non-zero fraction type, hence the extra step in the generation of the inland water fraction field was to set empty grid\_cells (i.e. grid\_cells that based on the data source are fully covered with ocean) as fully covered with inland water.

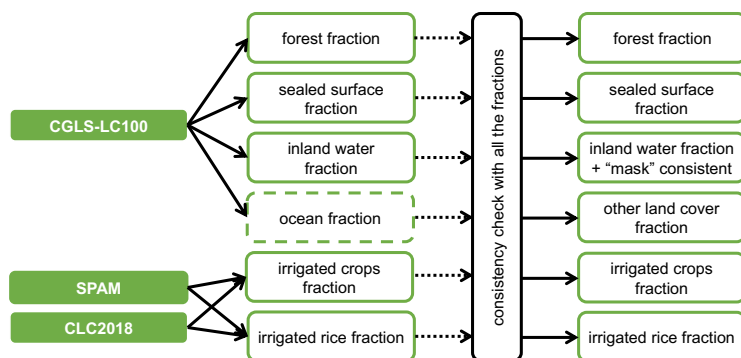


Figure 5. Workflow of complex manipulations to create land use fields; solid arrows indicate a function transformation, dotted – upscaling; dashed boxes indicate the intermediate fields used for other field generation.

718  
719  
720

**Table 2. Fraction of land use fields, their description, data source and applied transformations; ‘sum’ refers to the sum of all fractions except ‘other land cover fraction’; grey cells with bold italics show required intermediate fields; name in brackets in italics next to each field correspond to the name in the data repository.**

<i>Field type</i>	<i>Description</i>	<i>Data source (variable)</i>	<i>Transformation (in order)</i>
Forest fraction <i>(fracforest)</i>	Evergreen and deciduous needle leaf and broad leaf tree areas	CGLS-LC100 (tree-coverfraction)	Unit conversion % to fraction; Reprojecting and upscaling to final grid and resolution with mean; Consistency check with other fractions
Sealed surface fraction <i>(fracsealed)</i>	Urban areas, characterizing the human impact on the environment	CGLS-LC100 (urban-coverfraction)	Unit conversion % to fraction, scaled by 0.75 <sup>1</sup> ; Reprojecting and upscaling to final grid and resolution with mean; Consistency check with other fractions
Inland water fraction <i>(fracwater)</i>	Rivers, freshwater and saline lakes, ponds and other permanent water bodies over the continents	CGLS-LC100 (water-permanent-coverfraction)	Force Fox Basin and Caspian Sea to be fully covered with water; Unit conversion % to fraction; Reprojecting and upscaling to final grid and resolution with mean; Consistency check with other fractions; Cross-checking with ‘mask’ and forcing empty grid_cells as inland water
Irrigated crops fraction <i>(fracirrigated)</i>	Irrigated areas of all possible crops excluding rice	SPAM (spam2010v1r0_global_physical-area_CROP_i, 41 crops rice excluding)	Shapefile gridding to its native resolution (~10 km); Unit conversion ha to fractions; Reprojecting and downscaling to CLC2018 grid and resolution (~100 m) with nearest neighbour
		CLC2018 (landcover = ‘212’)	Unit conversion class to fraction
			Merging SPAM- and CLC2018-derived fractions, priority to CLC2018; Reprojecting and upscaling to final grid and resolution with mean; Consistency check with other fractions
Irrigated rice fraction <i>(fracrice)</i>	Irrigated areas of rice	SPAM (spam2010v1r0_global_physical-area_RICE_i)	Shapefile gridding to its native resolution (~10 km); Unit conversion ha to fractions; Reprojecting and downscaling to CLC2018 grid and resolution (~100 m) with nearest neighbour
		CLC2018 (landcover = ‘213’)	Unit conversion class to fraction
			Merging SPAM- and CLC2018-derived fractions, priority to CLC2018; Reprojecting and upscaling to final grid and resolution with mean; Consistency check with other fractions
Other land cover fraction <i>(fracother)</i>	Agricultural areas, non-forested natural area, pervious surface of urban areas	Non-negative residual from 1 subtracting ‘sum’ of all other fractions	<i>fracother</i> = max ((1 – sum),0)
<b><i>Ocean fraction</i></b> <i>(fracocean)</i>	Oceans	CGLS-LC100 (discrete_classification = ‘200’)	Unit conversion class to fraction; Forcing NoData to zero over ‘mask’ grid_cells, otherwise – fully covered; Reprojecting and upscaling to final grid and resolution with mean; Consistency check with other fractions

721  
722  
723  
724

For the sealed surface fraction, it is assumed that water can infiltrate in roughly 25 % of urban areas at kilometre scale through e.g. trees along the road, bushes along the fence, grass or moss between concrete tiles or cobble stones.

<sup>1</sup> For the sealed surface fraction, it is assumed that water can infiltrate in roughly 25 % of urban areas at kilometre scale through e.g. trees along the road, bushes along the fence, grass or moss between concrete tiles or cobble stones.

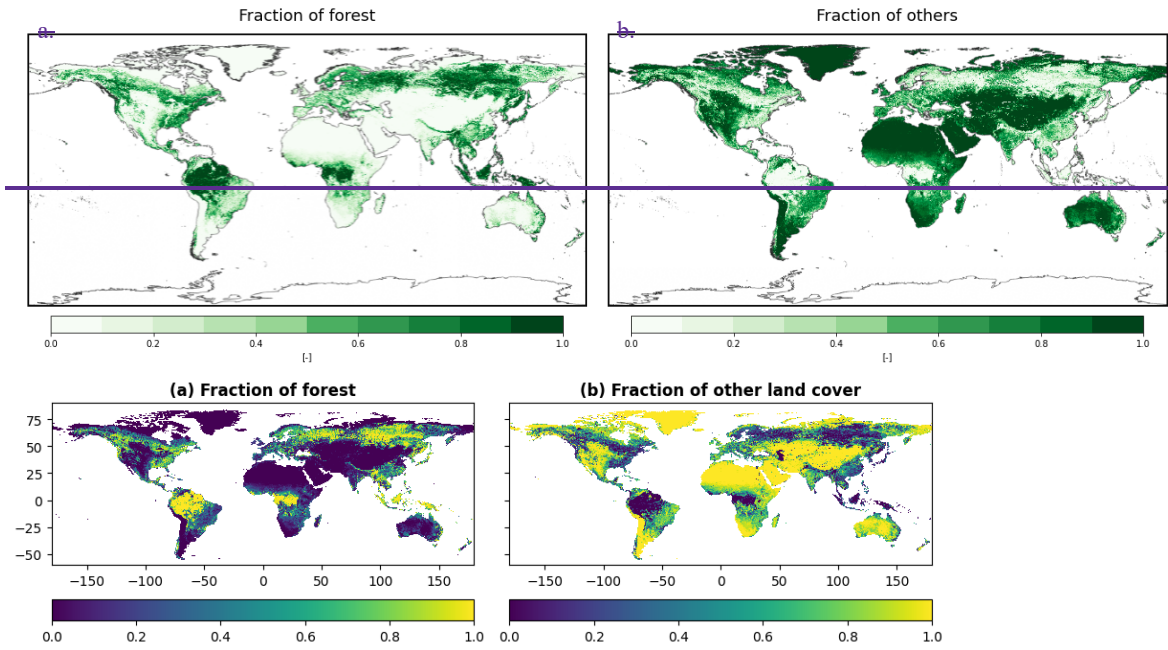
725 To ensure consistency between fractions, the sum of all fraction fields must be 1 at any resolution. When sum is  
 726 greater than 1, the inland water fraction value is assumed correct (input data corrected prior computation over Fox  
 727 Basin and Caspian Sea) and all other fractions are corrected ( $fr\_corr \cdot fracXX$ ) following Eq. (1):

$$728 \quad fr\_corr = fr \left( 1 - \frac{fr_{inlandWater} + fr_{ocean} + fr_{forest} + fr_{sealed} + fr_{irrigated} + fr_{rice}}{fr_{forest} + fr_{sealed} + fr_{irrigated} + fr_{rice}} \right), \quad (1)$$

$$729 \quad fracXX = fracXX_{raw} \left( 1 - \frac{fracwater_{raw} + fracocean_{raw} + fracforest_{raw} + fracsealed_{raw} + fracirrigated_{raw} + fracrice_{raw} - 1}{fracforest_{raw} + fracsealed_{raw} + fracirrigated_{raw} + fracrice_{raw}} \right), \quad (1)$$

730 where  $fr_{raw}$  refers to the original (i.e. before consistency check) fraction of  $XX$  which can be the forest, irrigated  
 731 crops, rice and sealed surfaces.

732 The generated fraction fields, e.g. forest (see Figure 4a Figure 6a) and other land cover (see Figure 4b Figure 6b),  
 733 have generally good consistency with other up-to-date products like ESA CCI Land Cover time-series v2.0.7  
 734 (ESA CCI map viewer <https://maps.elie.ucl.ac.be/CCI/viewer/>; Defourny et al., 2017).  
 735

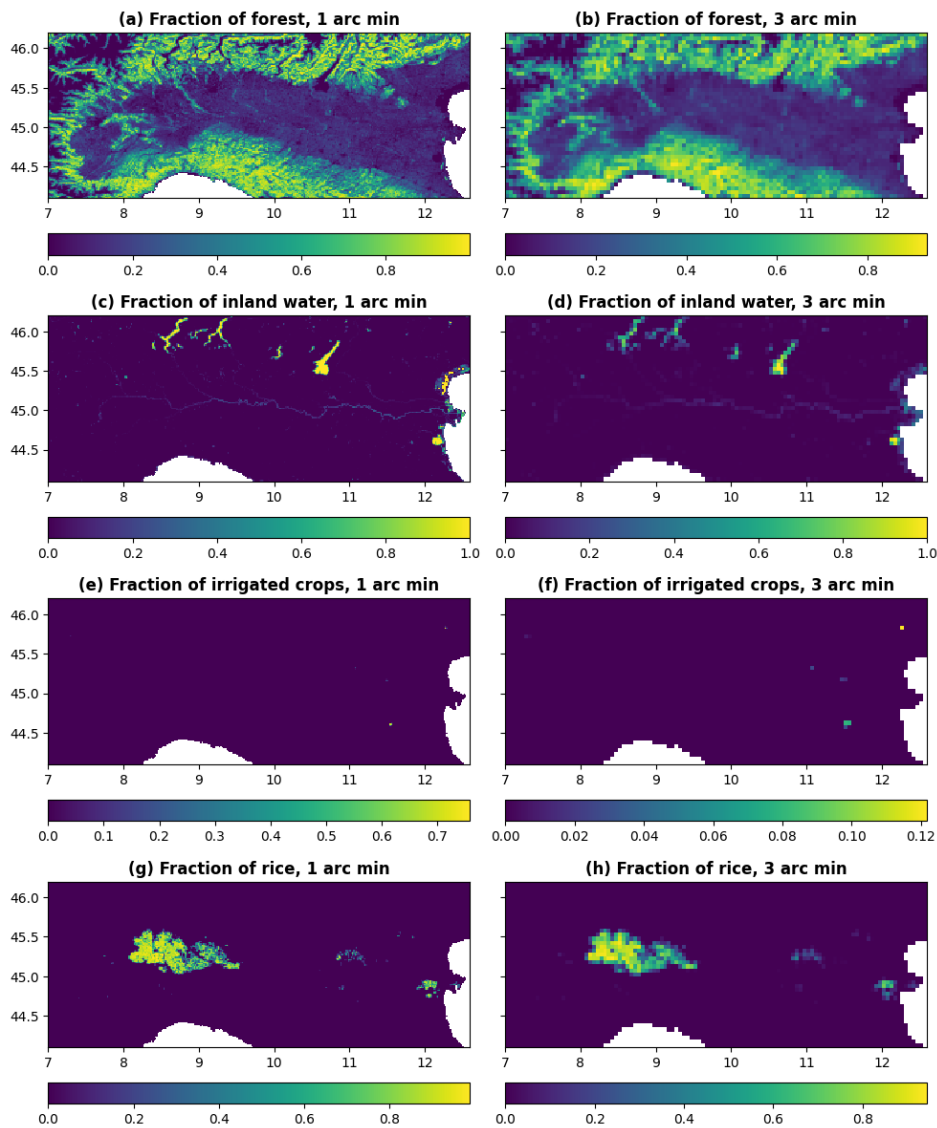


736

737 **Figure 4.6.** Fraction fields for forest (left column, plot a) and fraction of other land cover (right column, plot b) at 3  
 738 arc min (~5.6 km at the equator) resolution for global region.  
 739

### 740 4.3 Regional examples

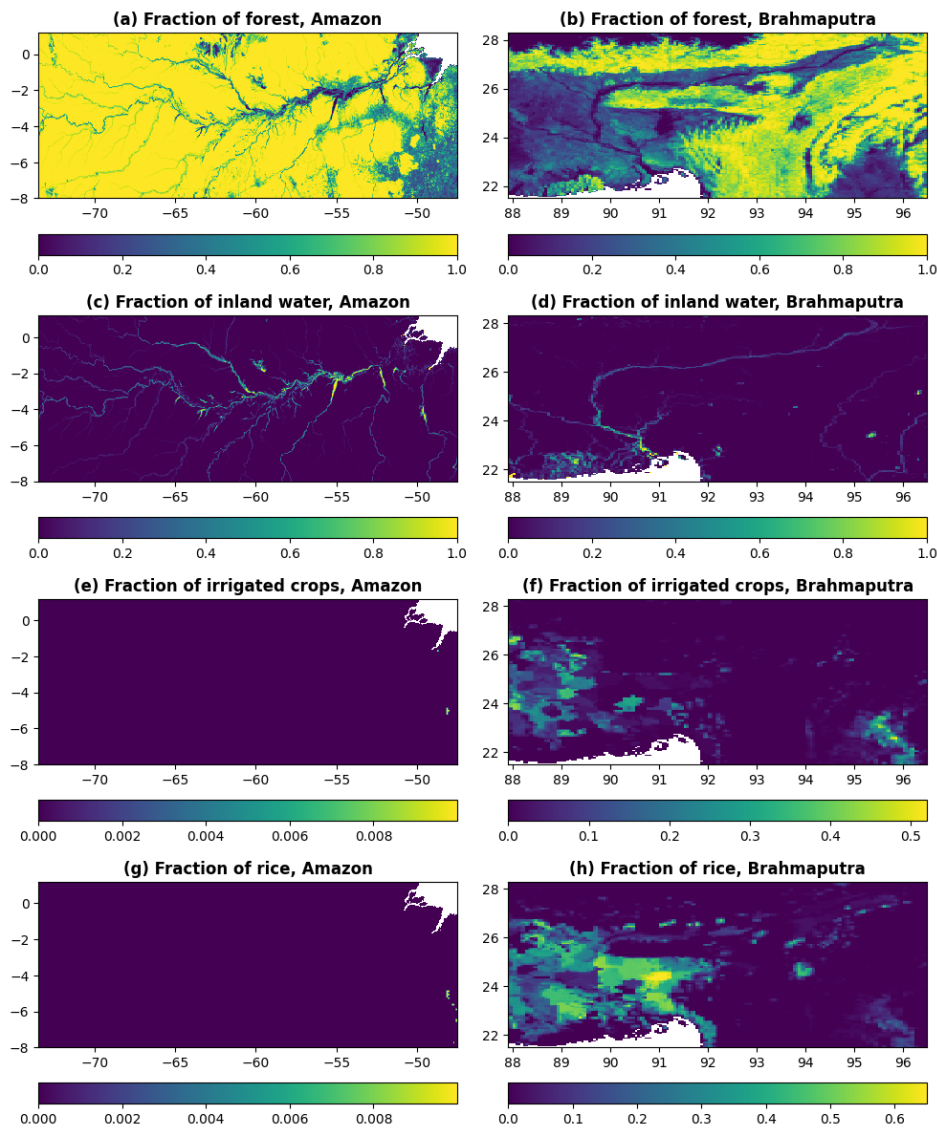
741 All fields in land use category are easy to interpret as they represent the fraction of grid cell covered by one or  
 742 another surface cover type. The most interesting ones are fraction of forest, fraction of inland water, fraction of  
 743 irrigated crops, and fraction of rice which are presented in Figure 7 for Po River area in 1 arc min and 3 arc min  
 744 resolution, and in Figure 8 for Amazon River and Brahmaputra River areas at 3 arc min resolution. With high  
 745 level of detail visible for the fields of fraction of forest and fraction of inland water (e.g. Amazon River) especially  
 746 at the highest spatial resolution (Po River).  
 747



748  
749  
750  
751  
752

Figure 7. Fraction of forest (upper row, plots a and b), fraction of inland water (second row, plots c and d), fraction of irrigated crops (third row, plots e and f), and fraction of rice (lower row, plots g and h) at 1 arc min (~1.9 km at the equator, left column, plots a, c, e and g) and 3 arc min (~5.6 km at the equator, right column, plots b, d, f and h) resolution for Po River area in Italy.





753 **Figure 8.** Fraction of forest (upper row, plots a and b), fraction of inland water (second row, plots c and d), fraction of  
 754 irrigated crops (third row, plots e and f), and fraction of rice (lower row, plots g and h) at 3 arc min (~5.6 km at the  
 755 equator) resolution for Amazon River area (left column, plots a, c, e and g) and Brahmaputra River area (right column,  
 756 plots b, d, f and h).  
 757

758 **5 Vegetation properties**

759 **5.1 General information**

760 Vegetation-related information contributes to the computation of precipitation interception, evaporation,  
 761 transpiration, and root water uptake. Depending on the model, vegetation dynamics can be represented with  
 762 different degrees of complexity including in hydrology processes, vegetation growth and feedback on climate  
 763 (Bonan et al., 2002). Rice being the world's most important food crop and having specific water demands, its  
 764 water cycle is often considered explicitly, with planting and harvesting dates being critical information to represent  
 765 the inter-annual variability in its water demand, provided the maximum three growing seasons. The variables  
 766 allow to model how vegetation affects the hydrology, with a particular focus on root water uptake and transpiration  
 767 depending on vegetation type and vegetation state (e.g. water stress conditions). For example, the crop group  
 768 number depends on the critical amount of soil moisture below which water uptake from plants is reduced as they  
 769 start closing their stomata. Alternative use of fields such as the Leaf Area Index LAI include biomass allocation,  
 770 which can be used for fire danger forecasting, and carbon stock monitoring, whilst rice planting/ harvesting days  
 771 are important for yearly cycle of methane modelling.

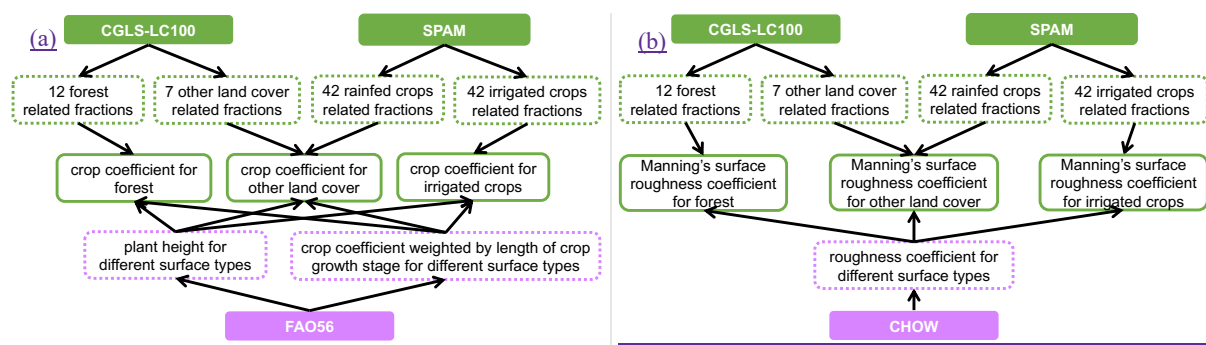
The dataset describes vegetation properties through four variables (note that LAI consists in total of 36 10-day average fields) for each of forest ( f ), irrigated crops ( i ) and other land cover types ( o ), and another six (two types times three seasons) variables for rice (name in brackets in italics correspond to the field's name in the data repository):

- Transpiration rate: crop coefficient (*cropcoef f*, *cropcoef i*, *cropcoef o*, dimensionless);
- Water uptake: crop group number (*cropgrp f*, *cropgrp i*, *cropgrp o*, dimensionless);
- Surface runoff generation and water routing: Manning's surface roughness coefficient (*manning's f*, *manning's o*,  $s/m^{1/3}$ ), rice planting and harvesting days (*riceplantingday1*, *riceplantingday2*, *riceplantingday3*, calendar day number; *riceharvestday1*, *riceharvestday2*, *riceharvestday3*, calendar day number);
- Water interception and evaporation: leaf area index (*laif*, *laii*, *laio*,  $m^2/m^2$ ).

### 4.3 Vegetation properties

### 5.2 Reference data and methodology

In complement to the land use fraction, the distribution of vegetation type and characteristics is required to capture the difference in environmental processes such as water intake of evaporation to be represented accurately (see Section 2). Here the vegetation properties are derived from many data sources using maps to account for the species spatial distribution and tables to obtain associated hydro-dynamics properties (i.e. CGLS-LC100 and SPAM2010) and tables to obtain associated hydro-dynamics properties for crops (i) **The Food and Agriculture Organisation (FAO) of the United Nations Irrigation and Drainage Paper No. 56** (further referred as FAO56) – a publication covering geographically referenced statistics for crop development stages, crop coefficients, crop height, rooting depth, and soil water depletion fraction for common crops found across the world, (ii) **Burek et al. (2014)** – a publication covering summarised information for crop coefficients, rooting depth, crop group number and Manning's surface roughness coefficient for different surface types, (iii) **Intara et al. (2018)** – a publication covering oil palm roots architecture, and (iv) **The Wofost 6.0 crop simulation model description** (further referred as SUPIT) – a publication covering crop group information for several crops as examples, and relation of a crop group from water depletion fraction; for river hydraulics **The Open-Channel Hydraulics manual** (further referred as CHOW) – a publication containing information on roughness coefficient over different surfaces. Time evolution of vegetation is based on **The Copernicus Global Land Service (CGLS) Leaf Area Index (LAI) 1km Version 2 collection** (further referred as CGLS-LAI) – a set of global maps without missing data describing vegetation dynamics at 10-day intervals at 1 km resolution covering land area from 90 N to 60 S and representative of the 10-year period of 2010-2019; time evolution of crops is based on **The RiceAtlas v3** (further referred as RiceAtlas) – a spatial database of global rice calendars and production at 1 km resolution for the national production totals to match the years 2010-2012 (for reference data details see Appendix 1). This requires assumptions to be made in case different sources did not contain the same information, and transformations to be applied depending on the vegetation type. The main data sources and general transformation steps (see Figure 9) to derive the 18 vegetation properties fields are summarised in Table-Table 3 and following text. Note that 'crop group number' variable corresponds to a water depletion value and can be averaged across different crop types.



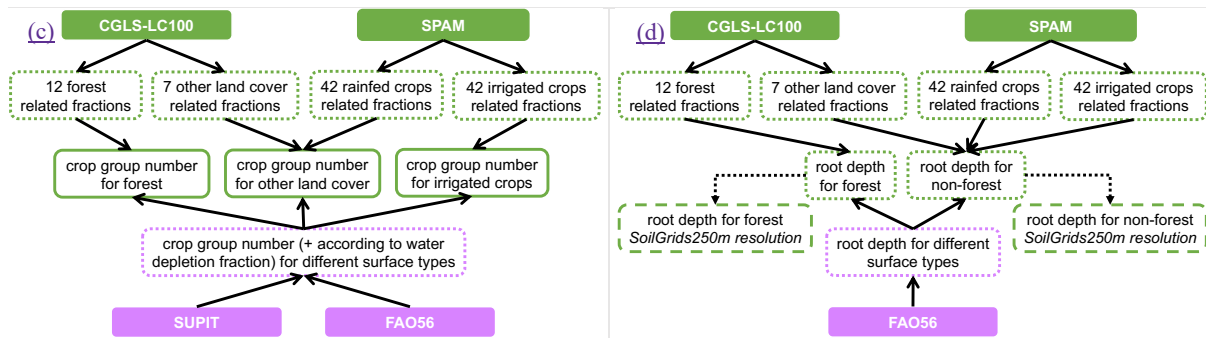


**Figure 9. Workflow of complex manipulations to create some of the vegetation property fields, e.g. crop coefficient (left column, upper row, plot a), Manning's surface roughness coefficient (right column, upper row, plot b), crop group number (left column, lower row, plot c), root depth (right column, lower row, plot d); solid arrows indicate a function transformation, dotted – upscaling; dashed boxes indicate the intermediate fields used for other field generation, dotted – the fields only used for the vegetation-related fields.**

**Table 3. Vegetation property fields, their description, data source and applied transformations; grey-cells with bold italics show required intermediate fields; name in brackets in italics next to each field correspond to the name in the data repository.**

Field type	Description	Data source	Transformation (in order)
Crop coefficient for forest, irrigated crops and other land cover type ( <i>cropcoef_f</i> , <i>cropcoef_i</i> , <i>cropcoef_o</i> )	Ratio between the potential (reference) evapotranspiration rate, in mm/day, and the potential evaporation rate of a specific crop (averaged by time and ecosystem type)	CGLS-LC100 (discrete_classification = '111', '112', '113', '114', '115', '116', '121', '122', '123', '124', '125', '126' [forest types], '20', '30', '40', '60', '70', '90', '100' [other land cover types])	Force Fox Basin and Caspian Sea to be fully covered with water; Unit conversion class to fraction (in total 12 forest related and 7 other land cover related fraction fields); Reprojecting and upscaling to final grid and resolution with mean
		SPAM (spam2010v1r0_global_physical-area_CROP_i/r, 42 crops, 'i' – irrigated, 'r' – rainfed)	Shapefile gridding to its native resolution (~10 km); Unit conversion ha to fractions (in total 42 irrigated crop related and 42 rainfed crop related fraction fields); Reprojecting and downscaling to final grid and resolution with nearest neighbour; Limiting values to 0.0-1.0 interval
		FAO56 (Table 11, 12 – information on crop coefficient and crop height); Intara et al. (2018); Burek et al. (2014)	Average crop coefficient value across climate zones for each crop growing stage and crop/ land cover type; Weighted average of crop coefficient per different crop growth stages (weighted by stage duration in days if available, otherwise mean); Average crop height value across climate zones for each crop/ land cover type
			Weighted average of relevant crop coefficient for forest, irrigated crops and other land cover type (weighted by crop height and fraction) following Eq. (2); Note: for other land cover type computation of crop coefficient of all rainfed crops is used for CGLS-LC100 (discrete_classification = '40'); Zero/ NoData filling with global mean
Crop group number for forest, irrigated crops and other land cover type ( <i>cropgrp_n_f</i> , <i>cropgrp_n_i</i> , <i>cropgrp_n_o</i> )	Represents a vegetation type and is an indicator of its adaptation to dry climate (averaged by ecosystem type)	CGLS-LC100 (discrete_classification = '111', '112', '113', '114', '115', '116', '121', '122', '123', '124', '125', '126' [forest types], '20', '30', '40', '60', '70', '90', '100' [other land cover types])	Same steps as for crop coefficient
		SPAM (spam2010v1r0_global_physical-	Same steps as for crop coefficient

		area_CROP_i/r, 42 crops, 'i' – irrigated, 'r' – rainfed)	
		FAO56 (Table 22 – information on crop depletion fraction); SUPIT (Table 6.1, 6.2 – information on crop groups); Burek et al. (2014)	Applying function (SUPIT) to water depletion fraction (FAO56) for each crop/ land cover type $cropgrpn = 10 \cdot fr_{dep} - 1.5$ , where $fr_{dep}$ – water depletion fraction; Limiting values to 1.0-5.0 interval; Note: if $fr_{dep}$ missing – using precomputed crop group number (Burek et al., 2014)
			<u>Same steps as for crop coefficient, but in Eq. (2) weighted by fraction only</u>
<u>Manning's surface roughness coefficient for forest and other land cover type (mannings_f, mannings_o)</u>	<u>Roughness or friction applied to the flow by the surface on which water is flowing (averaged by ecosystem type)</u>	<u>CGLS-LC100 (discrete classification = '111', '112', '113', '114', '115', '116', '121', '122', '123', '124', '125', '126' [forest types], '20', '30', '40', '60', '70', '90', '100' [other land cover types])</u>	<u>Same steps as for crop coefficient</u>
		<u>SPAM (spam2010v1r0_global_physical-area_CROP_i/r, 42 crops, 'i' – irrigated, 'r' – rainfed)</u>	<u>Same steps as for crop coefficient</u>
		<u>CHOW (Table 5, 6 – information on roughness coefficient n); Burek et al. (2014)</u>	<u>Matching roughness coefficient for each crop/ land cover type</u>
			Same steps as for crop coefficient, but in Eq. (2) weighted by fraction only
<u>Manning's surface roughness coefficient for forest, irrigated crops and other land cover type (mannings_f, mannings_o)</u>	<u>Roughness or friction applied to the flow by the surface on which water is flowing (averaged by ecosystem type)</u>	<u>CGLS-LC100 (discrete classification = '111', '112', '113', '114', '115', '116', '121', '122', '123', '124', '125', '126' [forest types], '20', '30', '40', '60', '70', '90', '100' [other land cover types])</u>	<u>Same steps as for crop coefficient</u>
		<u>SPAM (spam2010v1r0_global_physical-area_CROP_i/r, 42 crops, 'i' – irrigated, 'r' – rainfed)</u>	<u>Same steps as for crop coefficient</u>
		<u>CHOW (Table 5, 6 – information on roughness coefficient n, Burek et al. (2014)</u>	<u>Matching roughness coefficient for each crop/ land cover type</u>
			<u>Same steps as for crop coefficient, but in Eq. (2) weighted by fraction only</u>
Leaf area index for forest, irrigated crops and other land cover type ( <i>laif</i> , <i>laii</i> , <i>laio</i> )	Defined as half the total area of green elements of the canopy per unit horizontal ground area m <sup>2</sup> /m <sup>2</sup> (10-day average; 36 fields in total)	CGLS-LAI 10-day average for 2010-2019; <i>fracforest<sub>i</sub></i> ; <i>fracirrigated<sub>i</sub></i> ; <i>fracother</i>	Upscaling to final temporal resolution (in total 36 LAI fields); Reprojecting and upscaling to final grid and spatial resolution with unweighted mean; Filtering sparse areas of relevant fractions $fr < 0.7$ , where $fr$ – fraction; NoData filling DEEP (upsampling to 1, 3, 15 arc min, 1, 3, 15, 60 degrees spatial resolution with unweighted mean; replacing NoData at final resolution with first available precomputed less coarser resolution, if not – with zero)
Rice planting day ( <i>riceplantingday1</i> , <i>riceplantingday2</i> , <i>riceplantingday3</i> )	Most probable day of the year when rice is planted for the first, second and third time	RiceAtlas (PLANT_PKn, 3 seasons)	Ordering planting seasons by increasing Julian day (in total 3 planting dates per spatial unit); Shapefile gridding to final grid and spatial resolution (in total 3 fields); Note: if less than 3 seasons – repeating last available planting/ harvesting seasons date; NoData filling with global unweighted mode date of first planting/ harvesting
Rice harvest day ( <i>riceharvestday1</i> ,	Most probable day of the year when rice is	RiceAtlas (HARV_PKn, 3 seasons)	

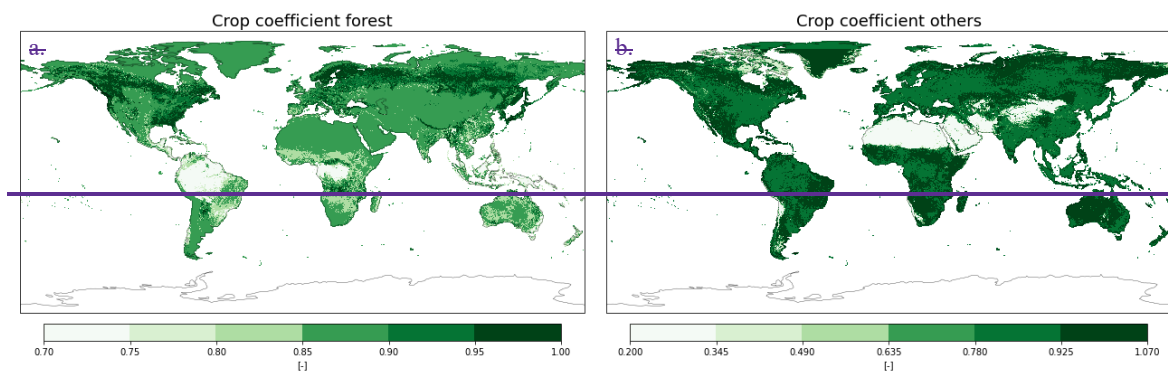
<i>riceharvestday2</i> , <i>riceharvestday3</i> )	harvested after planting for the first, second and third time		season (i.e. 105 – 15 <sup>th</sup> April/ 227 – 15 <sup>th</sup> August)
<b>Root depth for forest and non-forest</b> ( <i>root_depth_f</i> , <i>root_depth_o</i> )	Deepest soil depth reached by the crop roots	CGLS-LC100 (discrete_classification = ‘111’, ‘112’, ‘113’, ‘114’, ‘115’, ‘116’, ‘121’, ‘122’, ‘123’, ‘124’, ‘125’, ‘126’ [forest types], ‘20’, ‘30’, ‘40’, ‘60’, ‘70’, ‘90’, ‘100’ [other land cover types])	Same steps as for crop coefficient
		SPAM (spam2010v1r0_global_physical-area_CROP_i/r, 42 crops, ‘i’ – irrigated, ‘r’ – rainfed)	Same steps as for crop coefficient
		FAO56 (Table 22 – information on crop rooting depth); Burek et al. (2014)	Matching rooting depth for each crop/ land cover type
			Same steps as for crop coefficient, but in Eq. (2) weighted by fraction only; Downscaling to native SoilGrids250m resolution with nearest neighbour (for soil depth calculations)

819  
820  
821  
822  
823  
824  
825  
826  
827  
828  
829

The final step of the crop coefficient, crop group number, Manning’s surface roughness coefficient, and additional crop height (for crop coefficient calculation) and root depth (for soil depth calculation, see Section 4.46.2) for forest, irrigated crops and other land cover type is to compute weighted average of their components (e.g. different forest types) following Eq. (2):

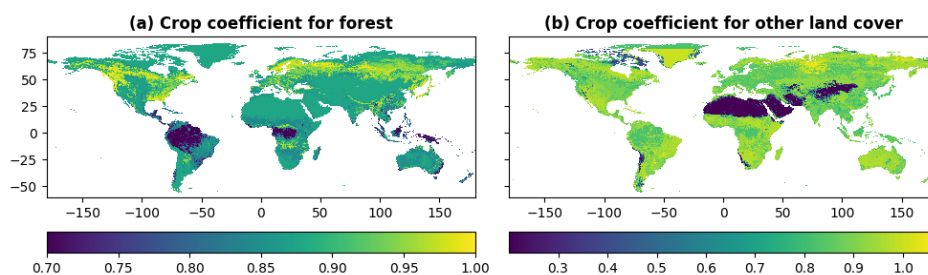
$$K = \frac{A_1 \cdot fr_1 \cdot K_1 + A_2 \cdot fr_2 \cdot K_2 + \dots + A_N \cdot fr_N \cdot K_N}{A_1 \cdot fr_1 + A_2 \cdot fr_2 + \dots + A_N \cdot fr_N} \quad (2)$$

where  $A$  is a scaling parameter (equals 1, except for crop coefficient where it equals to crop height),  $fr$  refers to the fraction of crop or land cover type,  $K$  – default (i.e. source table based) variable in question values,  $L..N$  – number of crop or land cover types included in the field (i.e. for forest  $N=12$ , irrigated crops  $N=41$ , other land cover type  $N=7$  and for CGLS-LC100 type ‘40’ (cropland) default values are based on 42 rainfed crops).



830  
831  
832  
833

The generated vegetation property fields, e.g. crop coefficient for forest (see Figure 5-10a) and other land cover (see Figure 10b), follow main features of e.g. generated forest fraction.



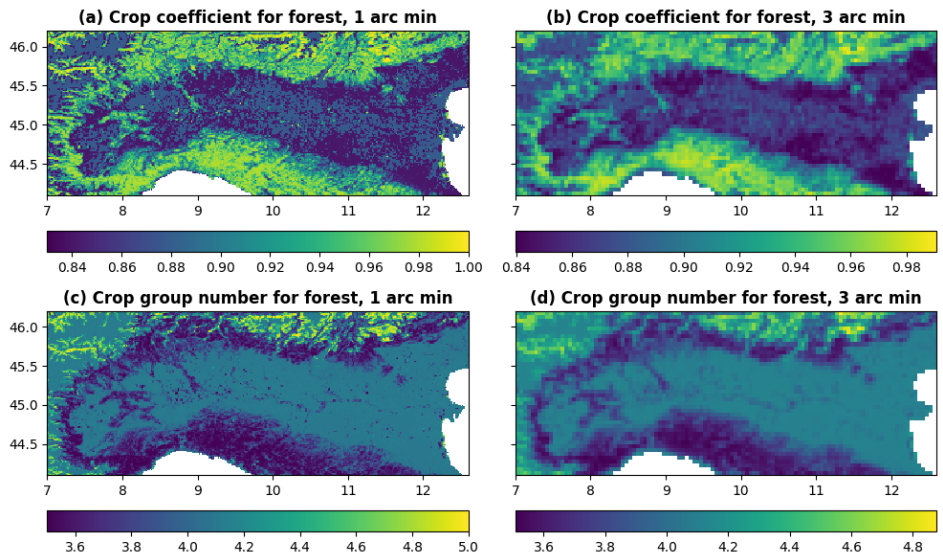
834  
835  
836

**Figure 10.** Crop coefficient for forest (left column, plot a) and crop coefficient for other land cover type (right column, plot b) at 3 arc min (~5.6 km at the equator) resolution for global region.

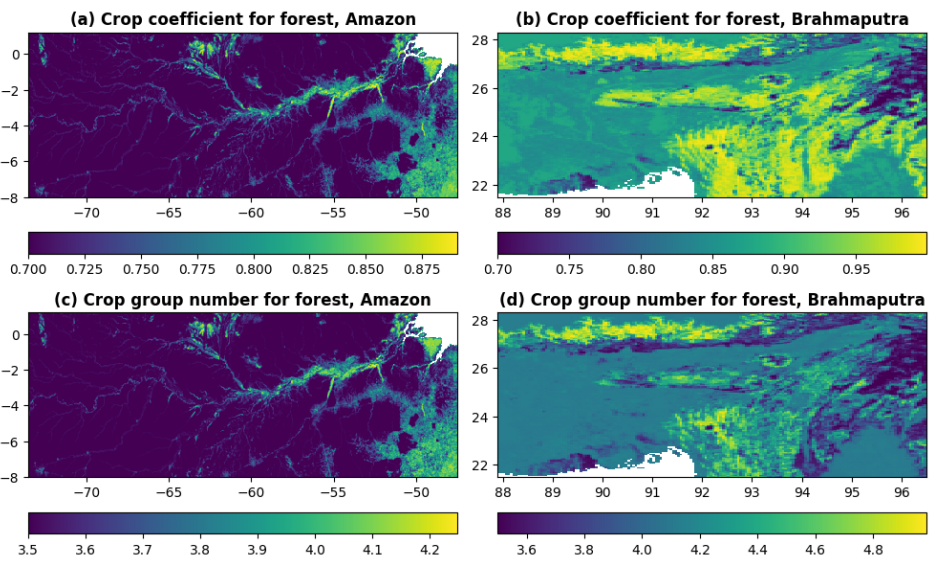


837 **5.3 Regional examples**

838 All fields in the vegetation properties category are complementary to the land use fractions, and help to understand  
839 for example the difference in evaporation water intake. The fields easiest to interpret are the crop coefficient and  
840 the crop group number which are presented for forest in Figure 11 for Po River area in 1 arc min and 3 arc min  
841 resolution, and in Figure 12 for Amazon River and Brahmaputra River areas at 3 arc min resolution. For example,  
842 fields of crop group number for forest (i.e. different forest type) show transition of vegetation resilience towards  
843 dry conditions in the Brahmaputra River area.  
844



845 **Figure 11. Crop coefficient for forest (upper row, plots a and b) and crop group number for forest (lower row, plots c**  
846 **and d) at 1 arc min (~1.9 km at the equator, left column, plots a and c) and 3 arc min (~5.6 km at the equator, right**  
847 **column, plots b and d) resolution for Po River area in Italy.**  
848



849 **Figure 12. Crop coefficient for forest (upper row, plots a and b) and crop group number for forest (lower row, plots c**  
850 **and d) at 3 arc min (~5.6 km at the equator) resolution for Amazon River area (left column, plots a and c) and**  
851 **Brahmaputra River area (right column, plots b and d).**  
852

853 **6 Soil properties**

854 **6.1 General information**

855 In land surface and distributed hydrological models, the water movement, storage and plants' water-uptake from  
856 the soil are often described by the soil-/water retention curve (SWRC). The SWRC is derived empirically by

measuring how water is retained and released by different soil types. Throughout time different SWRC have been developed and integrated into models, the most widely applied are Van Brooks and Corey (Brooks and Corey, 1964), Fredlund and Xing (Fredlund and Xing, 1994), van Genuchten (van Genuchten, 1980), and Gardner (Gardner, 1956) SWRCs. Different SWRC equations require different parameters, some shared between different SWRC concepts, e.g. referring physical soil characteristics such as water saturated and unsaturated content, hydraulic conductivity and pore size, others uniquely describing the SWRC function shape, not directly related to soil properties. Often, for computational reasons, the soil profile from ground level to bedrock depth is sliced into layers, at the modeller's choice, and the SWRC function is applied to each soil layer. Alternative use of soil properties is for soil moisture calculations.

The dataset includes variables required to apply the Van Genuchten SWRC equations (van Genuchten, 1980) to describe the water dynamics through a vertical soil profile composed of three layers (1, 2, 3), each variable is required for each soil layer and for forest ( f ) or non-forest ( o ) land use, with different soil depth in forest ( f ) and non-forest ( o ) areas following root depth values from Allen et al. (1998), further referred as FAO56, (total of 29 variables; name in brackets in italics correspond to the field's name in the data repository):

- Soil profile: surface layer depth (*soildepth1 f, soildepth1 o*, mm), middle layer depth (*soildepth2 f, soildepth2 o*, mm), subsoil depth (*soildepth3 f, soildepth3 o*, mm);
- Soil hydraulic properties: saturated (*thetas1 f, thetas1 o, thetas2 f, thetas2 o, thetas3, m<sup>3</sup>/m<sup>3</sup>*) and residual (*thetar1, thetar2, thetar3, m<sup>3</sup>/m<sup>3</sup>*) volumetric soil moisture content, pore size index (*lambda1 f, lambda1 o, lambda2 f, lambda2 o, lambda3, dimensionless*), Van Genuchten equation parameter (*genual f, genual o, genua2 f, genua2 o, genua3, cm<sup>-1</sup>*), saturated soil conductivity (*ksat1 f, ksat1 o, ksat2 f, ksat2 o, ksat3, mm/day*).

#### 4.4 Soil properties

#### Soil properties are derived from SoilGrids250m (see Section 3.4) 6.2 Reference data and methodology

Soil properties are derived from The International Soil Reference and Information Centre (ISRIC) SoilGrids250m global gridded soil information release 2017 (further referred as SoilGrids250m) – an output of special predictions produced by the SoilGrids system, as a set of global soil property and class maps on soil characteristics at six standard depths, including soil textures (clay, silt, sand), depth to bedrock, bulk density, organic carbon, pH and cation exchange capacity at 250 meters resolution covering land area with no permanent ice and representative for the year 2010 (for reference data details see Appendix 1); and are computed for both forested and non-forested (also known in literature as 'others') areas, expressed as fractions (main source is forest fraction based on CGLS-LC100, see Section 4.1), where non-forested area is the complementary fraction of forest. Soil depth layers are derived first and used as input to the soil hydraulic equations used to derive the properties, following a sequential workflow (see ~~Error! Reference source not found.~~ Figure 13 and Table 4). Equations used are from Toth et al. (2015).

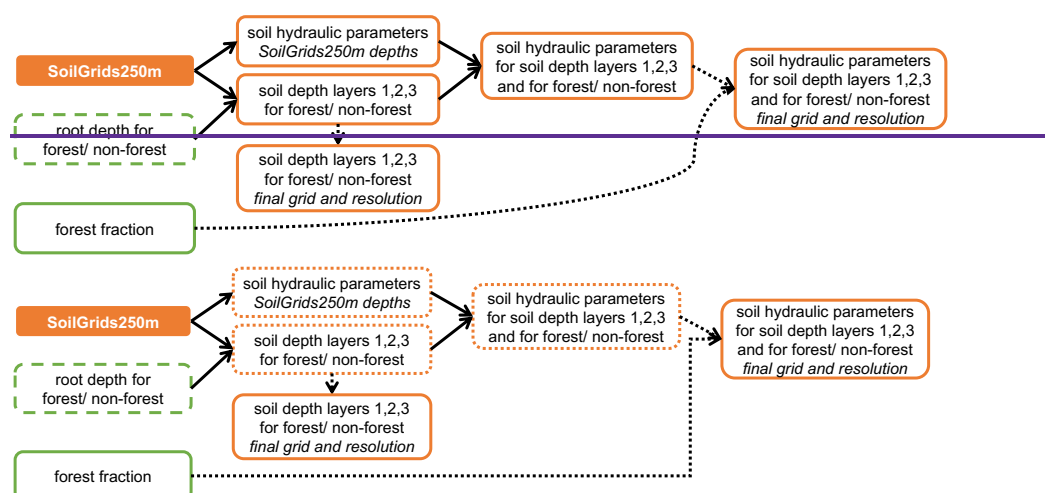


**Figure 6.13.** Workflow to generate the soil related fields; solid arrows indicate a function transformation, dotted – upscaling; dashed boxes indicate the intermediate fields used for other field generation, dotted – the fields only used for the soil-related fields; ‘SoilGrids250m depths’ – fields at the SoilGrids250m native grid and resolution with six default depths, ‘final grid and resolution’ – fields at the dataset’s final grid and resolution, boxes with no explicit indication – fields at SoilGrids250m native grid and resolution only.

899  
900

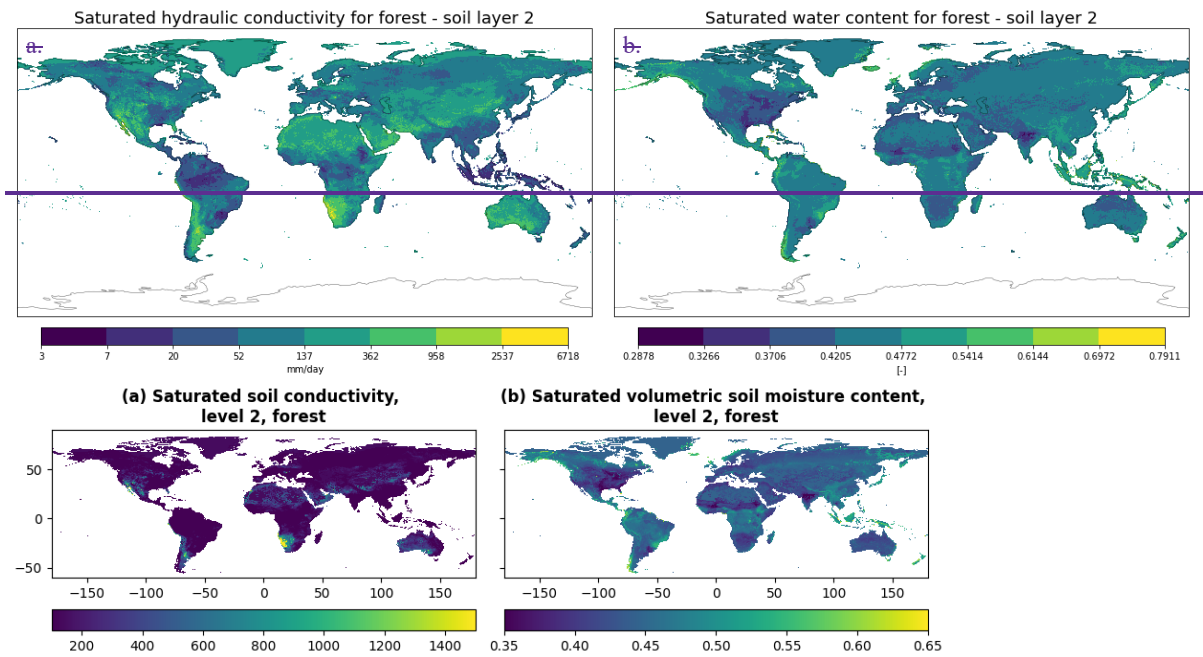
**Table 4. Soil property fields, their description, and applied transformations; name in brackets in italics next to each field correspond to the name in the data repository.**

<i>Field type</i>	<i>Description</i>	<i>Data Source</i>	<i>Transformation (in order)</i>
Soil depth layers 1, 2, 3 for forest and non-forest ( <i>soildepth1_f, soildepth1_o, soildepth2_f, soildepth2_o, soildepth3_f, soildepth3_o</i> )	Root depths assumed to divide the total soil depth between topsoil (surface [layer 1] and middle [layer 2]) and subsoil (bottom [layer 3])	SoilGrids250m (absolute_depth_to_bedrock); <i>root_depth_f; root_depth_o</i>	Transforming at SoilGrids250m native grid and resolution as described in <a href="#">Annex 2Appendix 3</a> ‘Soil Depth’ (in total 3 forest and 3 non-forest soil depth layer fields); Reprojecting and upscaling to final grid and resolution with unweighted mean; NoData filling DEEP (upsampling to 1, 3, 15 arc min, 1, 3, 15, 60 degrees spatial resolution with unweighted mean; replacing NoData at final resolution with first available precomputed less coarser resolution, if not – with zero)
Saturated volumetric soil moisture content for soil depth layers 1, 2, 3, and for forest and non-forest ( <i>thetas1_f, thetas1_o, thetas2_f, thetas2_o, thetas3</i> )	Saturated water content soil hydraulic property representing the maximum water content in the soil	SoilGrids250m (clay_content, silt_content, bulk_density); <i>soildepth1_f; soildepth1_o; soildepth2_f; soildepth2_o; soildepth3_f; soildepth3_o; fracforest</i>	Transforming at SoilGrids250m native grid and resolution as described in <a href="#">Annex 2Appendix 3</a> ‘Soil hydraulic parameters’ (in total 5 fields per soil hydraulic parameter, except <i>thetar</i> – only 3 as no forest/ non-forest separation); Limiting values and weighting by forest/ non-forest fraction (limits <i>thetas</i> < 1.0, <i>thetar</i> < <i>thetas</i> , $\lambda \leq 0.42$ , $g_{enua} \leq 0.055$ , $ksat > 0.0$ ); Upscaling to final grid and resolution with unweighted mean;
Residual volumetric soil moisture content for soil depth layers 1, 2, 3 ( <i>thetar1, thetar2, thetar3</i> )	Residual water content soil hydraulic property representing the minimum water content in the soil	SoilGrids250m (clay_content, silt_content); <i>soildepth1_f; soildepth1_o; soildepth2_f; soildepth2_o; soildepth3_f; soildepth3_o; fracforest</i>	NoData filling DEEP (upsampling to 1, 3, 15 arc min spatial resolution with unweighted mean; replacing NoData at final resolution with first available precomputed less coarser resolution, if not – with global unweighted mean)
Pore size index for soil depth layers 1, 2, 3, and for forest and non-forest ( <i>lambda1_f, lambda1_o, lambda2_f, lambda2_o, lambda3</i> )	Van Genuchten parameter $\lambda$ (also referred as ‘n-1’ in literature) soil hydraulic property representing the pore size index of the soil	SoilGrids250m (clay_content, silt_content, bulk_density, organic_carbon_content); <i>soildepth1_f; soildepth1_o; soildepth2_f; soildepth2_o; soildepth3_f; soildepth3_o; fracforest</i>	
Van Genuchten equation parameter for soil depth layers 1, 2, 3, and for forest and non-forest ( <i>genua1_f, genua1_o, genua2_f, genua2_o, genua3</i> )	Van Genuchten parameter $\alpha$ soil hydraulic property	SoilGrids250m (clay_content, silt_content, bulk_density, organic_carbon_content); <i>soildepth1_f; soildepth1_o; soildepth2_f; soildepth2_o; soildepth3_f; soildepth3_o; fracforest</i>	
Saturated soil conductivity for soil depth layers 1, 2, 3, and for forest and non-forest ( <i>ksat1_f, ksat1_o, ksat2_f, ksat2_o, ksat3</i> )	Saturated hydraulic conductivity soil hydraulic property representing the ease with which water moves through pore spaces of the soil	SoilGrids250m (clay_content, silt_content, soil_pH, cation_exchange_capacity); <i>soildepth1_f; soildepth1_o; soildepth2_f; soildepth2_o; soildepth3_f; soildepth3_o; fracforest</i>	

901  
902  
903  
904  
905  
906  
907  
908  
909

Two of the most common soil parameters of land surface and hydrological models, saturated hydraulic conductivity *ksat* and saturated water content, are shown in [Figure 7-Figure 14](#). Saturated hydraulic conductivity *ksat* (see [Figure 7aFigure 14a](#)) ranges from 2 to 7445 mm/day. The highest *ksat* values are concentrated in desertic areas such as the Sahara, Arabian Peninsula, Gobi, Patagonian, Sonoran-Mojave and Kalahari and Namib deserts. Low *ksat* between, 2 and 18 mm/day, are found in the Amazon river basin, the lower Mississippi river basin and South East Asia. *ksat* was visually compared against 8 global datasets developed with different input data and/ or PTFs (Zhang and Schaap, 2019; Gupta et al., 2021); a general agreement is noticeable in areas that show low variability across all datasets. Northern Russia, Canada, South East

910 Asia and Sonoran-Mojave Desert are the areas with high variability among datasets, with values ranging from  
 911 very low to very high  $ksat$ . Source of uncertainties in  $ksat$  values are primarily due to little availability of soil  
 912 samples and measurements carried out in those areas. Moreover, the climatic context plays a relevant role in clay  
 913 mineralogy composition, organic composition and soil pores structure (Hodnett and Tomasella, 2002), which  
 914 influence how water flows through the soil. Therefore, the PTF developed using soil samples collected in  
 915 temperate areas (such as Europe) are expected to have a different hydraulic behaviour compared to those collected  
 916 in tropical climates (Gupta et al., 2021), as also seen in Figure 7a14a.  
 917 Saturated water content (see Figure 7bFigure 14b) ranges between 0.27 to 0.79, with 80% of values between 0.40  
 918 and 0.46. A comparison with other global datasets was not carried out, however uncertainties are expected to be  
 919 of the same order of magnitude than those of  $ksat$  given the fact the saturated water content is calculated using  
 920 bulk density and clay content data.  
 921

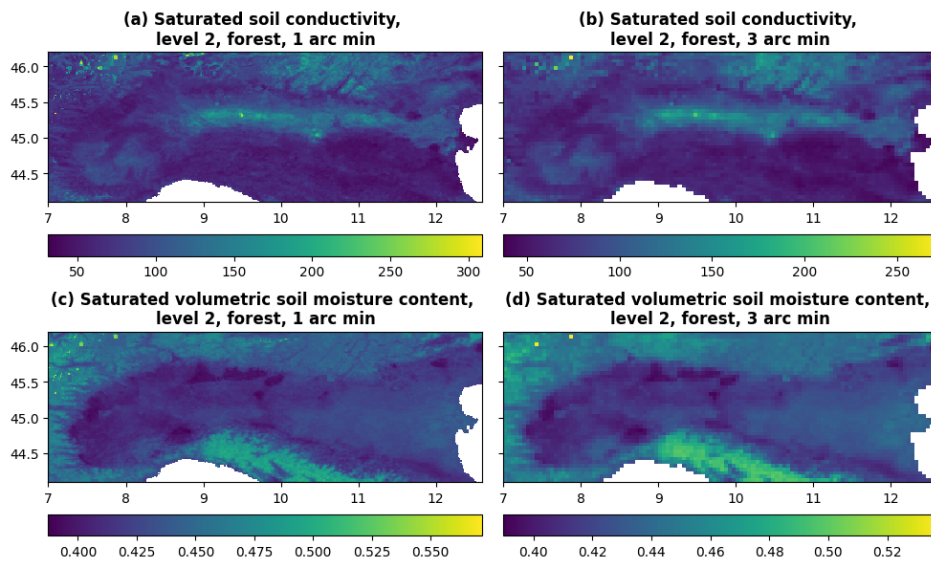


922  
 923  
 924 **Figure 7-14. Saturated soil hydraulic conductivity (a) and saturated water content (b) for forested areas of soil depth**  
 925 **layer 2 in mm per day (left column, plot a) and saturated volumetric soil moisture (i.e. water) content for forested areas**  
 926 **of soil depth layer 2 (right column, plot b) at 3 arc min (~5.6 km at the equator) resolution for global region.**

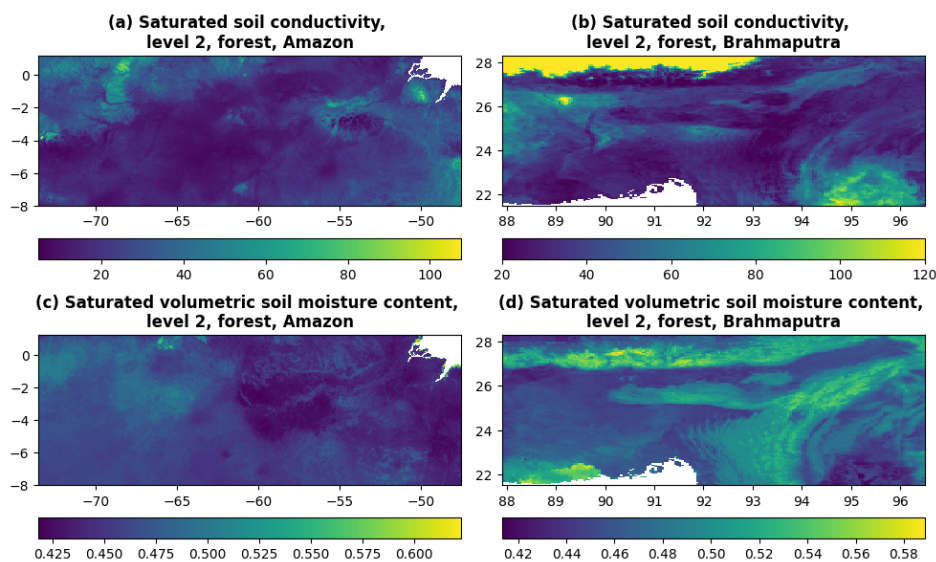
### 927 6.3 Regional examples

928 The majority of soil properties fields are easy to interpret. Saturated soil conductivity  $ksat$  and saturated volumetric  
 929 soil moisture content are presented for forested areas of soil depth layer 2 in Figure 15 for the Po River area in 1  
 930 arc min and 3 arc min resolution, and in Figure 16 for the Amazon River and the Brahmaputra River areas at 3  
 931 arc min resolution. The field of saturated soil conductivity for forest shows how easy it is for water to penetrate  
 932 soil depending on forest type, and the field of saturated volumetric soil moisture content shows what is the  
 933 maximum amount of water that the soil can absorb depending on forest type have interesting features over  
 934 Brahmaputra River area.  
 935





936  
937 **Figure 15.** Saturated soil hydraulic conductivity for forested areas of soil depth layer 2 in mm per day (upper row, plots  
938 **a and b**) and saturated volumetric soil moisture (i.e. water) content for forested areas of soil depth layer 2 (lower row,  
939 **plots c and d**) at 1 arc min (~1.9 km at the equator, left column, plots **a and c**) and 3 arc min (~5.6 km at the equator,  
940 **right column, plots b and d**) resolution for Po River area in Italy.



941  
942 **Figure 16.** Saturated soil hydraulic conductivity for forested areas of soil depth layer 2 in mm per day (upper row, plots  
943 **a and b**) and saturated volumetric soil moisture (i.e. water) content for forested areas of soil depth layer 2 (lower row,  
944 **plots c and d**) at 3 arc min (~5.6 km at the equator) resolution for Amazon River area (left column, plots **a and c**) and  
945 **Brahmaputra River area (right column, plots b and d).**

## 946 7 Lakes

### 947 4.5 Lakes

948 The lake field is derived from the GLWD database.

#### 950 7.1 General information

951 Lakes (and reservoirs) are important as they influence river discharge variability but also the atmosphere  
952 regionally and globally. The area covered by lakes can be used for computing evaporation from open water,  
953 freshwater storage, unregulated surface water extent, fresh water scarcity indexes, and biogenic green house gas



emission, as well as for reproducing different climate mitigation scenarios. The **CEMS - Surfacefields - 2023** dataset only includes data on lake extent and not reservoirs (generally smaller), described as a lake mask where the presence of lakes is consistent with fraction of inland water; the field's name in the data repository is *lakemask*, dimensionless).

## 7.2 Reference data and methodology

The lake mask field is derived from **The Global Lakes and Wetlands Database** (further referred as GLWD) – a global database of water bodies at spatial resolutions of up to 1:1 million – GLWD-1 with 3067 largest lake and 654 largest reservoir polygons, and GLWD-2 with ~250000 smaller lake and reservoir polygons (see Table 7).

**Table 5. Lake field, its description, data source and transformation; name in brackets in italics next to the lake field corresponds to the name in the data repository.**

Field type	Description	Data source	Transformation (in order)
Lake mask ( <i>lakemask</i> )	Area covered by lakes only (binary representation)	GLWD (GLWD-1, GLWD-2, lake type only); <i>fracwater</i>	Filtering non-lake spatial units; Shapefile gridding to final grid and resolution; If <i>fracwater</i> > 0 and GLWD is 'lake', then <i>lakemask</i> is 1, otherwise 0

## 4.6 Water demand

### 7.3 Regional examples

The lake mask field is easy to interpret as it shows which grid cells from fraction of inland water field have lakes. The lake mask field is presented in Figure 17 for Po River area in 1 arc min and 3 arc min resolution, and in Figure 18 for Amazon River and Brahmaputra River areas at 3 arc min resolution, where it shows the abundance of lakes over Amazon River area and detailed lake shapes over Po River area described by the 1 arc min resolution field.

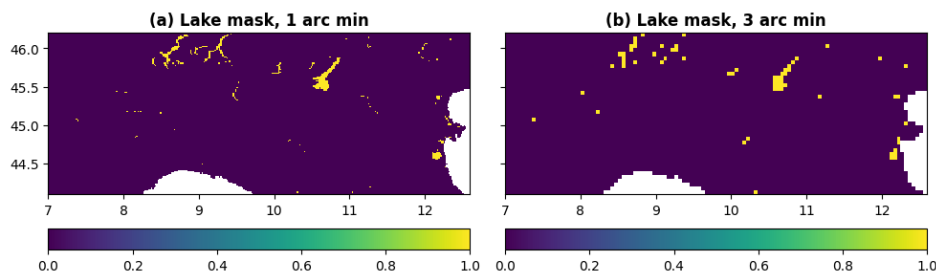


**Figure 17. Lake mask at 1 arc min (~1.9 km at the equator, left column, plot a) and 3 arc min (~5.6 km at the equator, right column, plot b) resolution for Po River area in Italy.**

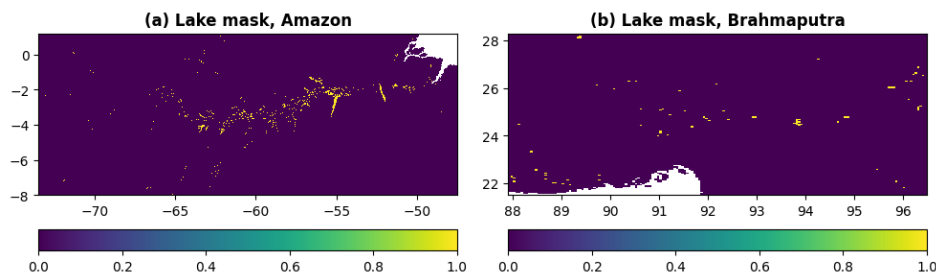


**Figure 18. Lake mask at 3 arc min (~5.6 km at the equator) resolution for Amazon River area (left column, plot a) and Brahmaputra River area (right column, plot b).**

## 8 Water demand

### 8.1 General information

Some environmental models explicitly represent a number of the human interventions impacting on the water cycle. One of the most common is water demand, which represents the withdrawal of water from natural water

982 [sources \(e.g. rivers, reservoirs, groundwater\) to satisfy the water demand for anthropogenic use. The segregation](#)  
983 [of the total water demand for anthropogenic use into four main sectors, namely domestic, energy, industrial, and](#)  
984 [livestock water withdrawal, enables a more accurate representation of the processes, and follows the Food and](#)  
985 [Agriculture Organisation of the United Nations \(FAO\) terminology \(Kohli et al., 2012\). Domestic water](#)  
986 [withdrawal represents indoor and outdoor household water use as well as other uses \(e.g. industrial and urban](#)  
987 [agriculture\) connected to the municipal system \(e.g., water use by shops, schools, and public buildings\). Electricity](#)  
988 [\(energy\) water withdrawal is the water use for the cooling of thermoelectric and nuclear power plants. Water](#)  
989 [withdrawal for industry is the water used for fabricating, processing, washing, cooling or transporting products,](#)  
990 [also includes water within the final products and water used for sanitation within the manufacturing facility.](#)  
991 [Livestock withdrawal is the demand for drinking and cleaning purposes of livestock.](#)  
992 [Higher accuracy in environmental modelling is achieved by differentiating water demand sources and by](#)  
993 [allocating different levels of priority to different usages. Within LISFLOOD, for instance, water demand for the](#)  
994 [energy sector and flooded irrigation \(rice crops\) is supplied by surface water bodies only, while non-flooded](#)  
995 [irrigation, domestic, industrial, livestock water demand can be supplied by both groundwater and surface water](#)  
996 [bodies. Moreover, domestic water demand has the highest priority in case of water scarcity conditions.](#)  
997 [It must be noted that the fields of water demand for agriculture are not included in this dataset because LISFLOOD](#)  
998 [computes crops water demand internally by accounting for climatic conditions, information on land cover \(see](#)  
999 [Section 4.2\), crops properties \(see Section 5.2\), and soil properties \(see Section 6.2\). Conversely, fields](#)  
1000 [representing the volume of water to satisfy the domestic, energy, industrial, and livestock demand must be](#)  
1001 [provided as input. Domestic, industrial, energy, and livestock water demand volumes have seasonal \(e.g. due to](#)  
1002 [temperature differences\) and inter-annual variations \(e.g. due to population changes and different economic](#)  
1003 [conditions\). In order to account for this variability, in LISFLOOD the four sectoral water demand fields provide](#)  
1004 [daily water demand data with monthly or annual variability from 01.01.1979 to 31.12.2019; the water demand](#)  
1005 [values are provided in mm/day, one field per month \(the first day of each month is used as representative](#)  
1006 [timestamp for the entire month\) for domestic and energy demand, one value per year \(the monthly fields are](#)  
1007 [repeated twelve times per each year\) for industrial and livestock demand.](#)  
1008 [Water availability, ecosystem long term ecological status, and anthropogenic needs must be accounted for to](#)  
1009 [evaluate the long term sustainability of water withdrawals. However, the spatial scales of water use data and](#)  
1010 [available water resources data often do not match due to different ways of data surveying and/or modelling](#)  
1011 [\(McManamay et al., 2021; Zhang et al., 2023\) and this creates a technical hurdle. Alternative use of the gridded](#)  
1012 [sectoral water demand information is e.g. for \(i\) the statistical analysis of long term spatiotemporal patterns and](#)  
1013 [trends of water demand; \(ii\) the evaluation of the long term sustainability and impacts of water withdrawals \(e.g.](#)  
1014 [in connection to remote sensing-derived datasets of surface water extent or groundwater total storage\); \(iii\) the](#)  
1015 [analysis of ecosystem–water–food–energy nexus \(Karabulut et al., 2016\); \(iv\) the evaluation of the impacts on](#)  
1016 [water resources of economical and price policies \(Dolan et al., 2021\); \(v\) the analysis of the responses in sectoral](#)  
1017 [water use during hydro climatic extremes \(Belleza et al., 2023\).](#)  
1018 [The CEMS SurfaceFields 2022 dataset includes water demand for four main sectors \(note that each sector](#)  
1019 [consists in total of 12 daily water demand fields per 41 \(1979–2019\) years, so 492 fields per sector\) for \(name in](#)  
1020 [brackets in italics correspond to the field’s name in the data repository\): livestock \(\*liv\*, mm/day\), industry \(\*ind\*,](#)  
1021 [mm/day\), energy production, \(\*ene\*, mm/day\) and domestic use \(\*dom\*, mm/day\). The temporal extension of the](#)  
1022 [water demand fields presented in this manuscript includes the most recent information of water demand at the](#)  
1023 [time of the dataset’s preparation. Readers that are interested in using more recent water demand data are invited](#)  
1024 [to follow the protocol presented in Section 8.2 to further extend in time the provided fields.](#)

## 1025 **8.2 Reference data and methodology**

1026 Global gridded water demand fields with monthly variability were generated for the four sectors using the data  
1027 sources listed [in Section 3.6 here](#) and following the transformations summarised in Table 8 (for additional  
1028 information and extra details see GitHub repository ‘[lisflood-utilities/water-demand-historic—at](#)  
1029 [feature/add\\_h\\_branches\\_upd · ec-jrc/lisflood-utilities · GitHub](#)’, last accessed: 21.02.2023).  
1030 [src/lisfloodutilities/water-demand-historic at master · ec-jrc/lisflood-utilities · GitHub](#)’, last accessed:  
1031 21.01.2024): (i) **AQUASTAT** – the FAO’s global information system with yearly country data on water resources  
1032 and agricultural water management for "Gross Domestic Product (GDP)", "Industry, value added to GDP",  
1033 "Agricultural water withdrawal", "Industrial water withdrawal", "Municipal water withdrawal", "Total water  
1034 withdrawal", and "Irrigation water withdrawal"; (ii) **United States Geological Survey National Water**  
1035 **Information System** (further referred as USGS NWIS) – a United States (US) database on water use data for the  
1036 annual state statistics for "Domestic total self-supplied withdrawals, fresh, in Mgal/d", "Public Supply total self-  
1037 supplied withdrawals, fresh, in Mgal/d", "Industrial total self-supplied withdrawals, fresh, in Mgal/d", "Total  
1038 Thermoelectric Power total self-supplied withdrawals, fresh, in Mgal/d", "Total Thermoelectric Power power  
1039 generated, in gigawatt-hours", and "Livestock total self-supplied withdrawals, fresh, in Mgal/d"; (iii) **Global**

1040 **Change Analysis Model** (further referred as GCAM) – an integrated, multi-sector model’s output that provides  
1041 estimates on water withdrawals for energy, agriculture, and municipal uses as lumped values of 235 hydrologic  
1042 basins; (iv) **Global-scale gridded estimates of thermoelectric power and manufacturing water use** (further  
1043 referred as Vassolo and Doll, 2005) – a global-scale gridded on 0.5° by 0.5° grid estimate of water withdrawal for  
1044 cooling of thermal power stations and for manufacturing, representative for the year 1995; (v) **The Gridded**  
1045 **Livestock of the World (GLW) version3** (further referred as GLW3) – a global-scale gridded on 0.083333° by  
1046 0.083333° (~10 km at the equator) grid of eight livestock species distribution, representative for the year 2010;  
1047 (vi) **World Bank manufacturing value added and gross domestic product** (further referred as World Bank) –  
1048 data provide "Manufacturing, value added (constant 2015 US\$)" values (further referred as MVA) and "Gross  
1049 Domestic Product GDP (constant 2015 US\$)" values; (vii) **The Global Human Settlement Population Grid**  
1050 **multitemporal version R2019A** (further referred as GHS-POP) – a global-scale gridded on 9 arc sec (~300 m at  
1051 the equator) grid distribution of population, expressed as the number of people per grid cell, representative for the  
1052 years 1975, 1990, 2000 and 2015; (viii) **Thematic Mapping Country Borders** shapefile (further referred as TM  
1053 ‘country borders’) – world country borders dataset; (ix) **The United States Census Bureau** Cartographic  
1054 **Boundary Files – Shapefile** (further referred as US CB) – the State boundaries for the USA, representative for the  
1055 year 2018; (x) **Multi-Source Weather** (further referred as MSWX) – a global-scale gridded high-resolution  
1056 (3-hourly, 0.1°), bias-corrected meteorological product with 2-meter daily and monthly maximum and minimum  
1057 air temperature; (xi) **Huang et al. (2018)** – a publication presenting 0.5° resolution global monthly gridded  
1058 sectoral water withdrawal dataset for the period 1971–2010 with calibrated R coefficient values and technique for  
1059 **temporal downscaling of domestic and energy water demands.**

1060 The water demand values are provided in mm/day, one field per month from 01.01.1979 to 31.12.2019 (the first  
1061 day of each month is used as the representative timestamp for the entire month). The methodology applied largely  
1062 follows Huang et al. (2018), with the key differences being the use of freely available datasets and the higher  
1063 resolution of the resulting fields. Spatial downscaling was achieved following the approach of Hejazi et al. (2014);  
1064 temporal downscaling was performed following the approaches of Wada et al. (2011), Voisin et al. (2013) and  
1065 Huang et al. (2018). It should be noted that country-scale estimates (from AQUASTAT) were integrated with  
1066 state-level water withdrawal estimates (from USGS NWIS). The protocol for the integration of local information  
1067 with global data sources was developed for further use in the future, to enable the integration of other regional or  
1068 national datasets as soon as they become available.

1070 **Table 6. Water demand fields, their description, data source and applied transformations; grey-cells with bold italics**  
1071 **show required intermediate fields; name in brackets in italics next to each field correspond to the name in the data**  
1072 **repository.**

<i>Field type</i>	<i>Description</i>	<i>Data source</i>	<i>Transformations (in order)</i>
<b><i>Population density (pop)</i></b>	Number of people per grid-cell	GHS-POP R2019A (1975, 1990, 2000, 2015)	Reprojecting and upscaling from native (9 arc sec) to the final grid and intermediate resolution of 0.01°x0.01° with sum (in total four fields); Transforming from population number to density per grid-cell (i.e. dividing by grid-cell area) and upscaling from intermediate to final resolution with mean (in total four fields); NoData filling (year) with linear interpolation till 2015, and with years 2000 and 2015 trend extrapolation 2016 onwards ( $pop_{year}^{grid}$ ; in total 41 fields)
		TM ‘country borders’, US CB ‘state borders’	Shapefile (country, US State) gridding to final grid and intermediate resolution of 0.01°x0.01°, then to final resolution; Transforming from population density per grid-cell to population per country (i.e. multiplying by grid-cell area and summing grid-cells according to the country mask from step above; $pop_{year}^{country}$ ; in total one table)
Water demand for domestic use ( <i>dom</i> )	Daily supply of water volume for indoor and outdoor household purposes and for all the uses that are connected to	AQUASTAT (per country), USGS NWIS (per US State), <i>pop</i>	Unit conversion from native to km <sup>3</sup> /year; NoData filling (year): for countries – with linear interpolation and forward/ backward extrapolation based on $pop_{year}^{country}$ , for US states – with linear interpolation and nearest neighbour extrapolation ( $demand_{year}^{country}$ , in total one table)
		<i>pop</i> , TM ‘country borders’, US CB ‘state borders’	Transforming water demand ( $demand_{year}^{country}$ ) to water demand per capita per country/ US State per year (in total one table): $perCapitaDemand_{year}^{country} = \frac{demand_{year}^{country}}{pop_{year}^{country}}$ ; NoData filling (country) with nearest neighbour;

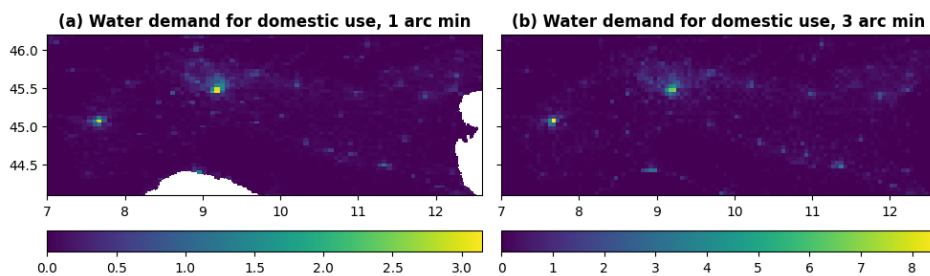
	the municipal system (e.g., water used by shops, schools, and public buildings)		Transforming from water demand per capita to water demand per grid-cell (i.e. weighting by $pop_{year}^{grid}$ ; in total one field per year): $demand_{year}^{grid} = perCapitaDemand_{year}^{country} \cdot pop_{year}^{grid}$
		MSWX, Huang et al. (2018) [Table 3, Eq. (2)].	Temporal downscaling (month) to account for the withdrawal fluctuations between the warmest and coldest months based on Huang et al. (2018) Eq. (2) (in total 12 fields per year): $demand_{month,year}^{grid} = \frac{demand_{year}^{grid}}{month_{number}} \cdot \left( \frac{\bar{T}_{month,year}^{grid} - avg_{year}^{grid}}{max_{year}^{grid} - min_{year}^{grid}} \cdot R + 1 \right)$ , where $avg_{year}^{grid}$ , $max_{year}^{grid}$ , $min_{year}^{grid}$ are the average, maximum, minimum monthly temperatures in a year; $\bar{T}_{month,year}^{grid}$ is the average temperature in a month of the year; $R$ is the amplitude of the monthly fluctuations from Huang et al. (2018) [Table 3]; $month_{number}$ is number of months in a year, i.e. 12; Temporal downscaling (day; in total 12 fields per year): $demand_{day,month,year}^{grid} = \frac{demand_{month,year}^{grid}}{day_{number}}$ , where $day_{number}$ is number of days in a month of a certain year
Water demand for industrial use ( <i>ind</i> )	Daily supply of water volume for fabricating, processing, washing and sanitation, cooling or transporting a product, incorporating water into a product	AQUASTAT (per country), USGS NWIS (per US State), GCAM (per region), Vassolo and Doll (2005), World Bank (MVA), <i>pop</i> , TM ‘country borders’	Unit conversion from native to km <sup>3</sup> /year; NoData filling (year; in total one table): <ul style="list-style-type: none"> <li>regional data – downscaling (spatial) to country values (i.e. weighting by <math>pop_{year}^{country}</math>), then linear interpolation (between years) and nearest neighbour extrapolation in time, finally rescaling values according to Vassolo and Doll (2005);</li> <li>country data – with linear interpolation (between years) and forward/ backward extrapolation based on <i>MVA</i> or <math>pop_{year}^{country}</math>, value disaggregation from industrial water demand to manufacturing and thermoelectric water demands according to regional data results;</li> <li>for US States data – with linear interpolation (between years) and nearest neighbour extrapolation;</li> <li>mosaicking results from US States and country data, from regional data, if not – with zero</li> </ul>
		<i>pop</i> , TM ‘country borders’, US CB ‘state borders’	Transforming from water demand per country/ US State to per grid-cell (i.e. weighting by $pop_{year}^{grid}/pop_{year}^{country}$ ; in total one field per year): $demand_{year}^{grid} = \frac{demand_{year}^{country}}{pop_{year}^{country}} \cdot pop_{year}^{grid}$ ; Temporal downscaling (day; in total one field per year): $demand_{day,year}^{grid} = \frac{demand_{year}^{grid}}{day_{number}}$ , where $day_{number}$ is number of days in a year
Water demand for thermoelectric use ( <i>ene</i> )	Daily supply of water volume for the cooling of thermoelectric and nuclear power plants	AQUASTAT (per country), USGS NWIS (per US State), GCAM (per region), Vassolo and Doll (2005), World Bank (MVA), <i>pop</i> , TM ‘country borders’	Same steps as for water demand for industrial use, but using the energy withdrawals as input data (in total one table)
		<i>pop</i> , TM ‘country borders’, US CB ‘state borders’	Same steps as for water demand for industrial use (in total one field per year)
		GCAM (per region), MSWX, Huang et al. (2018) [Eq. (3)-(10)].	Temporal downscaling (month) to account for the withdrawal fluctuations between the warmest and coldest months based on Huang et al. (2018) Eq. (3)-(10) (in total 12 fields per year)
Water demand for livestock use ( <i>liv</i> )	Daily supply of water volume for domestic animal needs	AQUASTAT (per country), USGS NWIS (per US State), GCAM (per region),	Unit conversion from native to km <sup>3</sup> /year; NoData filling (year; in total one table): <ul style="list-style-type: none"> <li>regional data – spatial downscaling from regional withdrawals to country values (i.e. weighting by total livestock mass</li> </ul>

	GLW3, TM 'country borders'	estimates per country from GLW3, $livestock_{year}^{country}$ ): $demand_{year}^{country} = \frac{withdrawal_{year}^{region}}{livestock_{year}^{region}} \cdot livestock_{year}^{country}$ , then value linear interpolation (between years) and nearest neighbour extrapolation, finally rescaled with country data (if available) <ul style="list-style-type: none"> <li>• for US States data – with linear interpolation (between years) and nearest neighbour extrapolation;</li> <li>• mosaicking results from US States and regional data, if not – with zero</li> </ul>
	GLW3, TM 'country borders', US CB 'state borders'	Transforming from water demand per country/ US State to per grid_cell (i.e. weighting by $\frac{livestockDensity_{year}^{grid}}{livestockDensity_{year}^{country}}$ ; in total one field per year): $demand_{year}^{grid} = \frac{demand_{year}^{country}}{livestockDensity_{year}^{country}} \cdot livestockDensity_{year}^{grid}$ ; Temporal downscaling (day; in total one field per year): $demand_{day,year}^{grid} = \frac{demand_{year}^{grid}}{number_{day,year}}$ , where $day_{year}^{number}$ is number of days in a year

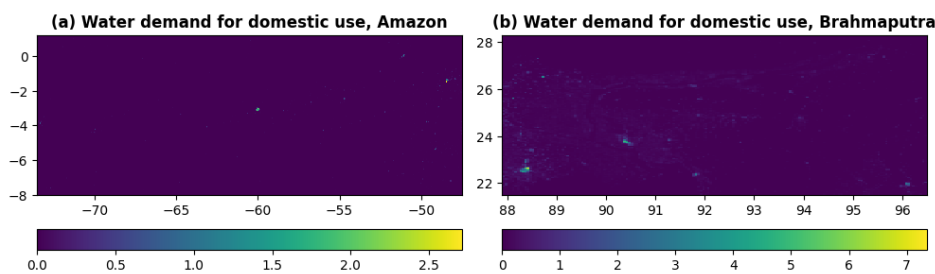
1073 To the best of the authors' knowledge, no other publicly accessible temporally varying global water demand field  
1074 set exists (only static datasets). A rigorous validation of the temporally varying water demand fields is not  
1075 straightforward at the global scale, as the only comprehensive global data source, FAO AQUASTAT, was used  
1076 to create the fields.

### 1077 8.3 Regional examples

1078 In general fields in water demand category are easy to interpret as they show how much water per day is needed  
1079 to satisfy certain type of human induced needs. In reality water demand fields are mainly covering urbanised areas  
1080 and are scattered around (i.e. not continuously looking field), with relatively small variations in field values from  
1081 month to month. Example for domestic water use is presented for August 2018 in Figure 19 for Po River area in  
1082 1 arc min and 3 arc min resolution, and in Figure 20 for Amazon River and Brahmaputra River areas at 3 arc min  
1083 resolution.



1085 Figure 19. Water demand for domestic use in mm per day at 1 arc min (~1.9 km at the equator, left column, plot a) and  
1086 3 arc min (~5.6 km at the equator, right column, plot b) resolution for Po River area in Italy.  
1087



1088 Figure 20. Water demand for domestic use in mm per day at 3 arc min (~5.6 km at the equator) resolution for Amazon  
1089 River area (left column, plot a) and Brahmaputra River area (right column, plot b).  
1090



59 Data, access, licensing, documentation

The new CEMS SurfaceFields 2022 is an open-source dataset of the Copernicus Emergency Management Service describing key components of the Earth surface generally required in environmental and hydrological modelling, including Earth system modelling and numerical weather prediction. The dataset includes static fields (e.g. forest fraction), yearly cycle fields (e.g. 10-day average LAI, in total 36 fields), and yearly varying fields (e.g. water demand). The surface fields are based on 25 different sources, including global and regional high resolution (up to 100 m) gridded and vector datasets. They were processed into two set of fields (i) at 1 arc min resolution (~1.86 km at the Equator) over Europe (72.25 N/ 22.75 N, 25.25 W/ 50.25 E; 4530x2970 grid-cells), and (ii) at 3 arc min resolution (~5.57 km at the Equator) over the Globe (90.00 N/ 90.00 S, 180.00 W/ 180.00 E; 7200x3600 grid-cells), to provide an up-to-date surface state for six main field groups: (1) catchment morphology and river network, (2) land use fields, (3) vegetation properties, (4) soil properties, (5) lakes, (6) water demand.

The CEMS\_SurfaceFields\_2022 dataset consist in total of 140 gridded fields at EPSG:4326 – WGS84: World Geodetic System projection in NetCDF format with information on Earth’s surface state (see Table 9 for the full list of fields), which are grouped thematically in sub-folders. The 1 arc min European fields have a total volume of 9.3 GB and the 3 arc min global fields have a total volume of 22.7 GB. The CEMS\_SurfaceFields\_2022 dataset is freely available for download from the JRC Data Catalogue (<https://data.jrc.ec.europa.eu/>). The set of global surface fields at 3 arc min resolution can be found here (JRC Data Catalogue – LISFLOOD static and parameter maps for GloFAS – European Commission (europa.eu), <https://data.jrc.ec.europa.eu/dataset/68050d73-9c06-499c-a441-dc5053cb0c86>) and the set of surface fields for the European domain at 1 arc min resolution can be found here (JRC Data Catalogue – LISFLOOD static and parameter maps for Europe – European Commission (europa.eu), <https://data.jrc.ec.europa.eu/dataset/f572c443-7466-4adf-87aa-c0847a169f23>). The README.txt file that can be found there contains the basic description of each surface fields including general information, data description, file overview, methodological information and data access and sharing information (for detailed technical description of how the surface fields were generated refer to the LISFLOOD User Guide, available online: [https://ec-jrc.github.io/lisflood-code/4\\_Static-Maps-introduction/](https://ec-jrc.github.io/lisflood-code/4_Static-Maps-introduction/)). The changelog.txt file – provides users with information on updates to the datasets. The copyright.txt file – information about the data license (CC BY 4.0).

**Table 9. Full list of surface fields with short description and units included in CEMS\_SurfaceFields\_2022 dataset; *name in italics correspond to the field’s file name in the data repository.***

Field group	Description	Name	Units
Main	model’s <i>field</i> (i.e. in technical <i>field</i> for model operation/ running sense)	<i>mask</i>	dimensionless
Catchment morphology and river network	local drainage direction (i.e. flow direction from one cell to another)	<i>LDD</i>	dimensionless
	grid-cell area	<i>pixarea</i>	m <sup>2</sup>
	grid-cell length	<i>pixlength</i>	m
	upstream <i>drainage</i> area	<i>upArea</i>	m <sup>2</sup>
	standard deviation of elevation	<i>elvstd</i>	m
	gradient	<i>gradient</i>	m/m
	channel bottom width	<i>chanbw</i>	m
	channel length	<i>chanlength</i>	m
	channel gradient	<i>changrad</i>	m/m
	Manning’s roughness coefficient for channels	<i>chanman</i>	s/m <sup>1/3</sup>
	channel mask (i.e. presence of river channel)	<i>chan</i>	dimensionless
	channel side slope (i.e. channel’s horizontal distance divided by vertical distance)	<i>chans</i>	m/m
	bankfull channel depth	<i>chanbnkf</i>	m
channel floodplain (i.e. width of the area where the surplus of water is distributed when the water level in the channel exceed the channel depth)	<i>chanflpn</i>	m	
Land use fields	fraction of forest	<i>fracforest</i>	dimensionless
	fraction of sealed surface	<i>fracsealed</i>	dimensionless
	fraction of inland water	<i>fracwater</i>	dimensionless
	fraction of irrigated crops	<i>fracirrigated</i>	dimensionless
	fraction of rice	<i>fracrice</i>	dimensionless
	fraction of other cover types	<i>fracother</i>	dimensionless
	crop coefficient	<i>cropcoef f, cropcoef i, cropcoef o</i>	dimensionless

Vegetation properties (for forest [f], irrigated crops [i], other land cover types [o])	crop group number	<i>cropgrp_n_f, cropgrp_n_i, cropgrp_n_o</i>	dimensionless
	Manning's surface roughness coefficient	<i>mannings_f, mannings_o,</i>	s/m <sup>1/3</sup>
	rice planting days (3 seasons)	<i>riceplantingday1, riceplantingday2, riceplantingday3</i>	calendar day number
	rice harvesting days (3 seasons)	<i>riceharvestday1, riceharvestday2, riceharvestday3</i>	calendar day number
Soil properties (for [1, 2, 3] layers; for forest [f], non-forest [o])	leaf area index	<i>laif, laii, laio</i>	m <sup>2</sup> /m <sup>2</sup>
	surface layer depth	<i>soildepth1_f, soildepth1_o</i>	mm
	middle layer depth	<i>soildepth2_f, soildepth2_o,</i>	mm
	subsoil depth	<i>soildepth3_f, soildepth3_o</i>	mm
	saturated volumetric soil moisture content	<i>thetas1_f, thetas1_o, thetas2_f, thetas2_o, thetas3</i>	m <sup>3</sup> /m <sup>3</sup>
	residual volumetric soil moisture content	<i>thetar1, thetar2, thetar3</i>	m <sup>3</sup> /m <sup>3</sup>
	pore size index	<i>lambda1_f, lambda1_o, lambda2_f, lambda2_o, lambda3</i>	dimensionless
	Van Genuchten equation parameter	<i>genua1_f, genua1_o, genua2_f, genua2_o, genua3</i>	cm <sup>-1</sup>
saturated soil conductivity	<i>ksat1_f, ksat1_o, ksat2_f, ksat2_o, ksat3</i>	mm/day	
Lakes	lake mask (i.e. presence of lakes)	<i>lakemask</i>	dimensionless
Water demand	livestock	<i>liv</i>	mm/day
	industry	<i>ind</i>	mm/day
	thermoelectric production	<i>ene</i>	mm/day
	domestic use	<i>dom</i>	mm/day

1122 Whilst the CEMS\_SurfaceFields\_2022 dataset followed strict requirements of the LISFLOOD-OS model (e.g.  
1123 format, treatment of missing values, number of soil layers, etc...) it definitely can be used outside the LISFLOOD  
1124 context, using the full dataset or its parts, for applications such as modelling risk assessment. The workflow and  
1125 methodology used to generate the dataset and published in this manuscript can be used as reference and be easily  
1126 modified if further adaptation to the dataset is needed (e.g. using different set of equations to describe the soil  
1127 properties, or sourcing new/ more relevant local datasets).  
1128

## 1129 **610 Conclusion**

1130 The Earth's surface has a strong impact on the surface energy and water balance that drives lower atmosphere  
1131 weather conditions and river discharge fluctuations. Depending on the surface type (e.g. land use, terrain or soil),  
1132 weather in the region can be colder/ warmer, more/ less humid, drier/ rainier, and/ or calmer/ windier than its  
1133 surroundings, and the terrestrial water cycle can differ, with water infiltrating more/ less in the soil, leaving as  
1134 evaporation in a larger/ smaller rate, and reaching rivers faster/ slower. Surface information is provided by land  
1135 use and ecosystem type (e.g., forest, rice paddy, bare ground, urban), river geometry (e.g., channel width, channel  
1136 length), soil properties (e.g., depth, porosity, hydraulic properties), amongst others.

1137 Information of underlying surface fields can be accounted for in Earth system and environmental models (e.g.  
1138 atmospheric, hydrological, etc.) to simulate the evolution in space and time of water, energy and carbon cycles. If  
1139 artificial influences and human intervention are included within the modelled processes (e.g. irrigation or water  
1140 management through reservoirs), the information required to describe the processes must also be integrated within  
1141 the modelling framework. Generally, this is achieved through a set of independent files used as input to the models.  
1142 Because of the temporal non-stationarity of some surface fields, typically associated with human intervention such  
1143 as land use and water use, but also due to climatic variation such as lake extent (new lakes forming or lakes  
1144 shrinking), input surface fields must be as representative as possible to the simulated period of interest. For  
1145 medium-range forecasting systems, this should be as close from present as possible, for example. When simulating  
1146 long periods, especially looking at past or future decades, caution must be given to results especially if some  
1147 surface fields which have substantially changed during the simulation period do not explicitly incorporate time  
1148 and instead are based on the most recent period, as they may not be representative to the full study period [and can](#)  
1149 [introduce substantial biases that grow with time. Same is applicable if surface fields are used for collecting](#)  
1150 [statistical data in general, as stats based on stationary fields represent only the period used to generate stationary](#)  
1151 [field in question.](#)

1152 In addition, in recent years the horizontal resolution of global Earth system and environmental models has been  
1153 constantly increasing reaching the kilometre scale milestone, supported by the technological developments in the  
1154 field of High Performance Computers and the wealth of high resolution datasets freely available. This imposes

1155 another condition to the input surface fields – it has to be of rather high horizontal resolution (i.e. ~2 and 6 km at  
1156 the [Equator](#) [equator](#)).

1157 Thanks to the availability of a wide range of high resolution environmental data derived from the use of ground,  
1158 unconventional and satellite measurement sensors, new high resolution datasets describing the Earth’s surface are  
1159 nowadays released regularly. Even though each dataset may have a very low absolute and root mean square errors  
1160 compared against available independent data, merging different datasets for modelling purposes (e.g. to model  
1161 hydrological surface parameters) might lead to questionable results and even model crash, due to possible  
1162 discontinuity or inconsistency in the combined datasets. In the specific case of hydrological modelling where river  
1163 flow is also represented, high horizontal resolution does not guarantee better modelling per se. Sources of  
1164 potentially large errors can be easily hidden in high resolution datasets. This is the case for instance of errors in  
1165 the Digital Elevation Models when they are used to obtain the rivers drainage network. Small errors in the  
1166 elevation of a grid cell can lead to a totally inaccurate representation of the location and the direction in which the  
1167 river is flowing in the model compared to reality. Mislocating a river or having a slightly inaccurate catchment  
1168 area can represent a trivial inaccuracy for most applications, but it can also lead to missed flood warning for  
1169 thousands of people within a flood awareness system. To benefit from different recent high resolution datasets  
1170 based on satellite and ground measurements, it is essential that a well-defined, thorough workflow is designed and  
1171 implemented so that the final products are consistent and compatible with each other, and can be used in  
1172 combination.

1173 The work presented in this manuscript is focused not only on the final surface field set generation (i.e.  
1174 CEMS\_SurfaceFields\_2022), but also on deriving robust reproducible methodology that could be re-applied once  
1175 new versions of 25 or less input sources are released. Understanding of the methodology applied helps to interpret  
1176 values in the final surface fields and possibly even numerical model results that use these surface fields. The  
1177 collection of input sources and their preparation for actual use is a very important step as it includes going through  
1178 all technical documentation, comparison and verification of papers, and investigation of the actual data, as well  
1179 as data gridding, interpolation, and scaling. All input sources for CEMS\_SurfaceFields\_2022 are ranked according  
1180 to their quality and up-to-date in order to favour one value in ambiguous situations when several datasets provide  
1181 different information for the same location. Consistency check between all surface type fractions is carried out to  
1182 address that ambiguity during the merge of information of different origin (i.e. adjust fractions to sum to one in  
1183 each grid\_cell). Some fields, like forest fraction, were rather straightforward to create from available source, yet  
1184 it was noted that prior correction of the source was needed to delete erroneous forest grid\_cells from the Fox  
1185 Basin in Canada (the mismatch was only spotted during the investigation of the actual data, as it was absent from  
1186 the documentation). Other fields, like soil hydraulic properties, are created not only from the source information  
1187 but also from the forest fraction that had to be generated prior; the soil hydraulic property methodology also  
1188 includes several steps that have to be performed at the data native resolution (i.e. 250 m) using information from  
1189 several global fields simultaneously which becomes technically and computationally challenging. Surface fields  
1190 with clear multi-annual changes, like water demand maps, are created using temporal interpolation and  
1191 extrapolation from multiple data sources to create time series fields. A final and non-trivial task is to have all  
1192 resulting fields on the identical required grid without deterioration of the actual value precision, even after several  
1193 file type translations (e.g. local drainage direction field can be automatically checked and corrected if needed for  
1194 required boundaries only in PCRaster format, not NetCDF). Due to the number of data sources and surface fields  
1195 required to represent the main variables (i.e. 70) used in Earth system and environmental models, the overall effort  
1196 to generate the CEMS\_SurfaceFields\_2022 dataset (both human and computing resources) was substantial.

1197 ~~The CEMS\_SurfaceFields\_2022 dataset at 1 arc min (over Europe) and 3 arc min (globally) were tested and~~  
1198 ~~indirectly validated using the LISFLOOD model through river discharge simulation (Grimaldi et al., 2024 in~~  
1199 ~~preparation); they are the underlying surface fields of the EFAS version 5 and GloFAS version 4 operational~~  
1200 ~~systems.~~

1201 The CEMS\_SurfaceFields\_2022 dataset is a new data source open to all offering a kilometre-scale resolution of  
1202 high-quality data describing the Earth’s surface; [\(openly available online from the data catalogue of the JRC for](#)  
1203 [Europe at ~1.9 km at the equator or 1 arc min resolution: https://data.jrc.ec.europa.eu/dataset/f572c443-7466-](#)  
1204 [4adf-87aa-c0847a169f23, and for Globe at ~5.6 km at the equator or 3 arc min resolution:](#)  
1205 [https://data.jrc.ec.europa.eu/dataset/68050d73-9c06-499c-a441-dc5053cb0c86, last accessed: 21.01.2024\),](#)  
1206 providing exceptional opportunity for the research and scientific community to extend and multiply European and  
1207 global applications in wide ranging fields of the water-energy-food nexus. [The CEMS\\_SurfaceFields\\_2022](#)  
1208 [surface fields use can be vast, e.g. standard deviation of elevation and other orographic sub-grid parameters are](#)  
1209 [critical for radiation parametrization, especially for shadowing effect; channel geometry fields are vital to describe](#)  
1210 [overbank inundation and infer inundated areas in wetland methane and soil carbon modelling; land use fractions](#)  
1211 [are needed for skin temperature calculations, biogenic flux calculations, urban planning, and climate mitigation](#)  
1212 [plan preparation; LAI use include biomass allocation, which can be used for fire danger forecasting, and carbon](#)  
1213 [stock monitoring, whilst rice planting/ harvesting days are important for yearly cycle of methane modelling; soil](#)  
1214 [properties are used for soil moisture calculations; and the area covered by lakes can be used for computing](#)

1215 [evaporation from open water, freshwater storage, unregulated surface water extent, fresh water scarcity indexes,](#)  
1216 [and biogenic green house gas emission, as well as for reproducing different climate mitigation scenarios. All of](#)  
1217 [the above state that CEMS SurfaceFields 2022 surface fields can be used for weather prediction, Earth system](#)  
1218 [modelling, hydrological and environmental modelling, or statistical analysis in general, with a spatial scale](#)  
1219 [allowing for global, regional and even national applications.](#)

1220  
1221 *Data availability.* The CEMS\_SurfaceFields\_2022 datasets are freely available for download from the JRC Data  
1222 Catalogue – global [at ~5.6 km at the equator or 3 arc min resolution:](https://data.jrc.ec.europa.eu/dataset/68050d73-9c06-499c-a441-dc5053cb0c86)  
1223 <https://data.jrc.ec.europa.eu/dataset/68050d73-9c06-499c-a441-dc5053cb0c86>), over Europe [at ~1.9 km at the](https://data.jrc.ec.europa.eu/dataset/f572c443-7466-4adf-87aa-c0847a169f23)  
1224 [equator or 1 arc min resolution: https://data.jrc.ec.europa.eu/dataset/f572c443-7466-4adf-87aa-c0847a169f23](https://data.jrc.ec.europa.eu/dataset/f572c443-7466-4adf-87aa-c0847a169f23),  
1225 [and are documented in this paper.](#)

1226  
1227 *Author contributions.* ~~AHCP and PS shaped initial plan of the authors participated research; MC and FM executed~~  
1228 [initial plan; CM, SG and JD reviewed initial results and provided guidance in surface field computation](#)  
1229 [\(methodology, data generation, verification\) further research. MC, FCFM and CP wrote prepared a first draft of](#)  
1230 [the manuscript with paper, which was adapted to its present state by contributions from all the other authors CM,](#)  
1231 [SG, JD, PS and HB.](#)

1232  
1233 *Competing interests.* The authors declare that they have no conflict of interest.

1234  
1235 *Acknowledgements.* CEMS\_SurfaceFields\_2022 is a product and service of the Copernicus Emergency  
1236 Management Service. Financial support for MC, FM, CM and CP was provided by contract 941462-IPR-2021.  
1237 [Authors thank two anonymous reviewers for their valuable comments and suggestions that helped to shape the](#)  
1238 [manuscript to it's current state.](#)

1239  
1240 *Financial support.* This research has been supported by contract 941462-IPR-2021.

## 1241 References

1242 [Alfieri, L., Lorini, V., Hirpa, F. A., Harrigan, S., Zsoter, E., Prudhomme, C., and Salamon, P.: A global streamflow](#)  
1243 [reanalysis for 1980–2018. Journal of Hydrology X, 6, 100049, ISSN 2589-9155,](#)  
1244 <https://doi.org/10.1016/j.hydroa.2019.100049>, 2020. (Available online  
1245 <https://www.sciencedirect.com/science/article/pii/S2589915519300331>, last accessed: 21.01.2024).

1246 [Allen, R. G., Pereira, L. S., Raes, D., and Smith, M.: FAO Irrigation and Drainage Paper No. 56: Crop](#)  
1247 [Evapotranspiration \(guidelines for computing crop water requirements\), 1998. \(Available online:](#)  
1248 [https://www.researchgate.net/publication/284300773\\_FAO\\_Irrigation\\_and\\_drainage\\_paper\\_No\\_56](https://www.researchgate.net/publication/284300773_FAO_Irrigation_and_drainage_paper_No_56), last  
1249 [accessed: 21.02.202301.2024\).](#)

1250 [Balsamo, G.: Interactive lakes in the Integrated Forecasting System. ECMWF Newsletter No. 137 – Autumn 2013,](#)  
1251 [pp. 30–34, 2013. <http://doi:10.21957/rffv1gir30-34>, <https://doi.org/10.21957/rffv1gir>, 2013. \(Available online:](#)  
1252 <https://www.ecmwf.int/en/eLibrary/80145-interactive-lakes-integrated-forecasting-system>, last accessed:  
1253 [21.02.202301.2024\).](#)

1254 [Bates, P. D., and De Roo, A. P. J.: A simple raster-based model for flood inundation simulation. Journal of](#)  
1255 [hydrology, vol. 236, 1-2, 54–77, Elsevier, 2000.236, 1-2, pp. 54–77, ISSN 0022-1694,](#)  
1256 [https://doi.org/10.1016/S0022-1694\(00\)00278-X](https://doi.org/10.1016/S0022-1694(00)00278-X), 2000. (Available online:  
1257 <https://www.sciencedirect.com/science/article/abs/pii/S002216940000278X>, last accessed: 21.01.2024).

1258 [Beck, H. E., van Dijk, A. I. J. M., Larraondo, P. R., McVicar, T. R., Pan, M., Dutra, E., and Miralles, D. G.:](#)  
1259 [MSWX: Global 3-Hourly 0.1° Bias-Corrected Meteorological Data Including Near-Real-Time Updates and](#)  
1260 [Forecast Ensembles. Bulletin of the American Meteorological Society, 103\(3\), pp. E710-E732, 2022.](#)  
1261 <https://doi.org/10.1175/BAMS-D-21-0145.1>, 2022. (Available online:  
1262 <https://journals.ametsoc.org/view/journals/bams/103/3/BAMS-D-21-0145.1.xml>, last accessed:  
1263 [21.02.202301.2024\).](#)

1264 [Belleza, G. A. C., Bierkens, M. F. P., and van Vliet M. T. H.: Sectoral water use responses to droughts and](#)  
1265 [heatwaves: analyses from local to global scales for 1990–2019. Environ. Res. Lett., 18 \(10\), 104008,](#)  
1266 <https://doi.org/10.1088/1748-9326/acf82e>, 2023.

1267 [Best, M. J., Pryor, M., Clark, D. B., Rooney, G. G., Essery, R. L. H., Menard, C. B., Edwards, J. M., Hendry, M.](#)  
1268 [A., Porson, A., Gedney, N., Mercado, L. M., Sitch, S., Blyth, E., Boucher, O., Cox, P. M., Grimmond, C. S. B.,](#)  
1269 [and Harding, R. J.: The Joint UK Land Environment Simulator \(JULES\), model description – Part 1: Energy and](#)  
1270 [water fluxes. Geosci. Model Dev., 4, 677–699, 2011, <https://doi.org/10.5194/gmd-4-677-2011>, 2011. \(Available](#)  
1271 [online: \[www.geosci-model-dev.net/4/677/2011/\]\(http://www.geosci-model-dev.net/4/677/2011/\), last accessed: 21.02.202301.2024\).](#)



1272 Bhardwaj, A.: Evaluation of Openly Accessible MERIT DEM for Vertical Accuracy in Different Topographic  
1273 Regions of India. 39th INCA International Congress, Dehradun (India), vol. 39, pp. 239–245, 2021. (Available  
1274 online:  
1275 [https://www.researchgate.net/publication/356726804\\_Evaluation\\_of\\_openly\\_Accessible\\_MERIT\\_DEM\\_for\\_](https://www.researchgate.net/publication/356726804_Evaluation_of_openly_Accessible_MERIT_DEM_for_vertical_accuracy_in_different_topographic_regions_of_India)  
1276 [vertical\\_accuracy\\_in\\_different\\_topographic\\_regions\\_of\\_India](https://www.researchgate.net/publication/356726804_Evaluation_of_openly_Accessible_MERIT_DEM_for_vertical_accuracy_in_different_topographic_regions_of_India), last accessed: 21.02.202301.2024).

1277 Bonan, G., Levis, S., Sitch, S., Vertenstein, M., and Oleson, K.: A dynamic global vegetation model for use with  
1278 climate models: Concepts and description of simulated vegetation dynamics. *Global Change Biology*, 9, pp. 1543–  
1279 1566, 2003. <https://doi.org/10.1046/j.1365-2486.2003.00681.x>, 2003.

1280 Brooks, R. H., and Corey, A. T.: Hydraulic properties of porous media. Hydrology paper No. 3, Colorado State  
1281 Univ., Fort Collins, 1964.

1282 Buchhorn, M., Smets, B., Bertels, L., De Roo, B., Lesiv, M., Tsendbazar, N.-E., Herold, M., and Fritz, S.:  
1283 Copernicus Global Land Service: Land Cover 100m: collection 3: epoch 2015: Globe (V3.0.1) [Data set]. Zenodo,  
1284 2020. <https://doi.org/10.5281/zenodo.3939038>, 2020.

1285 Buchhorn, M., Smets, B., Bertels, L., De Roo, B., Lesiv, M., Tsendbazar, N.-E., Li, L., and Tarko, A.: Copernicus  
1286 Global Land Service: Land Cover 100m: version 3 Globe 2015-2019: Product User Manual (Dataset v3.0, doc  
1287 issue 3.4). Zenodo, 2021. <https://doi.org/10.5281/zenodo.4723921>, 2021.

1288 Burek, P., Van Der Knijff, J., and De Roo, A.: LISFLOOD – Distributed Water Balance and Flood Simulation  
1289 Model – Revised User Manual. Luxembourg: Publications Office of the European Union, 2013, JRC78917, 2013.  
1290 (Available online: <https://publications.jrc.ec.europa.eu/repository/handle/JRC78917>, last  
1291 accessed: 21.02.202301.2024).

1292 Burek, P., Bianchi, A., and Gentile, A.: JRC Technical Report: A Pan-European Data Set for hydrological  
1293 modelling. Luxembourg: Publications Office of the European Union, 2014.

1294 Büttner, G., and Kosztra, B.: CLC2018 Technical Guidelines, 2017, Environment Agency, Austria, 2017.  
1295 (Available online: [https://land.copernicus.eu/user-corner/technical-](https://land.copernicus.eu/user-corner/technical-library/clc2018technicalguidelines-final.pdf)  
1296 [library/clc2018technicalguidelines-final.pdf](https://land.copernicus.eu/user-corner/technical-library/clc2018technicalguidelines-final.pdf), [https://land.copernicus.eu/en/technical-library/clc-2018-technical-](https://land.copernicus.eu/en/technical-library/clc-2018-technical-guidelines/@/download/file)  
1297 [guidelines/@/download/file](https://land.copernicus.eu/en/technical-library/clc-2018-technical-guidelines/@/download/file), last accessed: 21.02.202301.2024).

1298 Calvin, K., Patel, P., Clarke, L., Asrar, G., Bond-Lamberty, B., Cui, R. Y., Di Vittorio, A., Dorheim, K., Edmonds,  
1299 J., Hartin, C., Hejazi, M., Horowitz, R., Iyer, G., Kyle, P., Kim, S., Link, R., McJeon, H., Smith, S. J., Snyder, A.,  
1300 Waldhoff, S., and Wise, M.: GCAM v5.1: representing the linkages between energy, water, land, climate, and  
1301 economic systems. *Geosci. Model Dev.*, 12, 677–698, 2019. <https://doi.org/10.5194/gmd-12-677-2019>, 2019.

1302 Carver, G.: Ten years of OpenIFS at ECMWF. ECMWF Newsletter No. 170 – Winter 2021/22, pp. 6-7, 2022.  
1303 (Available online: <https://www.ecmwf.int/en/newsletter/170/news/ten-years-openifs-ecmwf>, last accessed:  
1304 21.02.202301.2024).

1305 Chai, L. T., Wong, C. J., James, D., Loh, H. Y., Liew, J. J. F., Wong, W. V. C., and Phua, M. H.: Vertical accuracy  
1306 comparison of multi-source Digital Elevation Model (DEM) with Airborne Light Detection and Ranging  
1307 (LiDAR). *IOP Conf. Ser.: Earth Environ. Sci.*, 1053, 012025, 2022. (Available online:  
1308 <https://iopscience.iop.org/article/10.1088/1755-1315/1053/1/012025/pdf>, last accessed: 21.02.202301.2024).

1309 Clark, D. B., Mercado, L. M., Sitch, S., Jones, C. D., Gedney, N., Best, M. J., Pryor, M., Rooney, G. G., Essery,  
1310 R. L. H., Blyth, E., Boucher, O., Harding, R. J., Huntingford, C., and Cox, P. M.: The Joint UK Land Environment  
1311 Simulator (JULES), model description – Part 2: Carbon fluxes and vegetation dynamics. *Geosci. Model Dev.*, 4,  
1312 701–722, 2011. <https://doi.org/10.5194/gmd-4-701-2011>, 2011. (Available online: [www.geosci-model-](http://www.geosci-model-dev.net/4/701/2011/)  
1313 [dev.net/4/701/2011/](http://www.geosci-model-dev.net/4/701/2011/), last accessed: 21.02.202301.2024).

1314 De Roo, A. P. J., Van Der Knijff, J., Schmuck, G., and Bates, P.: A simple floodplain inundation model to assist  
1315 in floodplain management. *New trends in water and environmental engineering for safety and life: Eco-compatible*  
1316 *solutions for aquatic environments*, 1–10, Balkema, Rotterdam, The Netherlands, 2000.

1317 De Roo, A., Odijk, M., Schmuck, G., Koster, E., and Lucieer, A.: Assessing the effects of land use changes on  
1318 floods in the Meuse and Oder catchment. *Physics and Chemistry of the Earth, Part B: Hydrology, Oceans and*  
1319 *Atmosphere*, vol. 26, 7-8, 593–599, Pergamon, 2001.

1320 Defourny, P., Lamarche, C., Bontemps, S., De Maet, T., Van Bogaert, E., Moreau, I., Brockmann, C., Boettcher,  
1321 M., Kirches, G., Wevers, J., and Santoro, M.: Land Cover CCI PRODUCT USER GUIDE VERSION 2.0 Tech.  
1322 Rep. ESA, 2017. (Available online: [https://maps.elie.ucl.ac.be/CCI/viewer/download/ESACCI-LC-Ph2-](https://maps.elie.ucl.ac.be/CCI/viewer/download/ESACCI-LC-Ph2-PUGv2_2.0.pdf)  
1323 [PUGv2\\_2.0.pdf](https://maps.elie.ucl.ac.be/CCI/viewer/download/ESACCI-LC-Ph2-PUGv2_2.0.pdf), last accessed: 21.02.202301.2024).

1324 Dolan, F., Lamontagne, J., Link, R., Hejazi, M., Reed, P., and Edmonds, J.: *Evaluating the economic impact of*  
1325 *water scarcity in a changing world*. *Nat Commun* 12, 1915, <https://doi.org/10.1038/s41467-021-22194-0>, 2021.

1326 Eerola, K., Rontu, L., Kourzeneva, E., Kheyrollah Pour, H., and Duguay, C.: Impact of partly ice-free Lake  
1327 Ladoga on temperature and cloudiness in an anticyclonic winter situation – a case study using a limited area  
1328 model. *Tellus A*, 66, 23929, 2014. <https://doi.org/10.3402/tellusa.v66.23929>, 2014.

1329 Florczyk, A. J., Corbane, C., Ehrlich, D., Freire, S., Kemper, T., Maffenini, L., Melchiorri, M., Pesaresi, M.,  
1330 Politis, P., Schiavina, M., Sabo, F., and Zanchetta, L., European Commission, Joint Research Centre: GHSL  
1331 Data Package 2019 – Public release GHS P2019, EUR 29788 EN, Publications Office of the European Union,



1332 Luxembourg, 2019, ISBN 978-92-76-13186-1, [JRC 117104](https://data.europa.eu/doi/10.2760/290498), <https://data.europa.eu/doi/10.2760/290498>, [JRC](https://doi.org/10.2760/290498)  
1333 [4471042019](https://doi.org/10.2760/290498).

1334 Fredlund, D.G., and Xing, A.: Equations for the Soil-Water Characteristic Curve. Canadian Geotechnical Journal,  
1335 31, 521–532, 1994. <http://dx.doi.org/10.1139/t94-061>, 1994.

1336 Freire, S., MacManus, K., Pesaresi, M., Doxsey-Whitfield, E., and Mills, J.: Development of new open and free  
1337 multi-temporal global population grids at 250 m resolution. Geospatial Data in a Changing World; Association of  
1338 Geographic Information Laboratories in Europe (AGILE), 2016.

1339 Gardner, W. R.: Calculation of capillary conductivity from pressure plate outflow data. Soil Science Society  
1340 Proceeding, 20(3), pp. 317–320, 1956. <https://doi.org/10.2136/sssaj1956.03615995002000030006x>, 1956.

1341 Google Earth Engine: Frequently Asked Questions (GEE: FAQ), 2023. (Available online:  
1342 <https://earthengine.google.com/faq/>, last accessed: 21.02.202301.2024).

1343 Gilbert, M., Nicolas, G., Cinardi, G., Van Boeckel, T. P., Vanwambeke, S. O., Wint, G. R. W., and Robinson, T.  
1344 P.: Global distribution data for cattle, buffaloes, horses, sheep, goats, pigs, chickens and ducks in 2010. Sci Data  
1345 5, 180227, 2018. <https://doi.org/10.1038/sdata.2018.227>, 2018.

1346 Gorelick, N., Hancher, M., Dixon, M., Ilyushchenko, S., Thau, D., and Moore, R.: Google Earth Engine:  
1347 Planetary-scale geospatial analysis for everyone. Remote Sensing of Environment, vol. 202, pp. 18–27, 2017,  
1348 <https://doi.org/10.1016/j.rse.2017.06.031>, 2017. (Available online:  
1349 <https://www.sciencedirect.com/science/article/pii/S0034425717302900>, last accessed: 21.02.202301.2024).

1350 Grimaldi, S., Salamon, P., Disperati, J., Zsoter, E., Russo, C., Ramos, A., Carton De Wiart, C., Barnard, C.,  
1351 Hansford, E., Gomes, G., and Prudhomme, C.: River discharge and related historical data from the Global Flood  
1352 Awareness System. v4.0. Copernicus Climate Change Service (C3S) Climate Data Store (CDS), 2022.  
1353 <http://10.24381/cds.a4fdd6b9> (Accessed on 21.02.2023) [Data set], <https://doi.org/10.24381/cds.a4fdd6b9>, 2022.  
1354 (Available online: <https://cds.climate.copernicus.eu/cdsapp#!/dataset/10.24381/cds.a4fdd6b9?tab=form>, last  
1355 accessed: 21.01.2024).

1356 Grimaldi, S., and al.: GloFAS v4: towards high resolution modelling of global hydrology. Journal of Hydrology  
1357 X, 2024 in preparation.

1358 Gupta, S., Lehmann, P., Bonetti, S., Papritz, A., and Or, D.: Global prediction of soil saturated hydraulic  
1359 conductivity using random forest in a Covariate-based GeoTransfer Function (CoGTF) framework. Journal of  
1360 Advances in Modeling Earth Systems, 13(4), e2020MS002242, 2021. <https://doi.org/10.1029/2020MS002242>,  
1361 2021.

1362 Harrigan, S., Zsoter, E., Cloke, H., Salamon, P., and Prudhomme, C.: Daily ensemble river discharge reforecasts  
1363 and real-time forecasts from the operational Global Flood Awareness System. Hydrol. Earth Syst. Sci., 27, 1–19,  
1364 2023. <https://doi.org/10.5194/hess-27-1-2023>, 2023. (Available online:  
1365 <https://hess.copernicus.org/articles/27/1/2023/>, last accessed: 21.02.202301.2024).

1366 Hejazi, M., Edmonds, J., Clarke, L., Kyle, P., Davies, E., Chaturvedi, V., Wise, M., Patel, P., Eom, J., and Calvin,  
1367 K., Moss, R., and Kim, S.: Long-term global water projections using six socioeconomic scenarios in an integrated  
1368 assessment modeling framework. Technol. Forecast. Social Change, 81, 205–226, 2014. pp. 205–226,  
1369 <https://doi.org/10.1016/j.techfore.2013.05.006>, 2014. (Available online:  
1370 <https://www.sciencedirect.com/science/article/abs/pii/S0040162513001169>, last accessed: 21.01.2024).

1371 Hengl, T., de Jesus, J. M., MacMillan, R. A., Batjes, N. H., Heuvelink, G. B. M., Ribeiro, E., Samuel-Rosa, A.,  
1372 Kempen, B., Leenaars, J. G. B., Walsh, M. G., and Ruiperez Gonzalez, M.: SoilGrids1km – Global Soil  
1373 Information Based on Automated Mapping. PLOS ONE 9(8): e105992, 2014.  
1374 <https://doi.org/10.1371/journal.pone.0105992>, 2014.

1375 Hengl, T., Mendes-de Jesus, J. M., Heuvelink, G. B. M., Ruiperez Gonzalez, M., Kilibarda, M., Blagotić, A.,  
1376 Shangguan, W., Wright, M. N., Geng, X., Bauer-Marschallinger, B., Guevara, M. A., Vargas, R., MacMillan, R.  
1377 A., Batjes, N. H., Leenaars, J. G. B., Ribeiro, E., Wheeler, I., Mantel, S., and Kempen, B.: SoilGrids250m: Global  
1378 gridded soil information based on machine learning. PLOS ONE 12(2): 1–40,  
1379 <https://doi.org/10.1371/journal.pone.0169748>, 2017. doi:10.1371/journal.pone.0169748

1380 Hirpa, F. A., Salamon, P., Beck, H. E., Lorini, V., Alfieri, L., Zsoter, E., and Dadson, S. J.: Calibration of the  
1381 Global Flood Awareness System (GloFAS) using daily streamflow data. Journal of Hydrology, vol. 566, 595–  
1382 606, 2018. <https://doi.org/10.1016/j.jhydrol.2018.09.052>, 2018.

1383 Hodnett, M. G., and Tomasella, J.: Marked differences between van Genuchten soil water-retention parameters  
1384 for temperate and tropical soils: a new water-retention pedo-transfer functions developed for tropical soils.  
1385 Geoderma, vol. 108 (3-4), pp. 155–180, ISSN 0016-7061, 2002. [https://doi.org/10.1016/S0016-7061\(02\)00105-](https://doi.org/10.1016/S0016-7061(02)00105-2)  
1386 [2](https://doi.org/10.1016/S0016-7061(02)00105-2), 2002.

1387 Huang, Z., Hejazi, M., Li, X., Tang, Q., Vernon, C., Leng, G., Liu, Y., Döll, P., Eisner, S., Gerten, D., Hanasaki,  
1388 N., and Wada, Y.: Reconstruction of global gridded monthly sectoral water withdrawals for 1971–2010 and  
1389 analysis of their spatiotemporal patterns. Hydrol. Earth Syst. Sci., 22, 2117–2133, [https://doi.org/10.5194/hess-](https://doi.org/10.5194/hess-22-2117-2018)  
1390 [22-2117-2018](https://doi.org/10.5194/hess-22-2117-2018), 2018.

1391 Huijnen, V., Le Sager, P., Köhler, M. O., Carver, G., Rémy, S., Flemming, J., Chabrillat, S., Errera, Q., and van  
1392 Noije, T.: OpenIFS/AC: atmospheric chemistry and aerosol in OpenIFS 43r3. *Geosci. Model Dev.*, 15, 6221–  
1393 6241, 2022, <https://doi.org/10.5194/gmd-15-6221-2022>, 2022.

1394 International Food Policy Research Institute (IFPRI): Global Spatially-Disaggregated Crop Production Statistics  
1395 Data for 2010 Version 2.0 [Data set]. Harvard Dataverse, 2019. doi:10.7910/DVN/PRFF8V (Available online:  
1396 <https://doi.org/10.7910/DVN/PRFF8V>, 2019. (Available online:  
1397 <https://dataverse.harvard.edu/dataset.xhtml?persistentId=doi:10.7910/DVN/PRFF8V>, last  
1398 21.02.202301.2024).

1399 Intara, Y. I., Nusantara, A. D., Supanjani, Caniago, Z., and Ekawita, R.: Oil Palm Roots Architecture in Response  
1400 to Soil Humidity. *International Journal of Oil Palm Vol. 1, Nr. 2, ISSN: 2614-2376*, 2018. (Available online:  
1401 <https://ijop.id/index.php/ijop/article/view/11/10>, last accessed: 21.02.202301.2024).

1402 Karabulut, A., Egoh, B. N., Lanzanova, D., Grizzetti, B., Bidoglio, G., Pagliero, L., Bouraoui, F., Aloe, A.,  
1403 Reynaud, A., Maes, J., Vandecasteele, I., and Mubareka, S.: Mapping water provisioning services to support the  
1404 ecosystem–water–food–energy nexus in the Danube river basin. *Ecosystem Services*, 17, 278–292,  
1405 <https://doi.org/10.1016/j.ecoser.2015.08.002>, 2016. (Available online:  
1406 <https://www.sciencedirect.com/science/article/pii/S221204161530019X>, last accessed: 21.01.2024).

1407 Karsenberg, D., Schmitz, O., Salamon, P., de Jong, K., and Bierkens, M. F. P.: A software framework for  
1408 construction of process-based stochastic spatio-temporal models and data assimilation. *Environmental Modelling*  
1409 & Software, 25(4), pp. 489–502, 2010. <https://doi.org/10.1016/j.envsoft.2009.10.004>, 2010.

1410 Kimpson, T., Choulga, M., Chantry, M., Balsamo, G., Boussetta, S., Dueben, P., and Palmer, T.: Deep learning  
1411 for quality control of surface physiographic fields using satellite Earth observations. *Hydrol. Earth Syst. Sci.*,  
1412 Learning for Verification of Earth System Parametrisation of Water Bodies. *EGUsphere*, vol. 2022, 1–34, 2023,  
1413 doi:10.5194/egusphere-2022-1177 (Available online: [https://egusphere.copernicus.org/preprints/egusphere-](https://egusphere.copernicus.org/preprints/egusphere-2022-1177/)  
1414 <https://doi.org/10.5194/hess-27-4661-2023>, 2023.  
1415 Köhler, M. O., Hill, A. A., Huijnen, V., and Le Sager, P.: Enhancing OpenIFS by adding atmospheric composition  
1416 capabilities. *ECMWF Newsletter No. 175 – Spring 2023*, pp. 27-31, 2023. <http://doi.org/10.21957/np36mk1s9d>,  
1417 2023. (Available online: [https://www.ecmwf.int/en/newsletter/175/earth-system-science/enhancing-openifs-](https://www.ecmwf.int/en/newsletter/175/earth-system-science/enhancing-openifs-adding-atmospheric-composition)  
1418 [adding-atmospheric-composition](https://www.ecmwf.int/en/newsletter/175/earth-system-science/enhancing-openifs-adding-atmospheric-composition), last accessed: 21.02.202301.2024).

1419 Kohli, A., Frenken, K., and Spottorno, C.: Disambiguation of water statistics. *FAO AQUASTAT Report*,  
1420 *AQUASTAT Programme*, FAO, pp. 1-6, 2012. (Available online: <https://www.fao.org/3/bc816e/bc816e.pdf>, last  
1421 21.02.202301.2024).

1422 Laborte, A. G., Gutierrez, M. A., Balanza, J. G., Saito, K., Zwart, S. J., Boschetti, M., Murty, M. V. R., Villano,  
1423 L., Aunario, J. K., Reinke, R., Koo, J., Hijmans, R. J., and Nelson, A.: RiceAtlas, a spatial database of global rice  
1424 calendars and production [Data set]. *Harvard Dataverse*, V3, 2017a. <https://doi.org/10.7910/DVN/JE6R2R>,  
1425 2017a.

1426 Laborte, A. G., Gutierrez, M. A., Balanza, J. G., Saito, K., Zwart, S. J., Boschetti, M., Murty, M. V. R., Villano,  
1427 L., Aunario, J. K., Reinke, R., Koo, J., Hijmans, R. J., and Nelson, A.: RiceAtlas, a spatial database of global rice  
1428 calendars and production. *Sci Data.*, 4:170074, PMID: 28556827, PMCID: PMC5448352, 2017b.  
1429 <https://doi.org/10.1038/sdata.2017.74>, 2017b. (Available  
1430 <https://www.ncbi.nlm.nih.gov/pmc/articles/PMC5448352/>, last accessed: 21.02.202301.2024).

1431 Lawrence, D. M., Fisher, R. A., Koven, C. D., Oleson, K. W., Swenson, S. C., Bonan, G., Collier, N., Ghimire,  
1432 B., van Kampenhout, L., Kennedy, D., Kluzek, E., Lawrence, P. J., Li, F., Li, H., Lombardozzi, D., Riley, W. J.,  
1433 Sacks, W. J., Shi, M., Vertenstein, M., Wieder, W. R., Xu, C., Ali, A. A., Badger, A. M., Bisht, G., van den  
1434 Broeke, M., Brunke, M. A., Burns, S. P., Buzan, J., Clark, M., Craig, A., Dahlin, K., Drewniak, B., Fisher, J. B.,  
1435 Flanner, M., Fox, A. M., Gentine, P., Hoffman, F., Keppel-Aleks, G., Knox, R., Kumar, S., Lenaerts, J., Leung,  
1436 L. R., Lipscomb, W. H., Lu, Y., Pandey, A., Pelletier, J. D., Perket, J., Randerson, J. T., Ricciuto, D. M.,  
1437 Sanderson, B. M., Slater, A., Subin, Z. M., Tang, J., Thomas, R. Q., Val Martin, M., and Zeng, X.: The Community  
1438 Land Model version 5: Description of new features, benchmarking, and impact of forcing uncertainty. *Journal of*  
1439 *Advances in Modeling Earth Systems*, 11(12), pp. 4245-4287, 2019. [https://doi-](https://doi.org/10.1029/2018MS001583)  
1440 [org.euiacar.idm.oclc.org/10.1029/2018MS001583](https://doi.org/10.1029/2018MS001583), 2019.

1441 Lehner, B., and Döll, P.: Development and validation of a global database of lakes, reservoirs and wetlands.  
1442 *Journal of Hydrology*, vol. 296-(1-4), pp. 1–22, <https://doi.org/10.1016/j.jhydrol.2004.03.028>, 2004. (Available  
1443 online: <http://dx.doi.org/10.1016/j.jhydrol.2004.03.028>, last accessed: 21.02.202301.2024).

1444 Lv, S., Zeng, Y., Wen, J., Zhao, H., and Su, Z.: Estimation of Penetration Depth from Soil Effective Temperature  
1445 in Microwave Radiometry. *Remote Sens.*, vol. 10(4), 519, 2018. <https://doi.org/10.3390/rs10040519>, 2018.

1446 Marthews, T. R., Dadson, S. J., Clark, D. B., Blyth, E. M., Hayman, G. D., Yamazaki, D., Becher, O. R. E.,  
1447 Martinez-de la Torre, A., Prigent, C., and Jimenez, C.: Inundation prediction in tropical wetlands from JULES-  
1448 CaMa-Flood global land surface simulations. *Hydrology and Earth System Sciences*, vol. 26-(12), 3151–3175,  
1449 2022. <https://doi.org/10.5194/hess-26-3151-2022>, 2022. (Available  
1450 <https://hess.copernicus.org/articles/26/3151/2022/>, last accessed: 21.02.202301.2024).

1451 Martínez-Sánchez, E.: Scientific Quality Evaluation of LAI/FAPAR/FCOVER Collection 1km Version 1 and  
1452 Version 2 Issue 11.00, 2020. (Available online: [https://land.copernicus.eu/global/sites/cgls.vito.be/files/products/CGLOPS1\\_SOE2019\\_LAI1km-](https://land.copernicus.eu/global/sites/cgls.vito.be/files/products/CGLOPS1_SOE2019_LAI1km-V1%26V2_11.00.pdf)  
1453 [V1%26V2\\_11.00.pdf](https://land.copernicus.eu/global/sites/cgls.vito.be/files/products/CGLOPS1_SOE2019_LAI1km-V1%26V2_11.00.pdf), last accessed: 21.02.202301.2024).

1454 <https://doi.org/10.1029/2020WR027751>, 2021.

1455 <https://doi.org/10.1029/2020WR027751>, 2021.

1456 <https://doi.org/10.1029/2020WR027751>, 2021.

1457 <https://doi.org/10.1029/2020WR027751>, 2021.

1458 Moiret-Guigand, A.: Copernicus Land monitoring services – CLC2018 / CLCC1218 VALIDATION REPORT,  
1459 Issue 1.3, 2021 (Available online: [https://land.copernicus.eu/user-corner/technical-library/clc-2018-and-clc-](https://land.copernicus.eu/user-corner/technical-library/clc-2018-and-clc-change-2012-2018-validation-report-view/@@download/file)  
1460 [change-2012-2018-validation-report-view/@@download/file](https://land.copernicus.eu/user-corner/technical-library/clc-2018-and-clc-change-2012-2018-validation-report-view/@@download/file), last accessed: 21.02.202301.2024).

1461 Notaro, M., Holman, K., Zarrin, A., Fluck, E., Vavrus, S., and Bennington, V.: Influence of the Laurentian Great  
1462 Lakes on Regional Climate. *J. Climate*, 26,(3), pp. 789–804, <https://doi.org/10.1175/JCLI-D-12-00140.1>, 2013.

1463 O’Callaghan, J. F., and Mark, D. M.: The Extraction of Drainage Networks from Digital Elevation Data.  
1464 *Computer Vision, Graphics, and Image Processing*, 28,(3), pp. 323–344, 1984.  
1465 [https://doi.org/10.1016/S0734-189X\(84\)80011-0](https://doi.org/10.1016/S0734-189X(84)80011-0), 1984.

1466 Pesaresi, M., and Politis, P.: [GHS-BUILT-S R2022A](https://doi.org/10.2905/D07D81B4-7680-4D28-B896-583745C27085) - GHS built-up surface grid, derived from Sentinel2  
1467 composite and Landsat, multitemporal (1975-2030) [Data set]. European Commission, Joint Research Centre  
1468 (JRC), 2022, <https://doi.org/10.2905/D07D81B4-7680-4D28-B896-583745C27085>, 2022. (Available online:  
1469 <http://data.europa.eu/89h/d07d81b4-7680-4d28-b896-583745c27085>, last accessed:  
1470 <http://data.europa.eu/89h/d07d81b4-7680-4d28-b896-583745c27085>,  
1471 21.02.202301.2024).

1472 Rosbjerg, D., and Madsen, H.: Concepts of hydrologic modeling. In *Encyclopedia of Hydrological Sciences* (eds  
1473 M.G. Anderson and J.J. McDonnell), 10, 1–9, 2005,  
1474 <https://doi.org/10.1002/0470848944.hsa009>, 2006.

1475 Samuelsson, P., Kourzeneva, E., and Mironov, D.: The impact of lakes on the European climate as simulated by  
1476 a regional climate model. *Boreal Environ. Res.*, 15, 113–129, 2010, *Res.*, 15(2), pp. 113–129,  
1477 <http://hdl.handle.net/10138/233079>, 2010. (Available online:  
1478 <https://helda.helsinki.fi/server/api/core/bitstreams/feb9f8de-e831-4e9e-9ee6-07ac7df898eb/content>, last  
1479 accessed: 21.01.2024).

1480 Schiavina, M., Freire, S., and MacManus, K.: [GHS-POP R2019A](https://doi.org/10.2905/42E8BE89-54FF-464E-BE7B-BF9E64DA5218) - GHS population grid multitemporal (1975,  
1481 1990, 2000, 2015) [R2019A](https://doi.org/10.2905/42E8BE89-54FF-464E-BE7B-BF9E64DA5218)). European Commission, Joint Research Centre (JRC), 2019. [Data set],  
1482 <https://doi.org/10.2905/42E8BE89-54FF-464E-BE7B-BF9E64DA5218>, PID:  
1483 <http://data.europa.eu/89h/0c6b9751-a71f0c6b9751-a71f-4062-830b-43c9f432370f>

1484 ~~Vassolo, S., and Döll, P.: Global scale gridded estimates of thermoelectric power and manufacturing water use.~~  
1485 ~~*Water Resour. Res.*, 41, 2005-830B-43C9F432370F, 2019. (Available online:~~  
1486 ~~<https://doi.org/10.1029/2004WR003360>~~[https://data.jrc.ec.europa.eu/dataset/0c6b9751-a71f-4062-830b-](https://data.jrc.ec.europa.eu/dataset/0c6b9751-a71f-4062-830b-43c9f432370f)  
1487 ~~[43c9f432370f](https://data.jrc.ec.europa.eu/dataset/0c6b9751-a71f-4062-830b-43c9f432370f), last accessed: 21.01.2024).~~

1488 Schiavina, M., Melchiorri, M., Pesaresi, M., Politis, P., Freire, S., Maffenini, L., Florio, P., Ehrlich, D., Goch, K.,  
1489 Tommasi, P., and Kemper, T., European Commission, Joint Research Centre: [GHSL Data Package 2022 – Public](https://doi.org/10.2760/19817)  
1490 [release GHSL P2022](https://doi.org/10.2760/19817), Publication Office of the European Union, JRC 129516, ISBN 978-92-76-53071-8,  
1491 <https://doi.org/10.2760/19817>, 2022, [doi:10.2760/19817](https://doi.org/10.2760/19817).

1492 Smets, B.: Product User Manual of LAI/FAPAR/FCOVER Collection 1km Version 2 Issue 1.33, 2019. (Available  
1493 online: [https://land.copernicus.eu/global/sites/cgls.vito.be/files/products/CGLOPS1\\_PUM\\_LAI1km-](https://land.copernicus.eu/global/sites/cgls.vito.be/files/products/CGLOPS1_PUM_LAI1km-V2_11.33.pdf)  
1494 [V2\\_11.33.pdf](https://land.copernicus.eu/global/sites/cgls.vito.be/files/products/CGLOPS1_PUM_LAI1km-V2_11.33.pdf), last accessed: 21.02.202301.2024).

1495 Smith, P. J., Pappenberger, F., Wetterhall, F., Del Pozo, J. T., Krzeminski, B., Salamon, P., Muraro, D., Kalas,  
1496 M., and Baugh, C.: On the operational implementation of the European Flood Awareness System (EFAS). *Flood*  
1497 *forecasting: A Global Perspective*, Academic Press, pp. 313–348, [https://doi.org/10.1016/B978-0-12-801884-](https://doi.org/10.1016/B978-0-12-801884-2.00011-6)  
1498 [2.00011-6](https://doi.org/10.1016/B978-0-12-801884-2.00011-6), 2016.

1499 Sparrow, S., Bowery, A., Carver, G. D., Köhler, M. O., Ollinaho, P., Pappenberger, F., Wallom, D., and  
1500 Weisheimer, A.: OpenIFS@home version 1: a citizen science project for ensemble weather and climate  
1501 forecasting. *Geosci. Model Dev.*, 14,(6), 3473–3486, 2021, <https://doi.org/10.5194/gmd-14-3473-2021>, 2021.

1502 Supit, I., Hoojer, A. A., and Van Diepen, C. A.: System description of the Wofost 6.0 crop simulation model  
1503 implemented in CGMS. Volume 1: Theory and Algorithms, 1994. (Available online:  
1504 <https://www.researchgate.net/publication/282287246> System description of the Wofost 60 crop simulation  
1505 [model implemented in CGMS Volume 1 Theory and Algorithms](https://www.researchgate.net/publication/282287246), last accessed: 21.02.202301.2024).

1506 Te Chow, V.: Open-channel Hydraulics. Civil engineering series (publisher McGraw-Hill, [isbn 9780070859067](https://books.google.co.uk/books?id=sL4\AAAAIAAJ)  
1507 [Book Company Inc.](https://books.google.co.uk/books?id=sL4\AAAAIAAJ)), ISBN 07-010776-9, 1959. <https://books.google.co.uk/books?id=sL4\AAAAIAAJ>  
1508 (Available online: [http://web.ipb.ac.id/~erizal/hidrolika/Chow%20-](http://web.ipb.ac.id/~erizal/hidrolika/Chow%20-%20OPEN%20CHANNEL%20HYDRAULICS.pdf)  
1509 [%20OPEN%20CHANNEL%20HYDRAULICS.pdf](http://web.ipb.ac.id/~erizal/hidrolika/Chow%20-%20OPEN%20CHANNEL%20HYDRAULICS.pdf), [https://heidarpour.iut.ac.ir/sites/heidarpour.iut.ac.ir/files/u3](https://heidarpour.iut.ac.ir/sites/heidarpour.iut.ac.ir/files/u32/open-chow.pdf)  
1510 [2/open-chow.pdf](https://heidarpour.iut.ac.ir/sites/heidarpour.iut.ac.ir/files/u32/open-chow.pdf), last accessed: 21.02.202301.2024).



- 1511 Tóth, B., Weynants, M., Nemes, A., Makó, A., Bilas, G., and Tóth, G.: New generation of hydraulic pedotransfer  
 1512 functions for Europe. *Eur J Soil Sci*, 66;(1), pp. 226-238, <https://doi.org/10.1111/ejss.12192>, 2015.  
 1513 <https://doi.org/10.1111/ejss.12192>
- 1514 Van Der Knijff, J., and De Roo, A.: LISFLOOD – Distributed Water Balance and Flood Simulation Model,  
 1515 Revised User Manual. EUR 22166 EN/2, Office for Official Publications of the European Communities,  
 1516 Luxembourg, 109 pp, 2008.
- 1517 Van Der Knijff, J. M., Younis, J., and De Roo, A. P. J.: LISFLOOD: A GIS-based distributed model for river  
 1518 basin scale water balance and flood simulation. *Int. J. Geogr. Inf. Sci.*, 24(2), 189–212, 2010.
- 1519 van Genuchten, M. T.: A closed-form equation for predicting the hydraulic conductivity of unsaturated soils. *Soil*  
 1520 *Sci. Soc. Am. J.*, 44, 892–898, 1980.
- 1521 Vanham, D., Alfieri, L., Flörke, M., Grimaldi, S., Lorini, V., De Roo, A., and Feyen, L.: The number of people  
 1522 exposed to water stress in relation to how much water is reserved for the environment: a global modelling study.  
 1523 *The Lancet Planetary Health*, vol. 5(11), pp. e766–e774, 2021, [https://doi.org/10.1016/S2542-5196\(21\)00234-5](https://doi.org/10.1016/S2542-5196(21)00234-5),  
 1524 2021. (Available online: <https://www.sciencedirect.com/science/article/pii/S2542519621002345>, last accessed:  
 1525 21.02.2024).
- 1526 Vassolo, S. and Döll, P.: Global-scale gridded estimates of thermoelectric power and manufacturing water use.  
 1527 *Water Resour. Res.* 41(4), <https://doi.org/10.1029/2004WR003360>, 2005.
- 1528 Vavrus, S., Notaro, M., and Zarrin, A.: The role of ice cover in heavy lake-effect snowstorms over the Great Lakes  
 1529 Basin as simulated by RegCM4. *Mon. Weather Rev.*, 141, 148–165, 2013.
- 1530 Voisin, N., Liu, L., Hejazi, M., Tesfa, T., Li, H., Huang, M., Liu, Y., and Leung, L. R.: One-way coupling of an  
 1531 integrated assessment model and a water resources model: evaluation and implications of future changes over the  
 1532 US Midwest. *Hydrol. Earth Syst. Sci.*, 17;(11), 4555–4575, <https://doi.org/10.5194/hess-17-4555-2013>, 2013.
- 1533 Wada, Y., van Beek, L. P. H., Viviroli, D., Dürr, H. H., Weingartner, R., and Bierkens, M. F. P.: Global monthly  
 1534 water stress: 2. Water demand and severity of water stress. *Water Resour. Res.*, 47;(7), W07518,  
 1535 [doi:10.1029/2010WR009792](https://doi.org/10.1029/2010WR009792), <https://doi.org/10.1029/2010WR009792>, 2011.
- 1536 Yamazaki, D., Oki, T., and Kanae, S.: Deriving a global river network map and its sub-grid topographic  
 1537 characteristics from a fine-resolution flow direction map. *Hydrol. Earth Syst. Sci.*, 13(11), 2241–2251,  
 1538 <https://doi.org/10.5194/hess-13-2241-2009>, 2009. ~~*Sci.*, 13, 2241–2251, 2009. doi:10.5194/hess-13-2241-2009.~~
- 1539 Yamazaki, D., Kanae, S., Kim, H., and Oki, T.: A physically based description of floodplain inundation dynamics  
 1540 in a global river routing model. *Water Resour. Res.*, 47, W04501, 2011. [doi:10.1029/2010WR009726](https://doi.org/10.1029/2010WR009726). *Res.*, 47(4),  
 1541 W04501, <https://doi.org/10.1029/2010WR009726>, 2011.
- 1542 Yamazaki, D., Ikeshima, D., Tawatari, R., Yamaguchi, T., O'Loughlin, F., Neal, J. C., Sampson, C. C., Kanae, S.,  
 1543 and Bates, P. D.: A high-accuracy map of global terrain elevations. *Geophys. Res. Lett.*, 44;(11), pp. 5844–5853,  
 1544 <https://doi.org/10.1002/2017GL072874>, 2017. ~~<https://doi.org/10.1002/2017GL072874>.~~
- 1545 Yamazaki, D., Ikeshima, D., Sosa, J., Bates, P. D., Allen, G. H., and Pavelsky, T. M.: MERIT Hydro: A high-  
 1546 resolution global hydrography map based on latest topography datasets. *Water Resources Research*, vol. 55;(6),  
 1547 pp. 5053–5073, 2019. [doi:10.1029/2019WR024873](https://doi.org/10.1029/2019WR024873) (Available online: <https://doi.org/10.1029/2019WR024873>,  
 1548 last accessed: 21.02.2023). 2019.
- 1549 Yu, Q., You, L., Wood-Sichra, U., Ru, Y., Joglekar, A. K. B., Fritz, S., Xiong, W., Lu, M., Wu, W., and Yang,  
 1550 P.: A cultivated planet in 2010 – Part 2: The global gridded agricultural-production maps. *Earth Syst. Sci. Data*,  
 1551 12;(4), 3545–3572, 2020. <https://doi.org/10.5194/essd-12-3545-2020>,  
 1552 2020.
- 1553 Zhang, Y., and Schaap, M. G.: Estimation of saturated hydraulic conductivity with pedotransfer functions: A  
 1554 review. *Journal of Hydrology*, vol. 575, pp. 1011–1030, ISSN 0022-1694, 2019.  
 1555 <https://doi.org/10.1016/j.jhydrol.2019.05.058> <https://doi.org/10.1016/j.jhydrol.2019.05.058>, 2019.
- 1556 **Annex**
- 1557 **Annex** Zhang, J., Liu, D., Guo, S., Xiong, L., Liu, P., Chen, J., and Yin, J.: High resolution annual irrigation  
 1558 water use maps in China based-on input variables selection and convolutional neural networks. *Journal of Cleaner*  
 1559 *Production*, 405, 136974, <https://doi.org/10.1016/j.jclepro.2023.136974>, 2023. (Available online:  
 1560 <https://www.sciencedirect.com/science/article/pii/S0959652623011320>, last accessed: 21.01.2024).

1561 **Appendix**

1562 **Appendix 1**

1563 All data sources used to produce dataset's surface fields, mentioned in Sections 3 to 9, are described here. All data  
1564 considered were open source, freely available, updated as recently as possible, with recognised reference on their  
1565 quality.

1566 **1.1 Catchment morphology and river network**

1567 **The MERIT DEM: Multi-Error-Removed Improved-Terrain Digital Elevation Model v.1.0.3 [15 October,**  
1568 **2018]** (further referred as MERIT DEM) is a high accuracy global DEM at 3 arc second resolution (~90 m at the  
1569 equator) covering land area from 90 N to 60 S, selected for its ability to clearly represent landscapes such as river  
1570 networks and hill-valley structures even in flat areas where height errors could be larger than topography  
1571 variability (Yamazaki et al., 2017; Bhardwaj, 2021; Chai et al., 2022). It is derived from seven different open-  
1572 source datasets, delivered as 57 GeoTiff files 30° by 30° region each, at ~90 m resolution (in total 90.0 GB),  
1573 representative of the year 2018. More detail on method, data content and access can be found in Yamazaki et al.  
1574 (2017) and MERIT DEM web-page [http://hydro.iis.u-tokyo.ac.jp/~yamadai/MERIT\\_DEM](http://hydro.iis.u-tokyo.ac.jp/~yamadai/MERIT_DEM).  
1575 The MERIT DEM was used to compute standard deviation of elevation, gradient and channel geometry fields.

1577 **The Catchment-based Macro-scale Floodplain (CaMa-Flood) Global River Hydrodynamics Model v4.0**  
1578 **maps** (further referred as CaMa-Flood) are used for the basic maps describing all physical properties of the river  
1579 network. It is derived from MERIT Hydro (MERIT Hydro is a global hydrography dataset, created by using  
1580 elevation (i.e. MERIT DEM) and several inland water maps; more detail can be found in Yamazaki et al. (2019)  
1581 and MERIT Hydro web-page [http://hydro.iis.u-tokyo.ac.jp/~yamadai/MERIT\\_Hydro](http://hydro.iis.u-tokyo.ac.jp/~yamadai/MERIT_Hydro)) for high resolution river  
1582 routing applications using the FLOW algorithm (Yamazaki et al., 2009; Yamazaki et al., 2011). The maps include  
1583 information on channel length, river topography parameters, floodplain elevation profile, channel width and  
1584 channel depth. The maps exist at 15, 6, 5, 3 and 1 arc min resolutions covering land area from 90 N to 60 S,  
1585 representative of the year 2017, and for each resolution, they are available as one single file with all variables in  
1586 NetCDF format (for 1 arc min 737.0 MB). More detail on method, data content and access can be found in  
1587 Yamazaki et al. (2011) and CaMa-Flood web-page [http://hydro.iis.u-tokyo.ac.jp/~yamadai/cama-](http://hydro.iis.u-tokyo.ac.jp/~yamadai/cama-flood/index.html)  
1588 [flood/index.html](http://hydro.iis.u-tokyo.ac.jp/~yamadai/cama-flood/index.html). Note that whilst the CaMaFlood maps were originally generated for the specific use of the  
1589 CaMa-Flood model, they can also serve as basic to derive alternative maps for other environmental models, as  
1590 done here.

1591 The CaMa-Flood maps were used to create the local drainage direction (LDD), upstream [drainage area](#), [channel](#)  
1592 [geometry](#) and [land masks](#) fields.

1593 **1.2 Land use fields**

1594 **The Copernicus Global Land Service (CGLS) Land Cover (LC) 100m map** (further referred as CGLS-LC100)  
1595 is a global land cover map of the year 2015 (Buchhorn et al., 2020). It is derived from the PROBA-V 100 m  
1596 satellite image collection, a database of high quality land cover training sites and ancillary datasets, reaching an  
1597 accuracy of 80 % at Level1 (Buchhorn et al., 2021). It contains 23 classes for discrete classification and 10 classes  
1598 for continuous cover fractions; and it is delivered as 15 files in GeoTiff format (in total 39.3 GB) at 100 m  
1599 resolution covering land area from 90 N to 60 S and representative of the year 2015. More detail on method, data  
1600 content and access can be found in Buchhorn et al. (2021) and Copernicus web-site  
1601 <https://land.copernicus.eu/global/products/lc>.

1602 The CGLS-LC100 was used to generate crop parameters and Manning's surface roughness coefficient for forest  
1603 and other land cover types, to generate forest, inland water, and sealed surface fraction fields, following a basic  
1604 quality check on large water bodies (i.e. correcting Fox Basin and Caspian Sea).

1606 **The Coordination of Information on the Environment (CORINE) Land Cover (CLC) inventory for 2018**  
1607 (further referred as CLC2018) is a set of maps describing the land cover/ land use status of 2018 covering  
1608 39 countries in Europe with a total area of over 5.8 Mkm<sup>2</sup>. The dataset is derived from satellite imagery (mainly  
1609 Sentinel-2, based on a constellation of two satellites orbiting Earth at altitude of 786 km 180° apart revisiting  
1610 equator every 5 days, and for gap filling Landsat-8, making a constellation together with Landsat-9 satellite  
1611 orbiting Earth at altitude of 705 km each revisiting equator every 16 days) and in-situ data and contains 44 classes,  
1612 delivered as one GeoTiff raster file (125.0 MB) at 100m resolution covering land area over Europe, representative  
1613 of the time period 2017-2018. The overall accuracy for CLC2018 is 92 % for the blind analysis (i.e. validation  
1614 team had no knowledge of the CLC2018 thematic classes) but there are regional variations: the Black Sea



1615 geographical region has the lowest accuracy of 84 %; country-wise overall accuracy vary from 86 % for Portugal  
1616 to 99 % for Iceland, lowest accuracy being linked to the landscape complexity (Moiret-Guigand, 2021). More  
1617 detail on method, data content and access can be found in Büttner and Kosztra (2017) and Moiret-Guigand (2021),  
1618 and Copernicus web-site <https://land.copernicus.eu/pan-european/corine-land-cover/clc2018>.  
1619 The CLC2018 was used to generate the irrigated crop fraction and rice fraction fields.

1620  
1621 **The Spatial Production Allocation Model (SPAM) – Global Spatially-Disaggregated Crop Production**  
1622 **Statistics Data for 2010 v2.0** (further referred as SPAM2010) is a global dataset generated in 2020, which  
1623 redistributes crop production information from country and sub-national provinces level to a finer grid cell level  
1624 (IFPRI, 2019). It is derived from numerous data sources, including crop production statistics, cropland data,  
1625 biophysical crop “suitability” assessments, spatial distribution of specific crops or crop systems, and population  
1626 density. SPAM2010 contains estimates of crop distributions within disaggregated units (based on a cross-entropy  
1627 approach) for 42 crops and two production systems (irrigated and rainfed), and is delivered as 84 files in shapefile  
1628 format at 10 km (5 arc min) resolution covering land area from 90 N to 60 S and representative of the year 2010  
1629 (in total 2.2 GB). Based on crop expert judgement from international (i.e. International Rice Research Institute,  
1630 International Maize and Wheat Improvement Center) and national organisations (i.e. The Chinese Academy of  
1631 Agricultural Sciences) SPAM2010 over Europe and America is more accurate than over Africa and South East  
1632 Asia, with best performance in allocating rice; grid-by-grid comparison of crop areas with independent Cropland  
1633 Data Layer (produced by using satellite images and vast amount of ground truth) over continental United States  
1634 shows coefficient of determination ( $R^2$ ) 0.7-0.9 and root mean square error (RMSE) 231-307 ha indicating a  
1635 relatively high reliability, with highest  $R^2$  and lowest RMSE values are for maize and soybean (Yu et al., 2020).  
1636 More detail on method, data content and access can be found in Yu et al. (2020) and MapSPAM web-site  
1637 <https://mapspam.info>.  
1638 SPAM2010 was used to compute the irrigated crop and rice fractions, crop parameters and Manning’s surface  
1639 roughness coefficient for irrigated crop fields.

### 1640 **1.3 Vegetation properties**

1641 **The Food and Agriculture Organisation (FAO) of the United Nations Irrigation and Drainage Paper No.**  
1642 **56** (further referred as FAO56) is a publication covering geographically referenced statistics for crop development  
1643 stages, crop coefficients, crop height, rooting depth, and soil water depletion fraction for common crops found  
1644 across the world; it also covers procedures for information aggregation, e.g. on the grid. It is delivered as an article  
1645 with a set of tables and equations and can be considered as the most complete source of information on crop  
1646 properties. More detail on method and data content can be found in Allen et al. (1998) and FAO online crop  
1647 information web-page <http://www.fao.org/land-water/databases-and-software/crop-information/tobacco/en/>.  
1648 FAO56 was used to compute the crop coefficients for forest, irrigated crops and other land cover types (online  
1649 crop information was specifically used for tobacco); and for intermediate computations such as depletion fraction  
1650 for different crop and surface types (table), crop height and root depth fields.

1651  
1652 Intara et al. (2018) is a publication covering oil palm roots architecture.  
1653 Intara et al. (2018) was used for oil palm root depth information in addition to FAO56.

1654  
1655 Burek et al. (2014) is a publication covering summarised information for crop coefficients, rooting depth, crop  
1656 group number and Manning’s surface roughness coefficient for different surface types.  
1657 Burek et al. (2014) was used for built-up, bare/ sparse vegetation, snow & ice, permanent inland water, ocean &  
1658 seas, herbaceous wetland, moss & lichen surface types crop coefficients, rooting depth, crop group number and  
1659 Manning’s surface roughness coefficient information in addition to FAO56 and other sources.

1660  
1661 **The Wofost 6.0 crop simulation model description** (further referred as SUPIT) is a publication on developing,  
1662 validating, and testing new or already existing agrometeorological models (Supit et al., 1994). It contains crop  
1663 group information for several crops as examples, and relation of a crop group from water depletion fraction. The  
1664 publication is delivered as a book with a set of tables and equations. Information on crop group is still considered  
1665 up-to-date. More detail on method and data content can be found in Supit et al. (1994).  
1666 SUPIT was used to compute the crop group fields for forest, irrigated crops and other land cover types.

1667  
1668 **The Open-Channel Hydraulics manual** (further referred as CHOW) is a publication on open-channel  
1669 hydraulics, including basic principles and different types of flows, i.e. uniform, gradually varied, rapidly varied,  
1670 and unsteady (Te Chow, 1959). It contains information on roughness coefficient over different surfaces. The  
1671 publication is delivered as a book with a set of tables and equations. More detail on method and data content can  
1672 be found in Te Chow (1959).

1673 CHOW was used to compute the Manning's surface roughness coefficient fields for forest, irrigated crops and  
1674 other land cover types.

1675  
1676 **The Copernicus Global Land Service (CGLS) Leaf Area Index (LAI) 1km Version 2 collection** (further  
1677 referred as CGLS-LAI) is a set of global maps without missing data describing vegetation dynamics – the annual  
1678 evolution of LAI at 10-day intervals over the period of 1999-2020. The dataset is derived from  
1679 SPOT/VEGETATION and PROBA-V data. The dataset's root mean square deviations over 20 GBOV sites over  
1680 the period 2014-2018 is 0.92, compared to 1.19 for MODIS C6 LAI product (Martinez-Sanchez, 2020). The  
1681 dataset is delivered as one multi-band file per year in NetCDF (netCDF4 CF-1.6) format (14.7 GB per year) at 1  
1682 km resolution covering land area from 90 N to 60 S and representative of the 10-year period of 2010-2019. More  
1683 detail on method, data content and access can be found in Smets (2019) and Martinez-Sanchez (2020), and  
1684 Copernicus web-site <https://land.copernicus.eu/global/products/lai>.  
1685 CGLS-LAI was used to compute the LAI fields for forest, irrigated crops and other land cover types.

1686  
1687 **The RiceAtlas v3** (further referred as RiceAtlas) is a spatial database of global rice calendars and production. It  
1688 contains information on start, peak and end dates of sowing, transporting and harvesting rice, derived from global  
1689 and regional databases, national publications, online reports, and expert knowledge. It is delivered as 7 files in  
1690 shapefile format (in total 195.8 MB) for administrative units (in total 2725 spatial units) at 1 km resolution for the  
1691 national production totals to match the years 2010-2012 (Laborte et al., 2017a). RiceAtlas is ~10 times more  
1692 spatially detailed, and has ~7 times more special units comparing with other global datasets (Laborte et al., 2017b).  
1693 More detail on method, data content and access can be found in Laborte et al. (2017a) and Laborte et al. (2017b).  
1694 RiceAtlas was used to compute rice planting and rice harvesting days for three different seasons.

#### 1695 **1.4 Soil properties**

1696 **The International Soil Reference and Information Centre (ISRIC) SoilGrids250m global gridded soil**  
1697 **information release 2017** (further referred as SoilGrids250m) is an output of special predictions produced by the  
1698 SoilGrids system, as a set of global soil property and class maps at 250 m resolution. It is derived from soil profile  
1699 data (from ~150,000 sites globally) with the use of machine learning, and contains information on soil  
1700 characteristics at six standard depths, including soil textures (clay, silt, sand), depth to bedrock, bulk density,  
1701 organic carbon, pH and cation exchange capacity. It is delivered as 43 files in GeoTiff format (in total 111.8 GB)  
1702 at 250 meters resolution covering land area with no permanent ice and representative for the year 2010 (according  
1703 to land cover) (Hengl et al., 2017). SoilGrids250m pH comparison with SSURGO data over California (depth 0-  
1704 200 cm) and Soil and Landscape Grid of Australia data over Tasmania (depth 0-5 cm) show high correlation, 0.79  
1705 and 0.71 respectively (Hengl et al., 2017). Despite its limited accuracy (i.e. between 30 and 70 %, according to  
1706 the SoilGrids web-site) due to the scarcity of soil profile observations (especially in Central Asia, Arctic regions  
1707 costal area and desert), low resolution of covariates data and algorithms, it was selected as the most recent source  
1708 of information. More detail on method, data content and access can be found in Hengl et al. (2017) and  
1709 SoilGrids250m web-site <https://www.isric.org/explore/soilgrids/faq-soilgrids-2017>.  
1710 SoilGrids250m was used to compute the soil depth and soil hydraulic properties for forest and non-forest.

#### 1711 **1.5 Lakes**

1712 **The Global Lakes and Wetlands Database** (further referred as GLWD) is a global database of water bodies. It  
1713 is derived from a combination of global and regional lake data sets, registers and inventories (i.e. point information  
1714 with descriptive attributes), and digital maps (i.e. polygons, rasterised global land cover and land use maps). The  
1715 database consists of two global files in shapefile format at spatial resolutions of up to 1:1 million – GLWD-1 with  
1716 3067 largest lake and 654 largest reservoir polygons (6.4 MB), and GLWD-2 with ~250000 smaller lake and  
1717 reservoir polygons (32.0 MB); and of one global file in ADF raster format at 30 arc sec resolution – GLWD-3  
1718 combines GLWD-1, GLWD-2 and additional information (8.9 MB). Validation against documented data shows  
1719 that GLWD represents good wetland maximum extent, and describes comprehensively lakes with surface area  
1720 greater or equal 1 km<sup>2</sup> (Lehner and Döll, 2004). More detail on method, data content and access can be found in  
1721 Lehner and Döll (2004) and GLWD web-site [https://www.worldwildlife.org/pages/global-lakes-and-wetlands-](https://www.worldwildlife.org/pages/global-lakes-and-wetlands-database)  
1722 database.  
1723 GLWD (i.e. only GLWD-1 and GLWD-2) was used to compute the discrete lake mask field.

#### 1724 **1.6 Water demand**

1725 **AQUASTAT** is the FAO's global information system on water resources and agricultural water management.  
1726 AQUASTAT collects information on water use via the network of AQUASTAT National Correspondents who

1727 are required to fill the annual questionnaire and collaborate with AQUASTAT team in the data validation process.  
1728 Five types of manual checks are followed by automatic implementation of almost 200 validation rules. The dataset  
1729 includes data for 180 countries worldwide, yearly data from 1979 to 2019 were used to produce the maps presented  
1730 by this manuscript. Float, lumped values for each country for the variables "Gross Domestic Product (GDP)",  
1731 "Industry, value added to GDP", "Agricultural water withdrawal", "Industrial water withdrawal", "Municipal  
1732 water withdrawal", "Total water withdrawal", and "Irrigation water withdrawal" were obtained in CSV format (2  
1733 files, in total 2.0 MB) from the AQUASTAT data acquisition dashboard  
1734 ([https://tableau.apps.fao.org/views/ReviewDashboard-v1/country\\_dashboard](https://tableau.apps.fao.org/views/ReviewDashboard-v1/country_dashboard)). More detail on method, data  
1735 content and access can be found in AQUASTAT web-site  
1736 <https://www.fao.org/aquastat/en/overview/methodology/>.  
1737 AQUASTAT variables were used accordingly to compute water demand fields for domestic, industrial, energy,  
1738 livestock use.

1739 **United States Geological Survey National Water Information System** (further referred as USGS NWIS) is a  
1740 national database on water use data for the United States (US) with annual statistics provided every 5 years since  
1741 1950. The water use data are best estimates produced by the USGS in cooperation with local, state, and federal  
1742 agencies as well as academic and private organisations. The water use data are lumped values (float numbers) for  
1743 each state, delivered in plain text format (52 files, in total 56.0 MB). Following variables were used: "Domestic  
1744 total self-supplied withdrawals, fresh, in Mgal/d", "Public Supply total self-supplied withdrawals, fresh, in  
1745 Mgal/d", "Industrial total self-supplied withdrawals, fresh, in Mgal/d", "Total Thermoelectric Power total self-  
1746 supplied withdrawals, fresh, in Mgal/d", "Total Thermoelectric Power power generated, in gigawatt-hours", and  
1747 "Livestock total self-supplied withdrawals, fresh, in Mgal/d". More detail on method, data content and access can  
1748 be found in USGS NWIS web-site <https://waterdata.usgs.gov/nv/nwis/wu>. For this study, data from 1985 to 2015  
1749 were used.

1750 USGS NWIS variables were used accordingly to refine the global water demand fields for the domestic, industrial,  
1751 energy, livestock use sectors for the US.

1752 **Global Change Analysis Model** (further referred as GCAM) is an integrated, multi-sector model developed by  
1753 the Joint Global Change Research Institute (JGCRI) to explore the overall behaviour of human and physical  
1754 systems dynamics and interactions. GCAM includes five main systems. One of these systems, the water module,  
1755 provides information about water withdrawals for energy, agriculture, and municipal uses as lumped values of  
1756 235 hydrologic basins; a detailed explanation can be found in Calvin et al. (2019). Estimates of industrial,  
1757 thermoelectric water withdrawals (energy sector) and electricity consumption were computed by running the  
1758 GCAM model, the output used are two files in CSV format (in total 4.0 MB). Data from the following sectors was  
1759 used: "biomass", "electricity", "nuclearFuelGenII", "nuclearFuelGenIII", "regional coal", "regional natural gas",  
1760 "regional oil", "SheepGoat", "Beef", "Dairy", "Pork", and "Poultry". More detail on method, data content and  
1761 access can be found in the documentation of the open source package <https://github.com/JGCRI/gcam-core/tree/gcam-v6.0>.

1762 GCAM variables were used accordingly to estimate water withdrawals for industrial, energy, livestock use.

1763 **Global-scale gridded estimates of thermoelectric power and manufacturing water use** (further referred as  
1764 Vassolo and Doll, 2005) is a global-scale gridded estimate of water withdrawal for cooling of thermal power  
1765 stations and for manufacturing. Estimates of values for the year 1995 are provided with a spatial resolution of 0.5°  
1766 by 0.5°. Thermoelectric power water use is based on the geographical location of 63590 thermal power stations.  
1767 Manufacturing water use is computed by estimating country-specific water withdrawal values, and spatial  
1768 downscaling using city night-time lights. Dataset verification of Vassolo and Doll (2005) showed satisfactory  
1769 representation of thermoelectric power water use but high uncertainty in the representation of manufacturing water  
1770 use. The data are delivered as one shapefile (2.5 MB). More details on method, data content and validation, and  
1771 data access can be found in Vassolo and Doll (2005).

1772 Vassolo and Doll (2005) dataset was used for the computation of energy demand fields.

1773 **The Gridded Livestock of the World (GLW) version3** (further referred as GLW3) is a spatial gridded dataset  
1774 of the global distribution of eight livestock species for 2010. It is delivered as 8 GeoTiff files at 0.083333° (~10  
1775 km at the equator) resolution (in total 208.0 MB). The species abundance was converted to total livestock mass.  
1776 More detail on method, data content and access can be found in Gilbert et al. (2018).  
1777 GLW3 was used to spatially disaggregate the water demand for livestock use.

1778 **World Bank manufacturing value added and gross domestic product** (further referred as World Bank) data  
1779 provide "Manufacturing, value added (constant 2015 US\$)" values (further referred as MVA) and "Gross  
1780 domestic product (constant 2015 US\$)" values (further referred as GDP).

1786 Domestic Product GDP (constant 2015 US\$)" values. The data provided as a table, downloaded in CSV format  
1787 (6 files, in total 6.0 MB) from <https://data.worldbank.org>.  
1788 World Bank dataset was used to temporally downscale the values of water demand fields for the industrial and  
1789 energy sectors.

1790  
1791 **The Global Human Settlement Population Grid multitemporal version R2019A** (further referred as GHS-  
1792 POP) is a spatial raster dataset that depicts the distribution of population, expressed as the number of people per  
1793 grid cell (Freire et al., 2016; Florczyk et al., 2019; Schiavina et al., 2019). GHS-POP residential population  
1794 estimates for target years provided by CIESIN GPWv4.10 were disaggregated from census or administrative units  
1795 to grid cells, informed by the distribution and density of built-up as mapped in the Global Human Settlement  
1796 Layer. The dataset has a spatial resolution of 9 arc sec (~300 m at the equator) resolution and is delivered as  
1797 individual files in GeoTiff format for 1975, 1990, 2000 and 2015 (4 files, in total 6.5 GB; available online:  
1798 [https://ghsl.jrc.ec.europa.eu/ghs\\_pop2019.php](https://ghsl.jrc.ec.europa.eu/ghs_pop2019.php), last accessed: 21.01.2024).  
1799 GHS-POP was used to spatially disaggregate the country, state, basin-level information of domestic, industrial,  
1800 energy water withdrawal.

1801  
1802 **Thematic Mapping Country Borders** shapefile (further referred as TM ‘country borders’) was derived from  
1803 Thematic Mapping™, which is a tool enabling web browsers to create thematic maps and associated world  
1804 datasets. For this work, the TM World Borders Dataset was downloaded as one shapefile (10.0 MB). **The United**  
1805 **States Census Bureau** Cartographic Boundary Files – Shapefile (further referred as US CB) provides the State  
1806 boundaries for the USA. For this work, the 2018 version was retrieved as one shapefile (3.2 MB; available online:  
1807 <https://www.census.gov/geographies/mapping-files/time-series/geo/carto-boundary-file.html>, last accessed:  
1808 21.01.2024). More detail on method, data content and access can be found in  
1809 <http://thematicmapping.org/downloads/>.  
1810 TM ‘country borders’ and US CB were used to spatially disaggregate the information of water withdrawal for  
1811 domestic, industrial, energy use.

1812  
1813 **Multi-Source Weather** (further referred as MSWX) is a high-resolution (3-hourly, 0.1°), bias-corrected  
1814 meteorological product with global coverage from 1979 to 7 months into the future. The data for 42 years  
1815 (~316700 files in NetCDF format, in total 128.0 GB) were retrieved via [www.gloh2o.org/mswx/](http://www.gloh2o.org/mswx/). For more  
1816 detailed information, see Beck et al. (2022).  
1817 MSWX 2-meter daily and monthly maximum and minimum air temperature were used to account for the climate-  
1818 induced intra- and inter- annual fluctuations of domestic, livestock, and energetic water demand.

1819  
1820 **Huang et al. (2018)** is a publication presenting 0.5° resolution global monthly gridded sectoral water withdrawal  
1821 dataset for the period 1971–2010.  
1822 Huang et al. (2018) Table 3 (calibrated R coefficient values) and Eq. (2) to (6) for temporal downscaling of  
1823 domestic and energy water demands were used in this study, respectively.

## 1824 **Appendix 2**

1825 Unit conversion to fraction  
1826 Hectare (ha):  $fraction = ha \cdot 10^4 / GridCellArea_{m^2}$ ;  
1827 Percentage (%):  $fraction = \% / 100$ ;  
1828 Class (landcover type):  $fraction = 1$ , i.e. assumes full 100 % coverage of the grid-cell.

## 1829 **Annex 2**

## 1830 **Appendix 3**

1831 Soil depth  
1832 Soil depth layers are derived following Burek et al. (2014) in which the total soil depth is horizontally divided in  
1833 three layers. The total soil depth is the ‘absolute depth to bedrock’ from SoilGrids250m, whereas root depths of  
1834 forest and non-forest are derived from FAO56 and CGLS-LC100 dataset at SoilGrids250m native (~250 m)  
1835 resolution (see Section 4.36.2 for more details). The methodology implemented for the creation of three soil layers  
1836 is the following:

1837 Soil depth layer 1 (surface)  $SD_1$  is assumed constant, equal to 50 mm all over the world for consistency with  
1838 satellite-derived datasets (satellite signal penetration depth of 50 mm is a good approximation to take into account  
1839 different meteorological conditions at different hour of the day globally based on Lv et al. (2018)), and follow Eq.  
1840 (A1):

$$1841 \quad SD_1 = 50mm \quad (A1)$$

1842  
1843 Soil depth layer 2 (middle)  $SD_2$  depends on the absolute depth to bedrock  $adb$  – if it is equal or less than 300 mm  
1844 computation follow Eq. (A2), otherwise it is conditional of the root depths as per Eq. (A3), and must meet  
1845 requirement from Eq. (A4):

$$1846 \quad SD_2 = (adb - SD_1)/2, \quad adb \leq 300mm \quad (A2)$$

$$1848 \quad SD_2 = \min(\text{root\_depth}, (adb - 300mm - SD_1)), \quad adb > 300m \quad (A3)$$

$$1849 \quad SD_2 = 50mm, \quad SD_2 < 50mm \quad (A4)$$

1850  
1851 Soil depth layer 3 (bottom)  $SD_3$ , is computed following Eq. (A5):

$$1852 \quad SD_3 = adb - (SD_1 + SD_2) \quad (A5)$$

1853  
1854 This set of equations is used twice, once with the root depth of forest area and a second time with the root depth  
1855 of non-forested areas, resulting in a total of six soil depth layers computed at SoilGrids250m native resolution.

#### 1856 1857 1858 Soil hydraulic parameters

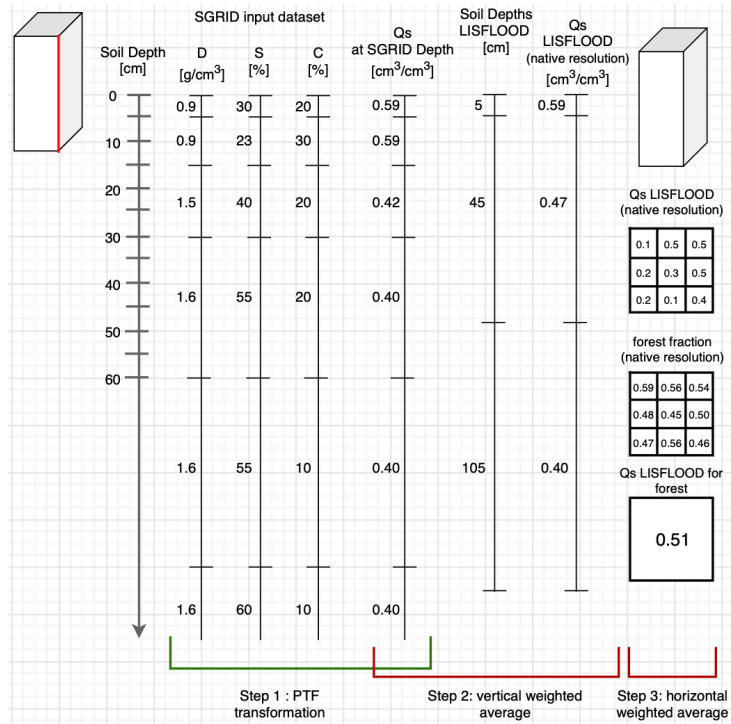
1859 Soil hydraulic parameters are derived by following three main steps (see Figure A1).

1860  
1861 First, soil hydraulic properties are derived at native resolution by applying pedotransfer functions (PTFs) to each  
1862 SoilGrids250m soil characteristics layer at each available depth. Pedotransfer functions translate field measured  
1863 soil information (such as soil texture, pH and structure) into proprieties and parameters needed to describe soil  
1864 processes. The PTFs implemented here are the ones proposed by Toth et al. (2015). Users can decide to derive  
1865 soil proprieties from different PTFs, but the general principle presented here remains valid.

1866  
1867 Second, the soil hydraulic parameters calculated at SoilGrids250m depths are vertically downscaled to the model  
1868 soil depth (previously computed) by weighted average (Figure A1, Step 2 with theta saturated as an example) at  
1869 the native SoilGrids250m resolution (~250 m).

1870  
1871 Third, the soil hydraulic parameters at the final soil depths are upscaled from native to final resolution by average  
1872 using forest and non-forest fraction layers as weights (Figure A1, Step 3).  
1873





1874  
1875  
1876

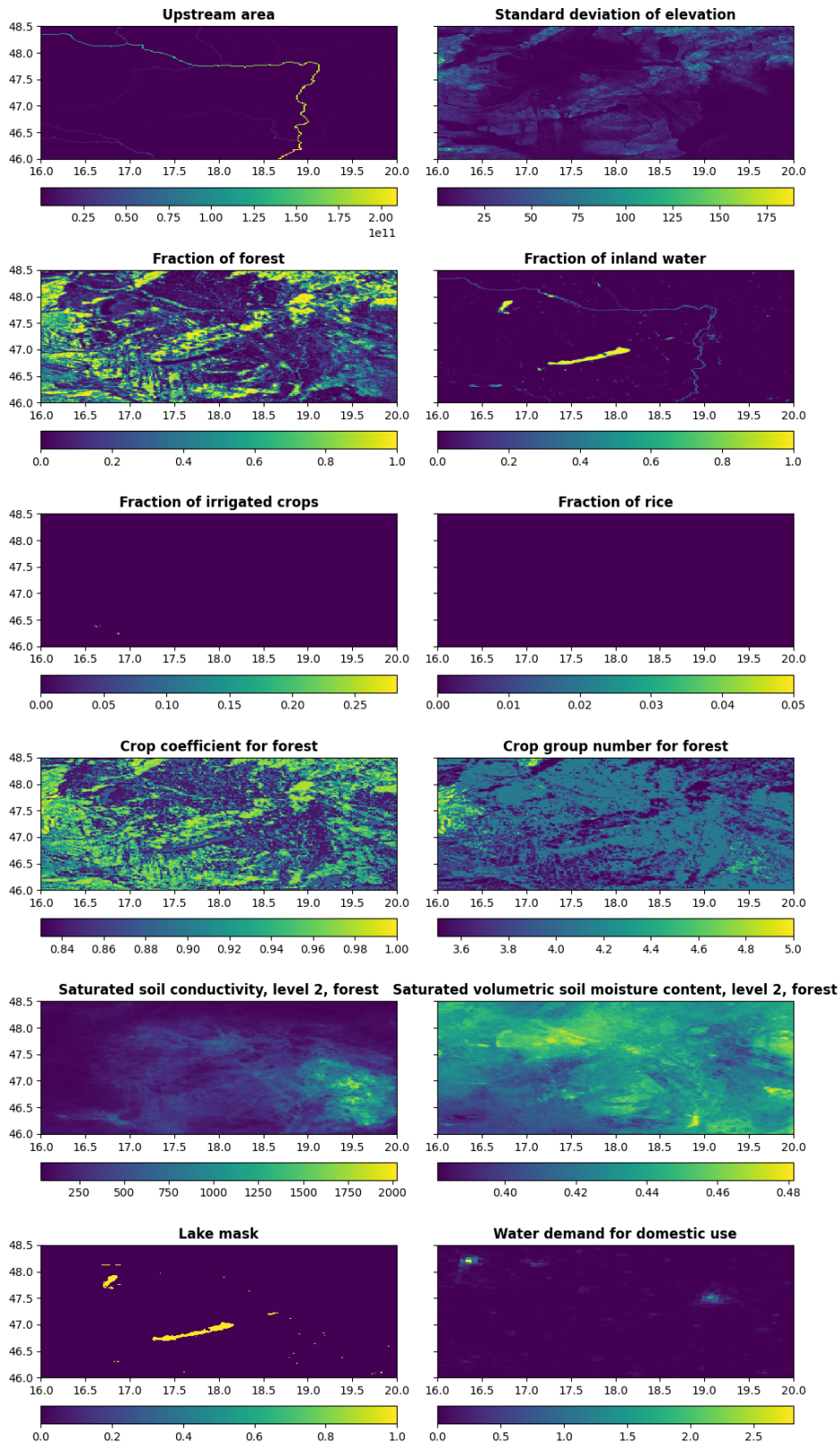
**Figure A1. Creation of theta saturated parameter 'Qs' using SoilGrids250m dataset 'SoilGRID' and forest fraction.**

1877

#### Appendix 4

1878  
1879  
1880  
1881

Here more regional examples of the most interesting surface fields of CEMS SurfaceFields\_2022 are provided to show what level of details is available at each resolution and field, and to emphasise consistency through all the fields that is the most valuable requirement when running any type of surface model.



1882  
1883  
1884  
1885  
1886  
1887

Figure A2. Upstream drainage area in square meters, standard deviation of elevation in meters, fraction of forest, fraction of inland water, fraction of irrigated crops, fraction of rice, crop coefficient for forest, crop group number for forest, saturated soil hydraulic conductivity for forested areas of soil depth layer 2 in mm per day, saturated volumetric soil moisture (i.e. water) content for forested areas of soil depth layer 2, lake mask, and water demand for domestic use at 1 arc min (~1.9 km at the equator) resolution for Danube River area in Europe.

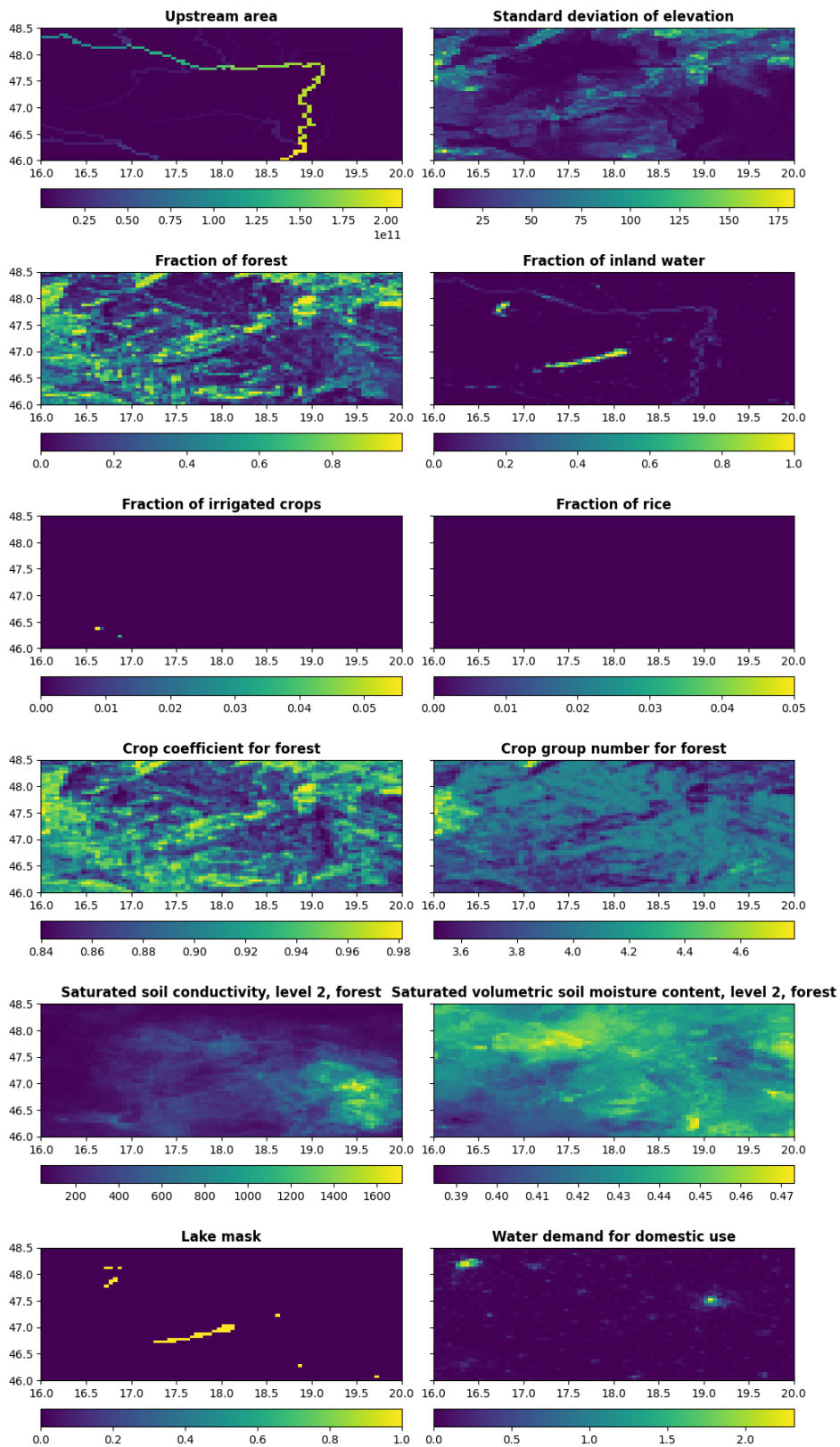
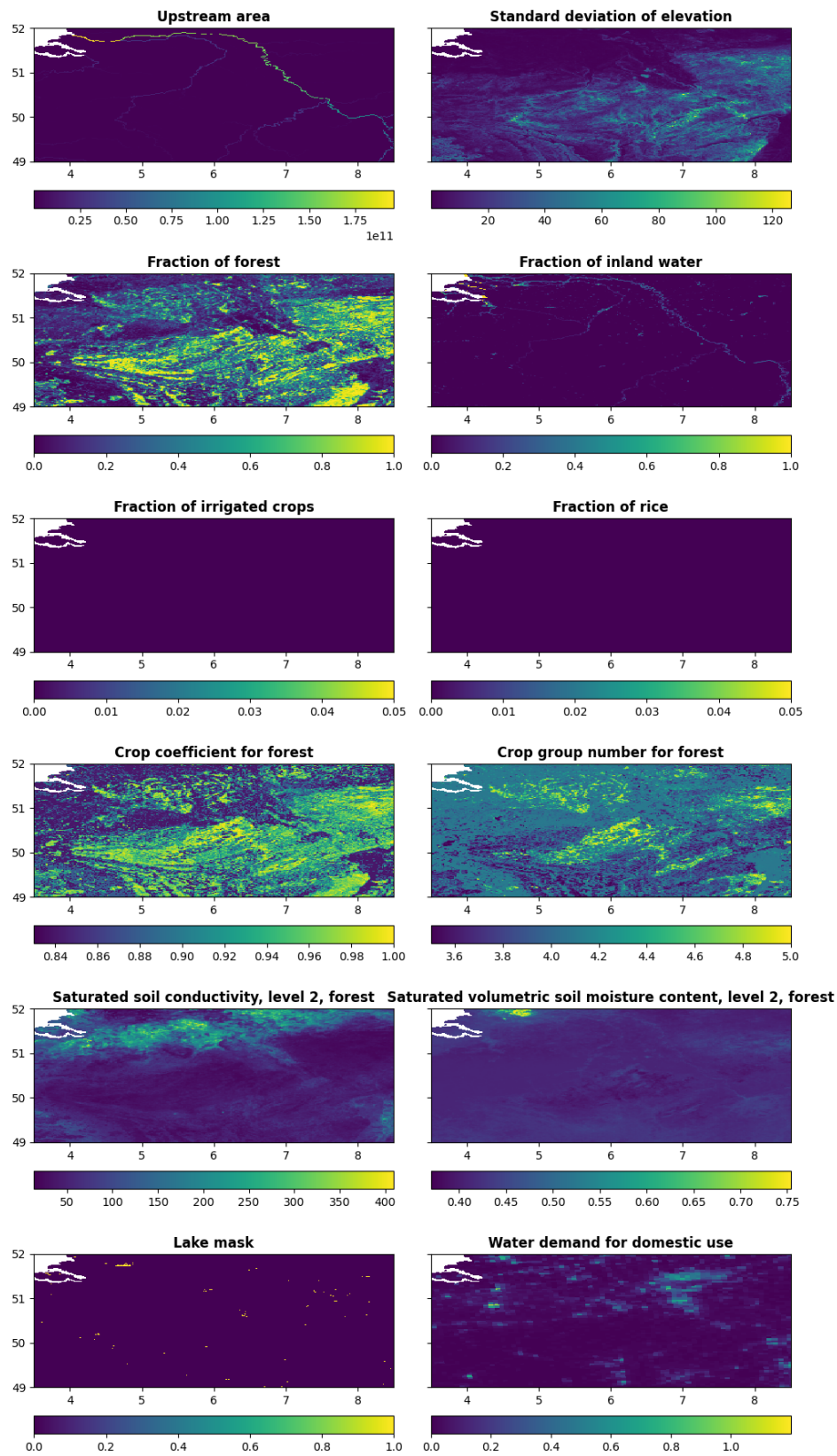


Figure A3. Same as Figure A2, but at 3 arc min (~5.6 km at the equator) resolution for Danube River area in Europe.

1888  
1889



1890  
1891

**Figure A4.** Same as Figure A2, but at 1 arc min (~1.9 km at the equator) resolution for Rhine River area in Germany.

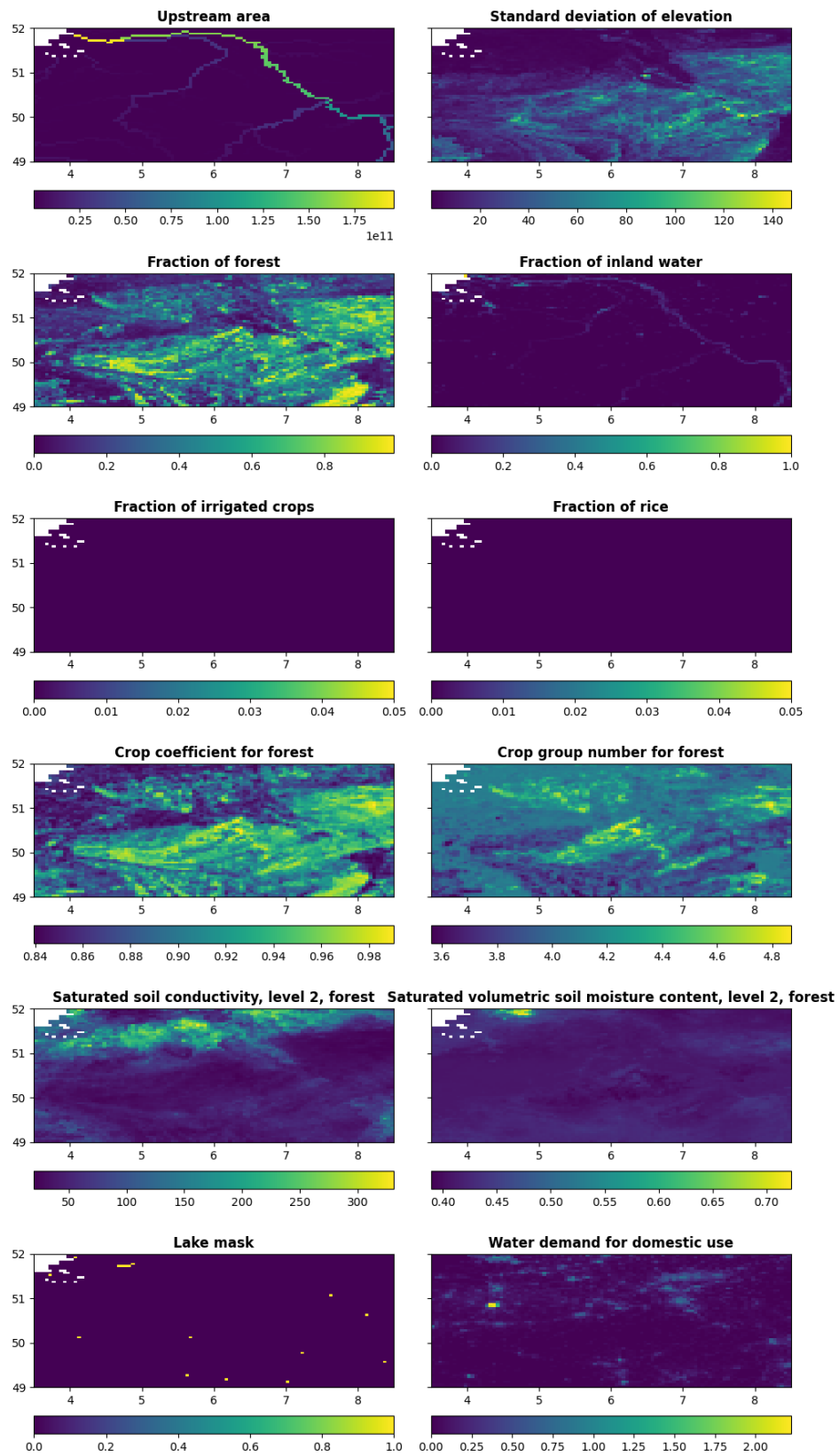


Figure A5. Same as Figure A2, but at 3 arc min (~5.6 km at the equator) resolution for Rhine River area in Germany.

1892  
1893



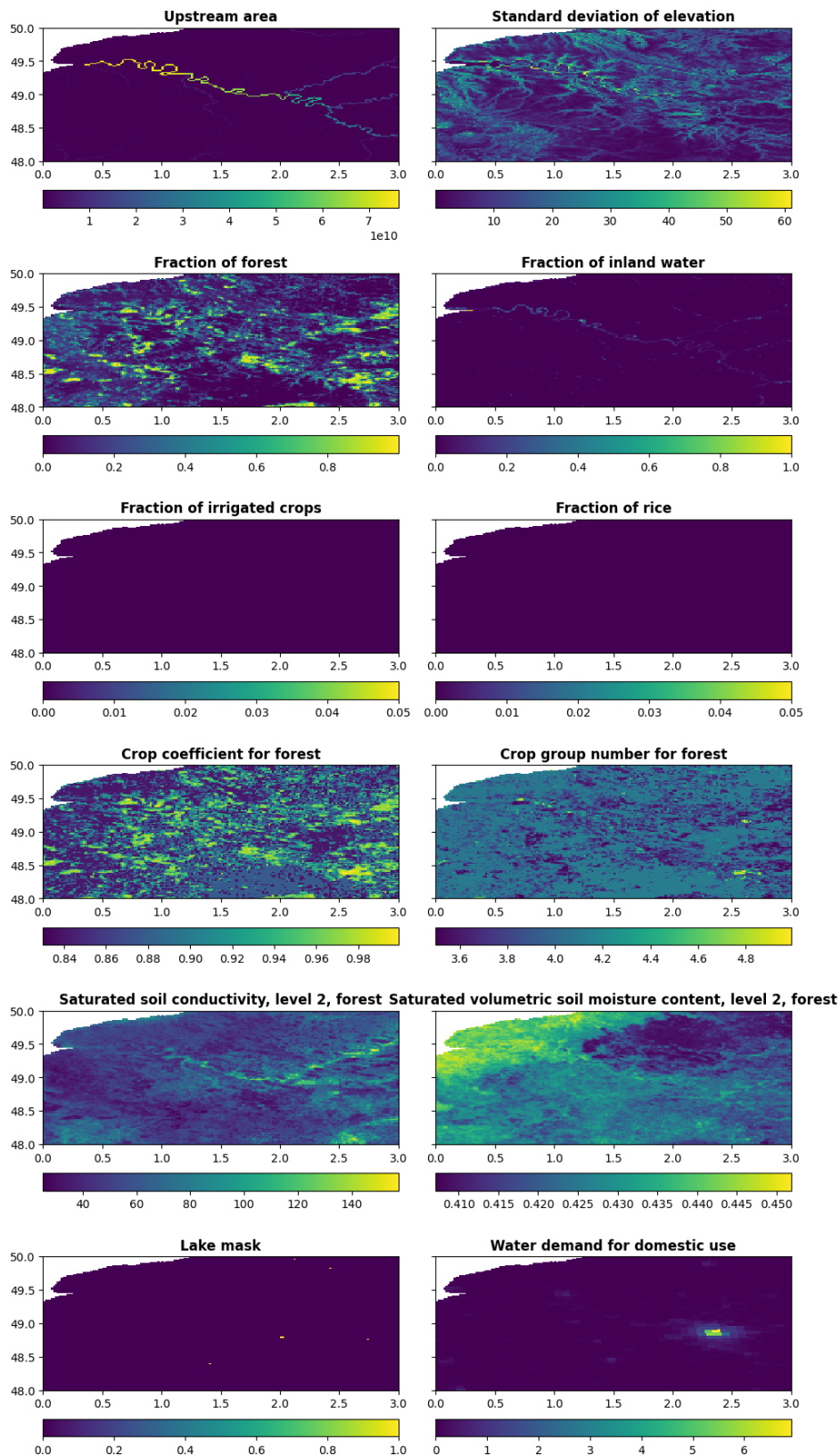


Figure A6. Same as Figure A2, but at 1 arc min (~1.9 km at the equator) resolution for Seine River area in France.

1894  
1895

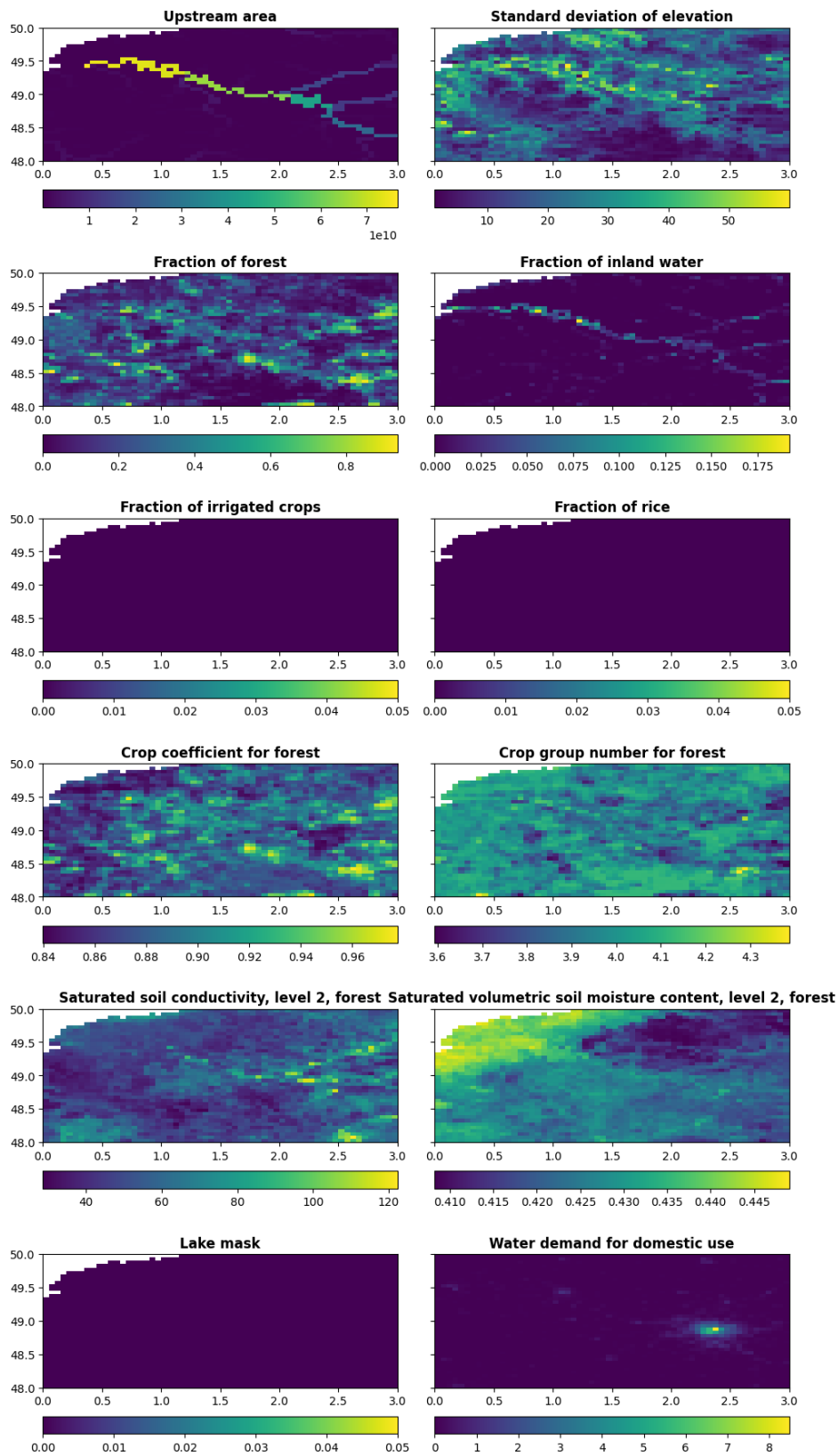
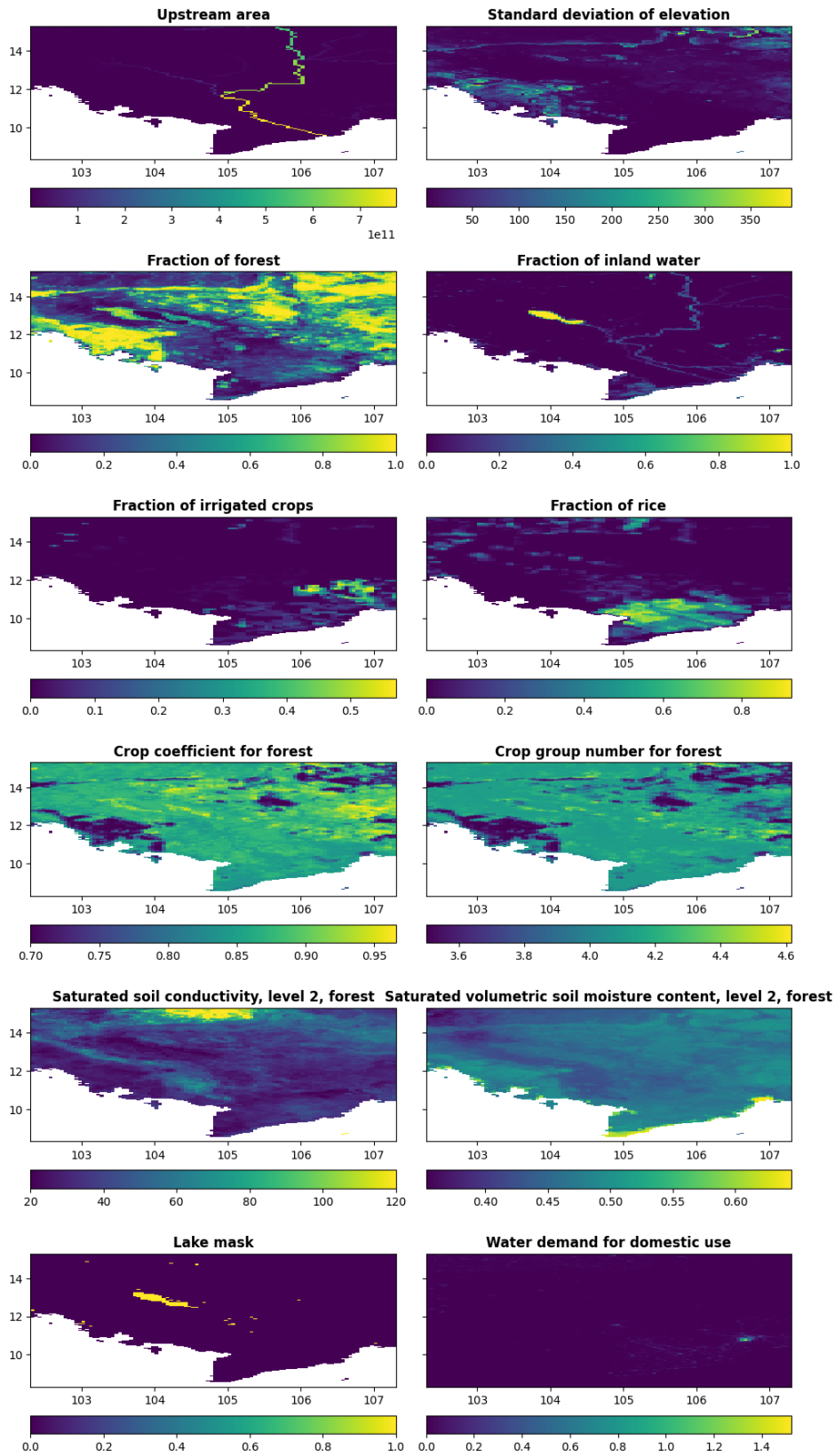


Figure A7. Same as Figure A2, but at 3 arc min (~5.6 km at the equator) resolution for Seine River area in France.

1896  
1897



**Figure A8.** Same as Figure A2, but at 3 arc min (~5.6 km at the equator) resolution for Seine Mekong area in Cambodia.

1898  
1899  
1900  
1901